NATIONAL TECHNICAL UNIVERSITY OF UKRAINE «IGOR SIKORSKY KYIV POLYTECHNIC INSTITUTE»

Faculty of electric power engineering and automatics

Automation of electromechanical systems and the electrical drives department

«On the rights of the manuscript»
UDC _____

«Defense allowed»

Head of Department
_____ Sergiy Peresada
(signature) (Name, Surname)
"___"_____2020 y.

Master thesis

specialty 141 – Electric power engineering, electrotechnics and electromechanics

specialization – Electromechanical systems of automation, electrical drives and electromobility

on the topic: Adaptive control of the interior permanent magnet synchronous motors

Performed by student VI year, group EP-81MN

Dmytro Illich Rodkin _____
(Name Surname) (signature)

Supervisor Dr. Sci., Prof. Sergiy Peresada _____
(post, academic degree, academic title, name and surname) (signature)

Advisor _____ _____ _____
(Section) (post, academic degree, academic title, name and surname) (signature)

Reviewer Dr. Sci., Research fellow Ivan Shapoval _____
(post, academic degree, academic title, name and surname) (signature)

Institution The Institute of Electrodynamics

I certify that in this master's thesis, there are no borrowings from the works of other authors without corresponding references.
Student _____
(signature)

Kyiv 2020

DIPLOMA PROJECT INFORMATION

№	Format	Marking	Designation	Pages	Note
1	A4		Task for the diploma project	2	
2	A4		Explanatory note	117	
3	A1		Structural scheme and block diagram for the speed control algorithm	1	
4	A1		Simulation and experimental results for the speed control algorithm	1	
5	A1		Structural scheme and block diagram for the position control algorithm	1	
6	A1		Simulation and experimental results for the position control algorithm	1	
7	A1		Structural scheme and block diagram for the adaptive position control algorithm	1	
8	A1		Structural scheme of the adaptive observer and simulation results for the position control algorithm	1	

Explanatory note

to the diploma project

topic: Adaptive control of the interior permanent magnet synchronous motors

Kyiv 2020

NATIONAL TECHNICAL UNIVERSITY OF UKRAINE «IGOR SIKORSKY KYIV POLYTECHNIC INSTITUTE»

Faculty of electric power engineering and automatics

Automation of electromechanical systems nad the electrical drives department

Higher education level - the second (master's) in educational and professional program

Specialty 141 – Electric power engineering, electrotechnics and electromechanics

Specialization – Electromechanical systems of automation, electric drive and electromobility

APPROVED
Head of Department
_____ Sergiy Peresada
(signature) (name, surname)
«___»_____2019 y.

TASK
for the master's thesis of the student
Rodkin Dmytro Illich
(full name)

1. Thesis topic «Adaptive control of the interior permanent magnet synchronous motors»
Supervisor Dr. Sci., Prof. Sergiy Peresada,
(post, academic degree, academic title, full name
approved by university order of «__» _____ 20__ y. №_____
2. Submission term _____
3. Object of study Processes of the electromechanical energy conversion of the interior permanent magnet synchronous motors.
4. Input data: Tested interior permanent magnet synchronous motor parameters: rated power 3 kW, rated current 5.4 A, rated torque 13.6 Nm, rated speed 220 rad/s, q-axis inductance 58mH, d-axis inductance 31mH, stator resistance 1.7Ohm.
5. The list of tasks to be completed:
   1. Survey of the existed methods for inductance determination considering saturation for the IPMSMs.
   2. Development of the tests for inductance determination methods that will combine simplicity, high accuracy and convenience of usage.

3. Development of the speed and position control algorithms for the IPMSMs. Verification of validity of usage of the control based on the non-saturated motor model for the small saturated IPMSMs.
4. Development of the position control algorithm with adaptation to the mechanical parameters for the IPMSMs.

6. List of graphic (illustrative) material: Structural scheme and block diagram for the speed control algorithm, Simulation and experimental results for the speed control algorithm, Structural scheme and block diagram for the position control algorithm, Simulation and experimental results for the position control algorithm, Structural scheme and block diagram for the adaptive position control algorithm, Structural scheme of the adaptive observer and simulation results for the position control algorithm.

7. Indicative list of publications 4 publications

8 Advisors to the thesis Sections

Section	post, academic degree, academic title, surname and initials)	Signature, date	
		Task issued	Task accepted

9. Date of issue of the assignment

Calendar plan

№	The name of the execution stages Master's Thesis	The term of completion of the stages of the master's thesis	Note
1	Analytical survey	13.01–02.02	
2	Derivation of the motor model	03.02-16.02	
3	Description of the inductance determination methods	17.02-01.03	
4	Derivation and research of the speed and position control methods of the motors	02.03-22.03	
5	Derivation and research of the adaptive position control of the motors	23.03-05.04	
6	Development of the start-up project	06.04-19.04	
7	Thesis formalization	20.04-04.05	

Student _____ _Dmytro Rodkin_
(signature) (name, surname)

Supervisor _____ ___Sergiy Peresada_
(signature) (name, surname)

SUMMARY

Thesis contains: pages – 117, drawings – 38, tables – 23.

The goal of the of the thesis lies in development of the control methods of the IPMSM with the purpose of its research and improvement of efficiency and performance of the electromechanical system.

In this thesis, analytical review of the inductance determination methods for the IPMSM is presented. After that two tests for inductance determination of the interior permanent magnet synchronous motors are proposed, analyzed and experimentally verified. Four methods are proposed to use to obtain static and dynamic inductances from the tests data.

Speed and position control algorithms are derived basing on the non-saturated model of the motor and its effectiveness was researched by means of experiment and simulation for small saturated motors. After that position control algorithm with adaptation to the mechanical parameters is designed and tested via simulation. Stability is proved using the second Lyapunov method.

Derived algorithms provide asymptotic tracking of the controlled coordinates, and decoupling of the direct current component and mechanic coordinate control subsystems.

INTERIOR PREMANENT MAGNET SYNCHRONOUS MOTORS, INDUCTANCE DETERMINATION, SATURATION OF THE MAGNETIC SYSTEM, ADAPTIVE CONTROL, MECHANICAL PARAMETERS ESTIMATION.

РЕФЕРАТ

Магістерська дисертація містить: 117 сторінок, 38 рисунків, 23 таблиці.

Метою роботи є розробка та розвиток методів керування явнополюсними синхронними двигунами з постійними магнітами, спрямований на покращення ефективності електромеханічної системи.

В роботі представлено аналітичний огляд методів визначення індуктивностей IPMSM. Запропоно та експериментально впроваджено два тести для визначення індуктивностей. Отримані в тестах дані пропонується обробити чотирьма методами для отримання значень статичної та динамічної індуктивностей.

Розроблено алгоритми керування швидкістю та подоженням на основі моделі, що не враховує насичення. Ефективність алгоритмів досліджена шляхом моделювання та експериментально для двигуна з низьким рівнем насичення. Після цього синтезовано алгоритм керування положенням з адаптацією до механічних параметрів. Стабільність системи доведена за допомогою другого методу Ляпунова.

Отримані алгоритми забезпечують асимптотичне відпрацювання контрольованих координат та розв’язку підсистеми керування прямою компонентою струму та підсистемою керування механічними координатами.

ЯВНОПОЛЮСНИЙ СИНХРОННИЙ ДВИГУН З ПОСТІЙНИМИ МАГНІТАМИ, ВИЗНАЧЕННЯ ІНДУКТИВНОСТЕЙ, НАСИЧЕННЯ МАГНІТНОЇ СИСТЕМИ, АДАПТИВНЕ КЕРУВАННЯ, ВИЗНАЧЕННЯ МЕХАНІЧНИХ ПАРАМЕТРІВ.

CONTENT

INTRODUCTION

Interior permanent magnet synchronous motors (IPMSM) find their application in high dynamics and high precision drives. Due to presence of permanent magnets (PMs), torque and power density of the motors is significantly higher comparing to the other AC machines. Unlike the surface PM motors (SPMSMs) where permanent magnets are attached to the surface of the rotor, IPMSM is more reliable, maximum speed is usually higher. The only drawback of the motor is its cost, as nowadays technologies do not allow creating PMs artificially with equivalent flux density comparing to the ones from rare earth materials.

The PMs are implemented into the rotor structure in the IPMSM. Due to this geometry, rotor of the motor has saliency. It leads to the several consequences: motor torque is created not only from PMs, but also from the reactive component caused by the difference between direct and quadrature axis inductances of the rotor; effect of saturation and cross-coupling on the motor behavior is significantly higher comparing to the non-salient analog.

Thesis actuality. Conventional vector control algorithms demand information about six motor parameters for proper operation. Moreover, parameters are considered as constant values. Inductances variation due to saturation have to be considered in the motor model and control algorithm in order to avoid performance deterioration due to parameter mismatch. Therefore, derivation of the motor model where saturation and cross-coupling are considered is an open-ended question and has to be solved. Several approaches are proposed to determine inductances considering saturation effects. The most of the methods require special tests or ignore system nonlinearities with the purpose of simplification of the calculation, but it leads to output data accuracy deterioration.

On the other hand, if motor saturation is comparatively small, development of more complex algorithm with considered saturation is questionable. In this manuscript, verification of validity of usage of the control based on the non-saturated model for the small saturated IPMSMs is made.

Another aspect of IPMSMs control that is also considered in the manuscript is online estimation of mechanical parameters of the motors. Proper estimation of the moment of inertia, friction coefficient and load torque are highly important in high dynamic applications, such as robotics or servo drives.

Thesis relation with science programs, topics and plans. The thesis is based on the research made in the Automation of electromechanical systems and the electrical drives department of the National Technical University of Ukraine "Igor Sikorsky Kyiv Polytechnic Institute" and in the School of Engineering of the Warwick University during student exchange program.

Research goals and tasks.

The *goal* of the thesis lies in the improvement of efficiency and performance of the electromechanical systems based on IPMSMs by means of development of the advanced control techniques. The *tasks* of the thesis are following:

1. Survey of the existed methods for inductance determination considering saturation for the IPMSMs.
2. Development of the tests for inductance determination methods that will combine simplicity, high accuracy and convenience of usage.
3. Development of the speed and position control algorithms for the IPMSMs. Verification of validity of usage of the control based on the non-saturated motor model for the small saturated IPMSMs.
4. Development of the position control algorithm with adaptation to the mechanical parameters for the IPMSMs.

Research object. Processes of the control of the electromechanical energy conversion of the IPMSMs.

Research subject. Speed and position control algorithms of the IPMSMs with adaptation to the mechanical parameters.

Research methods. Research is based on the modern control theory of the nonlinear systems. Following methods are used: second Lyapunov method, feedback linearizing control method and methods of modelling and experimental research.

Scientific novelty of the obtained results is following:

1. Novel speed and position control algorithms for IPMSM is designed. Despite of the existing analogues, it allows decoupling of direct current component control subsystem and mechanical coordinates control subsystem. From the experimental and simulation analysis follows that proposed algorithms can be used for small saturated IPMSMs without significant performance degradation.

2. Novel position control algorithm with online adaptation to the mechanical parameters for the IPMSM is designed. Unlike the existed algorithms, mechanical parameters are observed during operation and algorithm adapts to its variation.

Practical value of the obtained results. Designed speed and position algorithms provide asymptotic tracking of the controlled coordinates that leads to improvement of the high-dynamics systems performance. Designed adaptive position algorithm observes mechanical parameters during operation that allows improving system performance especially if mechanical parameters are variable values.

Publications. The main idea of the Master thesis is presented in 4 scientific articles, where 1 of them is an IEEE conference paper and 3 are published in Ukrainian scientific journals.

Publications:

1. Rodkin D., Zinchenko O., Peresada S. "Survey of the interior permanent magnet synchronous motor models considering saturation and cross-magnetization", International scientific and technical journal of young scientists, graduate students and students "MODERN PROBLEMS OF ELECTRIC POWER ENGINEERING AND AUTOMATION", Kyiv, Ukraine, 2020.

2. Rodkin D., Zinchenko O., Peresada S., Kiselychnyk O. "Inductance determination of interior permanent magnet synchronous motor considering saturation", International scientific and technical journal of young scientists, graduate students and students "MODERN PROBLEMS OF ELECTRIC POWER ENGINEERING AND AUTOMATION", Kyiv, Ukraine, 2020.

3. S. Peresada, V. Reshetnyk, D. Rodkin, O. Zinchenko, "Linearizing speed control and self-commissioning of interior permanent magnet synchronous motors", Bulletin of the National Technical University "KhPI". Problems of automated

electrodrive. Theory and practice, Kharkiv, 2019. no. 9, vol. 1334. pp. 36-42. (in Ukrainian).

4. S. Peresada, Y. Nikonenko, V. Reshetnyk and D. Rodkin, "Adaptive position control and self-commissioning of the interior permanent magnet synchronous motors," 2019 IEEE International Conference on Modern Electrical and Energy Systems (MEES), Kremenchuk, Ukraine, 2019, pp. 498-501.

1 ANALYTICAL SURVEY OF PARAMETER DETERMINATION METHODS

Interior permanent magnet synchronous motors (IPMSMs) find their application in high-dynamic and precision drives, such as robotics and electric vehicles, because of high torque/inertia ratio, high reliability, high power factor and high efficiency. Most of these advantages are achieved because of presence of permanent magnets in motors structure (usually in the rotor). At the same time, the main disadvantage of the motors comparing to the other AC machines – its cost – is also caused by existence of permanent magnets.

A lot of types of the structure of the synchronous motors are existed. The most significant examples are presented in Fig. 1.1 [1].

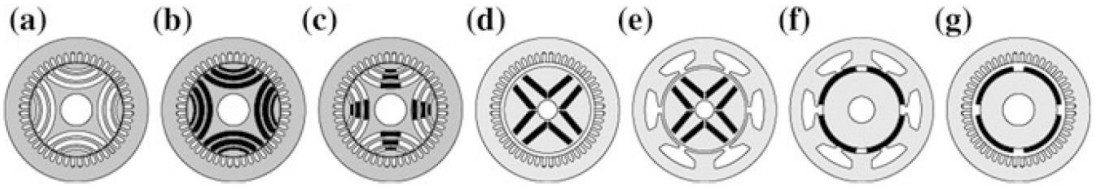

Fig. 1.1 – Different types of the PM synchronous machines. a) Synchronous reluctance motor (SynRM); b) PM reluctance motor with ferrite magnets; c) PM reluctance motor with rare-earth magnets; d) IPMSM with distribution windings; e) IPMSM with concentrated windings; f) SPMSM with concentrated windings; g) SPMSM with distributed windings [1]

In case of synchronous motors, total torque is combination of magnet torque (caused by PMs) and reluctance torque (caused by rotor saliency). Depending on the rotor structure in the configurations presented in Fig. 1.1, dominant torque source is different. Saliency and PM flux linkage relation define motor behavior in field weakening region. According to [2], configurations in Fig. 1.1 can be organized in "IPM design plane" (Fig. 1.2). The p.u. PM flux linkage is relation between nominal voltage and open circuit voltage at nominal speed; saliency equals to $\xi = L_d / L_q$.

In Fig. 1.2 optimal design line is shown. This line corresponds to the special matches of magnet and saliency that leads to the optimal flux weakening capability, in

particular - possibility to operate with constant power at any speed with limited current and voltage.

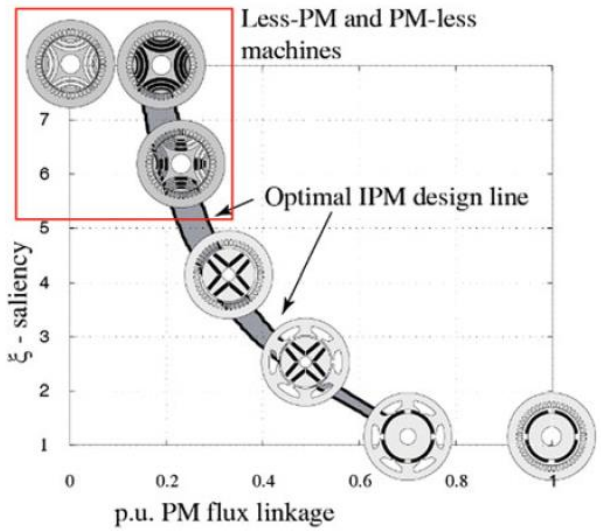

Fig. 1.2 – IPM design plane that shows optimal design line [1]

Because of saliency, saturation effects of the machine are very distinct. Saturation effects cause parameters to vary nonlinearly, especially inductances along two axes. Modern control techniques require precise knowledge of the motor parameters for the proper motor operation. Therefore, variation of the inductances makes huge impact on the control performance [3] unless its change is a known function.

A lot of methods exist to determine inductance values of the synchronous motors. They can be conditionally divided into two groups: a) *those that require additional equipment* [4]-[17] and b) *those that does not* [18]-[37].

Overall, methods that require additional equipment are more precise and magnetic saturation can be considered during the test, however, as it follows from the name of the first group, equipment, such as blocking mechanisms, loading machines, hardware filters, DC supplies and so on, is required.

Methods that does not require additional equipment, also known as self-commissioning with free rotor or adaptive control method, require only common electric drive system with fully controlled inverter. Despite of the convenience of usage of the methods from the second group, their accuracy of parameter identification is influenced by many factors, such as external noises, the inverter nonlinearities, and

errors in reference frame transformation. Moreover, in the mentioned algorithms, all motor parameters are considered as constants, saturation and cross-coupling effects are neglected.

The third group, that is not considered in the thesis, proposes to calculate inductances using Finite Element Analysis (FEA). This method allows to calculate motor parameters based on its geometry and materials [38]-[41]. Manufacturers use this technique to predict characteristics of the motor that has to be produced.

IPMSMs model in rotor reference frame (d-q) considering cross coupling and saturation is following [4]:

$$\begin{aligned}
u_d &= Ri_d + L_{dd}\left(i_d, i_q\right)\frac{di_d}{dt} + L_{dq}\left(i_d, i_q\right)\frac{di_q}{dt} - \omega p_n \Psi_q\left(i_d, i_q\right), \\
u_q &= Ri_q + L_{qq}\left(i_d, i_q\right)\frac{di_q}{dt} + L_{qd}\left(i_d, i_q\right)\frac{di_d}{dt} + \omega p_n \Psi_d^*\left(i_d, i_q\right), \\
\Psi_d^*\left(i_d, i_q\right) &= \Psi_d\left(i_d, i_q\right) + \Psi_M\left(i_d, i_q\right), \\
\Psi_d\left(i_d, i_q\right) &= L_d\left(i_d, i_q\right) i_d, \\
\Psi_q\left(i_d, i_q\right) &= L_q\left(i_d, i_q\right) i_q,
\end{aligned} \tag{1.1}$$

where u_d, u_q are stator voltages; i_d, i_q are stator currents; ω is rotor speed; p_n is pole pairs number, R_s is stator windings resistance; Ψ_m is permanent magnets flux, $L_d\left(i_d, i_q\right)$ and $L_q\left(i_d, i_q\right)$ are d- and q-axis static inductances; $L_{dd}\left(i_d, i_q\right)$ and $L_{qq}\left(i_d, i_q\right)$ are d- and q-axis dynamic inductances; $L_{dq}\left(i_d, i_q\right)$ and $L_{qd}\left(i_d, i_q\right)$ are cross inductances; $\Psi_d^*\left(i_d, i_q\right)$ and $\Psi_q\left(i_d, i_q\right)$ are total flux along d- and q- axis respectively; $\Psi_d\left(i_d, i_q\right)$ - flux along d-axis caused by currents.

1.1 Inductance determination methods that require additional equipment

Mainly two approaches are used to determine inductances from the model (1.1). The first one proposes to lock the rotor. In this case motor model converts into two independent series RL circuits, if cross coupling is neglected. The second approach is

to consider motor operation at nonzero constant speed at steady-state. Differential current components decay to zero in (1.1).

1.1.1 Stand-still rotor methods

There are several ways for inductance determination if rotor is locked. The first option is to observe current response to the voltage change, another words, to observe system behavior during transient. The second option is to apply AC high frequency voltage and observe current magnitude. In this case inductances are determined from frequency method. These methods will be thoroughly described below.

Method proposed in [6] can be described requires locking mechanism. Disadvantages are following: additional DC supply is used and cross-coupling and saturation is neglected. Phases B and C are connected. Voltage step is applied between phases A and B. Phase A current and voltage between phases A and B are measured using current and voltage probe respectively.

For d-axis inductance calculation, magnetic axis of the rotor has to be aligned with phase A voltage vector. Similarly, q-axis inductance is calculated if magnetic axis is orthogonal to phase A voltage vector. After that rotor has to be locked.

In stand-still, IPMSM model converts to RL series circuit. Therefore, exponential change of current is expected if voltage step is applied. Time constant τ is computed as time between transient start and moment when current value reaches 63.2% of its steady state value.

Inductance is calculated from time constant and resistance as

$$L_{dq} = \frac{2}{3}\tau R_s. \tag{1.2}$$

In [4] method based on flux calculation is presented. In the paper cross-coupling and saturation are considered, however nonlinearities caused by inverter are neglected. Rotor has to be locked during the test, and its position is known value. The idea is to calculate dynamic and cross inductances (1.1) from fluxes $\Psi_q\left(i_d, i_q\right)$ and $\Psi_d\left(i_d, i_q\right)$ values. Inductances can be determined as [4], [7], [8]:

$$L_{dd}\left(i_d,i_q\right)=\frac{\partial\Psi_d\left(i_d,i_q\right)}{\partial i_d},L_{qq}\left(i_d,i_q\right)=\frac{\partial\Psi_q\left(i_d,i_q\right)}{\partial i_q},$$
$$L_{dq}\left(i_d,i_q\right)=\frac{\partial\Psi_d\left(i_d,i_q\right)}{\partial i_q},L_{qd}\left(i_d,i_q\right)=\frac{\partial\Psi_q\left(i_d,i_q\right)}{\partial i_d}. \quad (1.3)$$

Flux linkages can be calculated from current and voltage transients. For instance, for $\Psi_q\left(i_d,i_q\right)$ computation, current i_d is maintained as constant, voltage u_q is changing in stepwise manner as presented in Fig. 1.3. Current response is shown in Fig. 1.4. Time dependent flux $\Psi_q=\Psi_q\left(t\right)$ is calculated from voltage $u_q\left(t\right)$ and current response $i_q\left(t\right)$ based on model equation in flux linkage terms:

$$u_q=R_s i_q+\frac{d\Psi_q\left(i_d,i_q\right)}{dt}. \quad (1.4)$$

$$\Psi_q\left(i_d,i_q\right)=\int_0^t\left(u_q-R_s i_q\right)dt. \quad (1.5)$$

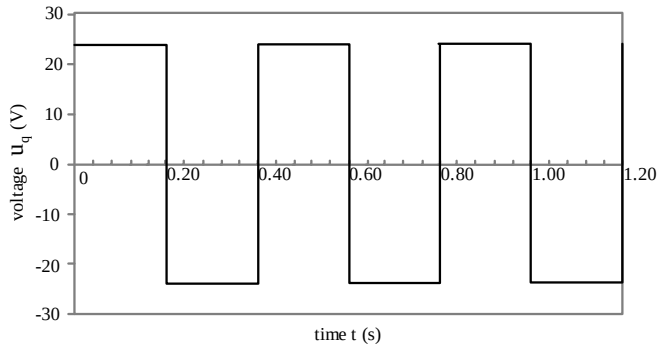

Fig. 1.3 – Stepwise voltage change u_q for standstill test [4]

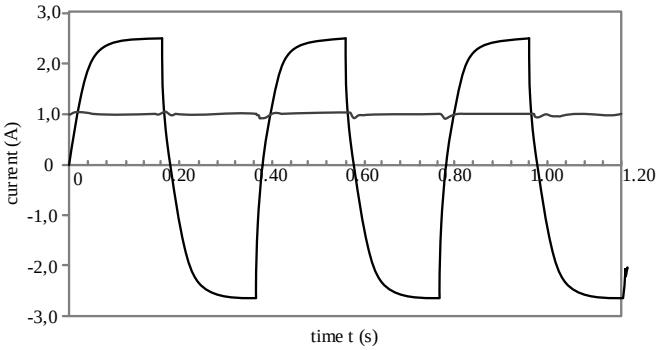

Fig. 1.4 – Currents i_d and i_q during the standstill test [4]

Time dependent flux $\Psi_q = \Psi_q(t)$ is determined for different i_d current in order to obtain flux values for each currents value. Applied voltage value is selected so that current i_q values cover all operational range of the motor. Figure for dependence $\Psi_q = \Psi_q(i_q)$ for one i_d current (in this case $i_d = 1A$) is presented in Fig. 1.5

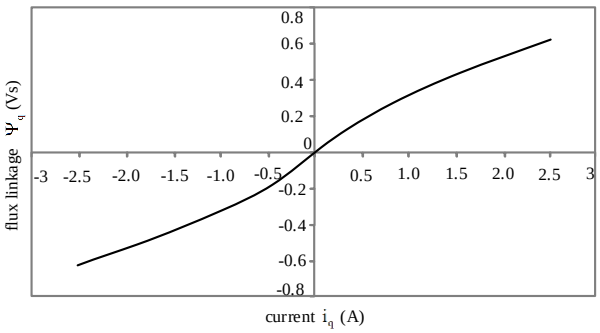

Fig. 1.5 – Characteristic $\Psi_q = f(i_d = 1, i_q)$ obtained from the test data in standstill test [4]

After that inductances $L_{qq}(i_d, i_q)$ and $L_{qd}(i_d, i_q)$ can be determined from (1.3). Similar approach is proposed for $L_{dq}(i_d, i_q)$ and $L_{dd}(i_d, i_q)$ determination. Static inductance can also be calculated from fluxes or model with fluxes (1.1) can be used instead.

In [9] stator AC voltage method is proposed. Worth mentioning that voltage is applied in stator reference frame. Cross-coupling and saturation are neglected; motor has to have access to neutral point; AC power supply is required. Initially, rotor has to be locked so that magnetic axis is aligned with phase A. Method allows determining both axes inductances after three stages test. As saturation and cross coupling are neglected, motor model (1.1) is simplified and has a form of the series RL circuit:

1. Small phase A voltage (v_{an}) is applied and the induced phase current i_a is measured. Considering that rotor is locked, steady-state voltage-current relation for PMSM is

$$v_{an} = \left(R_s + j\omega_s\left(L_{ls} + L_A + L_B\right)\right)i_a, \tag{1.6}$$

where ω_s is voltage frequency, L_{ls} is the stator leakage inductance, L_A and L_B are components of the magnetizing inductances.

2. Similarly, small AC voltage is applied to phase B for the same rotor position. After that open-circuit v_{an} voltage is applied and phase B current i_b are measured. This condition is represented as

$$v_{an} = \left(-j\omega_s \left(\frac{L_A + L_B}{2} \right) \right) i_b \tag{1.7}$$

3. After that rotor is realigned. Rotor d-axis is aligned with phase B by means of applying small DC voltage. After that rotor is locked. AC voltage is applied to phase C and open-circuit v_{an} voltage and phase C current i_c are measured. Voltage - current relation can be expressed as

$$v_{an} = \left(-j\omega_s \left(\frac{L_A - 2L_B}{2} \right) \right) i_c. \tag{1.8}$$

Considering that resistance is known, magnetizing inductances and stator leakage inductances are calculated from (1.6)-(1.8). D- and q-axis inductances are computed as

$$\begin{aligned} L_d &= L_{ls} + 3/2\left(L_A + L_B\right), \\ L_q &= L_{ls} + 3/2\left(L_A - L_B\right). \end{aligned} \tag{1.9}$$

Frequency method is presented in [10]. In the test, inverter nonlinearities are considered. Test requires inverter-controlled motor. Drawback is that Cross-coupling and saturation are neglected. Initially rotor has to be locked. Determination is based on measurements of peak values of current and voltage if small AC voltage is applied to one of the motor phases. In order to exclude nonlinearities, AC voltage with two different amplitudes is applied and two current amplitudes are measured.

In order to calculate d-axis inductance, magnetic axis of the rotor has to be aligned with phase A voltage vector. Inductance is determined as

$$L_d = \frac{1}{\omega_s}\sqrt{\left(\frac{V_{a,amp1} - V_{a,amp2}}{I_{a,amp1} - I_{a,amp2}}\right) - R_s^2}, \quad (1.10)$$

where $V_{a,amp1}, V_{a,amp2}$ - voltage amplitudes, $I_{a,amp1}\, I_{a,amp2}$ - current amplitudes

Similar situation is for q-axis inductance calculation. However magnetic axis of the rotor has to be orthogonal to applied voltage vector.

In [11] frequency method using multisinusoidal signal is presented. Test requires motor connection to the voltage source inverter (VSI). Saturation is considered during the test. In order to study influence of cross coupling, additional dc supply is needed. The paper shows the procedure of generation multisinusoidal signal for identification of the d-q axis inductances considering saturation and cross-coupling. Test signal includes first 15 harmonics based on the fundamental $\omega_0 = 2\pi 20$ rad/s. Phase displacement for each harmonic is chosen using Schroeder phases method. Proposed method allows to decrease amplitude of the output current signal comparing to the similar test with one harmonic.

Saturation effects can be evaluated when VSI is connected to phases B and C of the motor. Phase A is disconnected. Rotor d-axis is aligned with phase A voltage vector for L_q calculation, and orthogonal to phase A for L_d calculation. By controlling the average phase voltages, the dc component of the phase currents can be altered. In this way, the machine impedance can be measured for different dc values of the quadrature and direct-current components. Cross coupling can be evaluated if additional DC voltage is applied between phases A and C.

In stand-still, motor model converts to series RL circuit, and total impedance along q-axis can be determined as

$$Z_{q,i} = \frac{V_{q,i}}{I_{q,i}} = \sqrt{R_{q,i}^2 + \left(\omega_0 i L_{q,i}\right)^2}, \quad (1.11)$$

where $i = (1,2,...,15)$ - harmonic number.

Theoretically, $L_{q,i}$ and $R_{q,i}$ can be measured for each harmonic; however, resistance in this case is frequency dependent value. Therefore, it is proposed to measure resistance separately from DC test. Measurement $V_{q,i}/I_{q,i}$ is presented for each harmonic. $Z_{q,i}$ is fitted to this measurement by a variation of $L_{q,i}$. For this purpose, the least-square curve fitting method is used. Similar approach is proposed for L_d inductance calculation.

1.1.2 Constant speed methods

Overall, constant speed methods consider motor operation in steady state and calculate inductances from back EMF components. Inverter nonlinearities have less impact on these tests. PI controllers are used to track reference current values.

Constant speed steady state method without requirement of the prime mover is presented in [12]. Tested motor has to be vector-controlled. Such configuration allows to consider saturation and cross-coupling effects only partially, as inductances can be determined not for every d-q axis current. Constant motor speed is achieved for different current angles. Paper considers operation at three different speeds: 200rpm, 300rpm and 400rpm. Inductances are calculated basing on two consecutive measurements of currents and voltages for the same torque but with different d-axis current. Determination equations are following:

$$\begin{aligned} L_d\left(i_{d1},i_{q1}\right) &= \frac{\left(v_{q1}-v_{q2}\right)-R_s\left(i_{q1}-i_{q2}\right)}{\omega_s\left(i_{d1}-i_{d2}\right)}, \\ L_q\left(i_{d1},i_{q1}\right) &= \frac{-v_{d1}+R_s i_{d1}}{\omega_s i_{q1}}, \end{aligned} \tag{1.12}$$

where $\left(v_{q1},i_{q1},i_{d1}\right),\left(v_{q2},i_{q2},i_{d2}\right)$ - the first and the second current and voltage reading respectively, stator resistance is known value.

Proposed calculation (1.12) allows to exclude PM flux from determination equation.

Method [13] is similar to [12], however resistance and PM flux variation due to temperature change are considered. In this case on one measurement of currents and voltages is done for one calculation. Initial values of R_s and Ψ_M are assumed to be known. Two methods are proposed to evaluate temperature effects: where temperature of the end winding is used; where both end winding temperature and estimated temperature of the PMs obtained from a temperature distribution analysis are used. Results are compared to the data obtained from FEA. Estimated values of resistance $\hat{R}_s$ and PM flux $\hat{\Psi}_M$ for the second method are calculated as follows:

$$\begin{aligned} \hat{R}_s &= R_{s\_ambient}\left(1+\alpha_R\frac{\Delta T}{100}\right), \\ \hat{\Psi}_M &= \Psi_{M\_ambient}\left(1+\alpha_\Psi\frac{\Delta \hat{T}}{100}\right), \end{aligned} \tag{1.13}$$

where $R_{s\_ambient}$ and $\Psi_{M\_ambient}$ are values of resistance and PM flux at ambient temperature; ΔT - difference between measured end winding and ambient temperature; $\Delta\hat{T}$ denotes difference between estimated PM flux temperature and ambient temperature; α_R and α_Ψ are temperature coefficients.

Inductance estimations $\hat{L}_d(i_d,i_q)$ and $\hat{L}_q(i_d,i_q)$ are determined from (1.13) as

$$\hat{L}_d(i_d,i_q)=\frac{u_q-\hat{R}_s i_q-\omega\hat{\Psi}_M}{\omega i_d},\ \hat{L}_q(i_d,i_q)=\frac{u_d-\hat{R}_s i_d}{\omega i_q}. \tag{1.14}$$

Constant speed steady state method considering iron losses is proposed in [14]. In the method additional machine is required to maintain constant speed. Saturation along one axis is considered only. Inductance calculation is based on previously calculated PM flux and core loss resistance. If $i_q = 0A$, resistance is excluded from d - axis inductance calculation:

$$L_d(i_d)=\frac{u_q-\omega\Psi_M}{\omega i_d}. \tag{1.15}$$

Q-axis inductance is determined similarly ($i_d = 0A$):

$$L_q(i_d) = -\frac{u_d}{\omega i_q - \frac{\omega^2 \Psi_M}{R_C}}, \tag{1.16}$$

where R_C - core loss resistance.

Active resistance influence is excluded during the test in [15]. Unlike test in [14], saturation and cross-coupling are fully considered. Motor is rotated with prime mover at the constant speed. D-q axes voltage values are measured two times at steady state altering polarity of the q-axis current. Researches propose to use reference values of the voltages, so test inaccuracies associated with inverter operation. As a result, for one pair of currents, four measurement has to be done: $v_d(i_d, i_q), v_d(i_d, -i_q)$ and $v_q(i_d, i_q), v_q(i_d, -i_q)$. Inductances are determined as

$$\begin{aligned} L_d(i_d, i_q) &= \frac{v_q(i_d, i_q) + v_q(i_d, -i_q) - 2\omega\Psi_M}{2\omega i_d}, \\ L_q(i_d, i_q) &= \frac{v_d(i_d, -i_q) - v_d(i_d, i_q)}{2\omega i_q}. \end{aligned} \tag{1.17}$$

Researches in [16] propose method of calculation flux linkages from the steady-state model excluding high order harmonic influence. Saturation and cross – coupling are considered. Motor is rotated with constant speed during the test. Method requires measurement of rotor position and phase A current and voltage. Sources of harmonics are non-sinusoidal distribution of windings (5^{th}, 7^{th}, 11^{th} and 13^{th} harmonic), slotting harmonics, inverter dead time (in case if it is not compensated, sixth-harmonic component is presented in current), switching harmonics and so on. Presence of this harmonics has negative impact on accuracy of inductance determination.

Harmonics exclusion can be done in the following way. Phase A voltage can be measured directly; however, it requires high sampling rate. Since our interest is to extract fundamental component only, RC low-pass filter is proposed to use. Fast

Fourier transformation proposed to extract fundamental harmonics from current and voltage curves. When angle from position sensor is zero, current and voltage values correspond to d-axis current and voltage. When angle is 90 degrees – q-axis current and voltage.

Currents and voltages are measured for each possible combination of d-q axis currents. After that fluxes are determined as

$$\Psi_q\left(i_d,i_q\right)=\frac{-v_q+R_s i_q}{\omega},\ \Psi_d\left(i_d,i_q\right)=\frac{v_d-R_s i_d}{\omega}. \tag{1.18}$$

Self- and cross-inductances are determines from (1.3).

1.2 Inductance determination methods that does not require additional equipment

As was mentioned before, these methods can be conditionally divided into two categories: offline methods, also known as self-commissioning with free rotor, and online methods with adjustable and adaptive control algorithms. In general, motor has to be connected to voltage source inverter (VSI) for both methods Fig. 1.6.

Self-commissioning procedure is a procedure of self-identification of electrical or/and mechanical parameters. The majority of the proposed methods assume that inductances are constants that leads to accuracy deterioration. Existing methods propose to use observers. Mainly observer design is based on Lyapunov second method, recursive least square (RLS) method, affine projection method, sliding mode or can be compiled manually. In case of adaptive algorithms, stability analysis has to be provided.

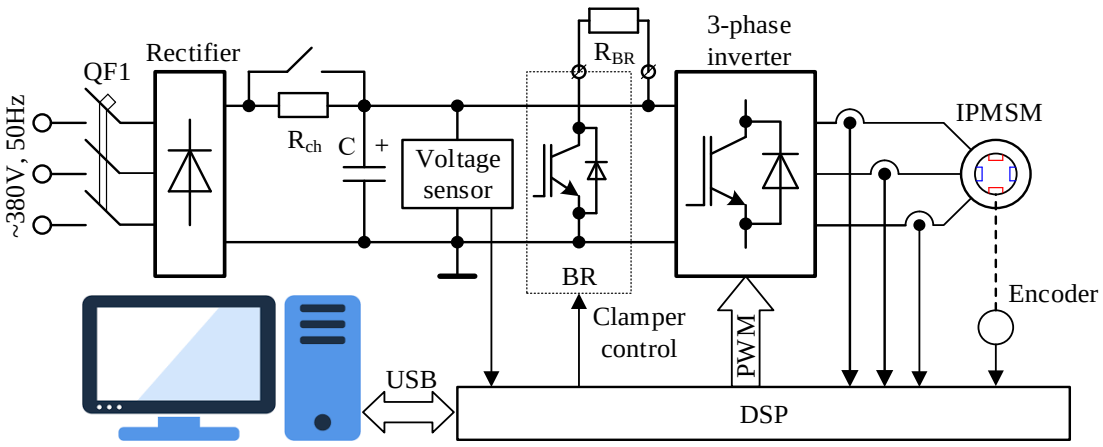

Fig. 1.6 – General functional diagram of the experimental setup for online and offline methods implementation

1.2.1 Offline identification methods

Self-commissioning procedure using high frequency signal injection is proposed in [18]. As reference signal frequency is comparatively high, motor remains motionless during the test. Drawback is that inductances are considered as constant parameters. High frequency voltage is injected along d- and q-axis of the motor. Considering that speed $\omega = 0$, flux, caused by currents, can be found as

$$\Psi_s = \frac{s}{s^2 + K_p s + K_i}\left(u_s - R_s i_s\right), \tag{1.19}$$

where u_s - stator voltage vector; $i_s = \left(i_d, i_q\right)$ - stator current vector; $s = d/dt$; $\Psi_s = \left(\Psi_d, \Psi_q\right)$ - current caused flux linkage vector, K_p, K_i - proportional and integral gain.

Bandpass filter is used in order to exclude flux caused by PMs from calculation and to reduce signal noises. Inductances are determined as follows:

$$\begin{aligned} L_d &= L_{d0} + K_{Ld}\frac{1}{s}\left(\left|\Psi_d\right| - \left|L_d i_d\right|\right), \\ L_q &= L_{q0} + K_{Lq}\frac{1}{s}\left(\left|\Psi_q\right| - \left|L_q i_q\right|\right), \end{aligned} \tag{1.20}$$

where $K_{Ld} = K_{Lq} > 0$ - inductance estimation gains; L_{d0}, L_{q0} - initial best estimations.

During the test, following voltage is applied:

$$u_s = u_{s\alpha} + j u_{s\beta} = u_{dc} + U_h \cos 2\pi f_s t + j U_h \sin 2\pi f_s t. \tag{1.21}$$

Voltage DC component u_{dc} is utilized to align d-axis with α -axis of the stator reference frame. Authors propose to inject voltage with amplitude $U_h = 20\text{V}$ and frequency $f_s = 400\text{Hz}$. Proposed test can be run for different values of the DC component in order to evaluate cross coupling effects between d- and q-axis.

Frequency method where inverter nonlinearities are considered is proposed in [19] and [20]. Method requires fully controlled electric drive. Saturation and cross-coupling are neglected during the test. The idea of the method lies in compensation and exclusion of inverter nonlinearities during the test. Inductance is determined using frequency method:

$$\hat{L}_x = \frac{U_{inj}}{I_{xh}\omega_s}, \tag{1.22}$$

where U_{inj} - amplitude of the injected voltage; I_{xh} - amplitude of induced HF current. $\hat{L}_x$ - estimated value of inductance along one of the rotor reference frame axes.

If high frequency (HF) voltage signal is injected using fully controlled inverter, effect of nonlinearities will be considerable and as a result determined inductance value will not be accurate. In the paper, voltage error caused by inverter nonlinearities is presented in the following form:

$$\Delta u_{err-x} = \text{sign}\left(i_{fx}\right)\Delta U + R_{xh} i_{xh}, \tag{1.23}$$

where i_{xh} denotes fundamental current of arbitrary phase x; ΔU - saturated voltage error in Region II (Fig. 1.7); R_{xh} - high frequency equivalent resistance.

Transient of phase voltage error and HF equivalent resistance as functions of phase current are presented in Fig. 1.7.

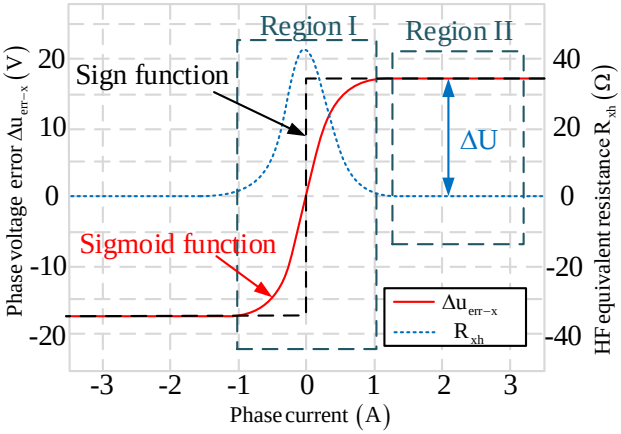

Fig. 1.7 – Phase voltage error and the HF equivalent resistance that represents inverter nonlinearities for offline identification test [20]

D-axis inductance determination: The first term from (1.23) can be excluded if constant DC component is implemented into d-axis current. It allows pulling stator current out of the zero-current clamping (ZCC) zone. Moreover, injection of DC current component allows reducing R_{xh} drastically. Fig. 1.8 shows that value of the HF resistance depends on rotor position. If the DC component of an arbitrary phase current turns to zero, HF current component is also zero, and therefore there will be no errors caused by inverter for these positions. Estimated valued of d-axis inductance $\hat{L}_d$ is presented in Fig. 1.9(a). Error decays to zero at $\theta_r = (2k+1)\pi/6$, $k \in \{0,1,2,3,4,5\}$. As a result, it is possible to obtain accurate value of the d-axis inductance using proposed method for particular rotor positions without any compensations.

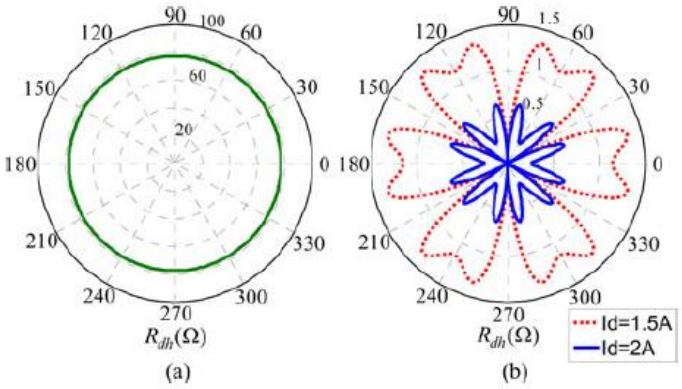

Fig. 1.8 – HF equivalent resistance R_{dh} in polar coordinate with an electrical cycle for offline identification test (a) DC current component $I_d = 0$ A; (b) $I_d = 1.5$ and 2.5 A [20]

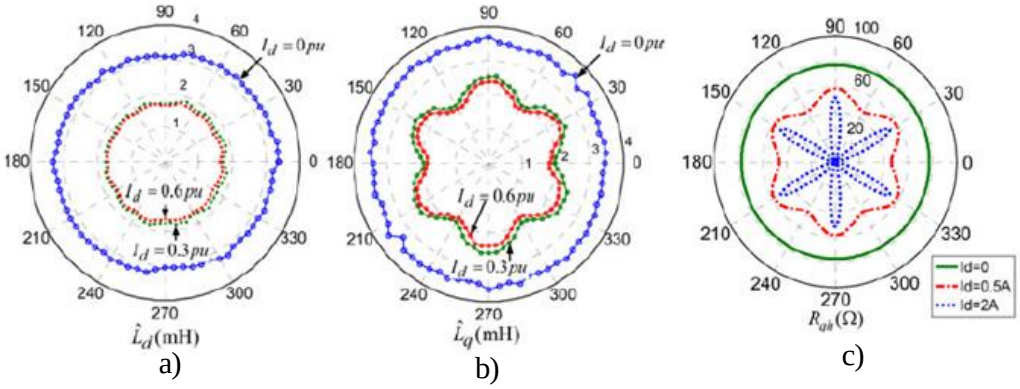

Fig. 1.9 – Estimated d-q axis inductances in an electric cycle for offline identification test [20]

Q-axis inductance determination: Procedure is the same, however injection of DC current component has less influence on q-axis HF resistance Fig. 1.9c. Moreover, point of the least R_{qh} corresponds to points where DC component of the arbitrary phase is the highest. Therefore, at least value of ΔU has to be known for accurate q-axis inductance determination. Estimated values of q-axis inductance are presented in Fig. 1.9(b).

Flux determination method with estimation error compensation is proposed in [21]. In the paper inverter nonlinearities and saturation effects are considered, rotor movement during identification procedure is taken into account.

Flux linkage are determined from model in flux linkage terms (1.5), and voltage error caused by inverter nonlinearities is considered:

$$\Psi_{dq}\left(i_d, i_q\right) = \int_0^t \left(u_{dq} - R_s i_{dq} - u_{dq\,err}\left(i_{dq}\right)\right) dt, \tag{1.24}$$

where $u_{dq\,err}\left(i_{dq}\right)$ - voltage error caused by inverter nonlinearities.

Inverter nonlinearities are considered in the same way is proposed in [19], [20]. In the paper, error is determined in the following way. In Fig. 1.10 procedure of stator resistance determination is presented. Series of current and voltage measurements is done to compute resistance R_{dn}, where $n = 0..5$, which is gradient of voltage line. It is seen that u_d curve is highly nonlinear. Resistance $R_{d5} \approx R_s$, as inverter nonlinearities can be neglected at high current level. Voltage u_d is proposed to interpolate by Hermite polynomial. After that voltage error is determined is follows:

$$u_{derr} = \begin{cases} R_{d0} i_d - R_{d5} i_d, \; 0 \le i_d < i_{d0} \\ U_{hermite}\left(i_d\right) - R_{d5} i_d, \; i_{d0} \le i_d < i_{d5} \\ u_{d5} - R_{d5} i_d, \; i_{d5} \le i_d \end{cases}. \tag{1.25}$$

Voltage error along q-axis as determined by means of inverse and direct Park transformation.

Fluxes are determined for each of (d-q) current combination. In order to do that hysteresis control is proposed:

$$u_{dq\,ref}(k)=\begin{cases} U_{dq\,out}, & \text{if } i_{dq}(k)<-I_{dq\,set} \\ -U_{dq\,out}, & \text{if } i_{dq}(k)>I_{dq\,set} \\ u_{k\,ref}(k-1), & \text{otherwise} \end{cases}, \tag{1.26}$$

where $U_{dq\,out}$ is the amplitude of injected voltage; $I_{dq\,set}$ is the value of current setting which controls the magnitude of injection current.

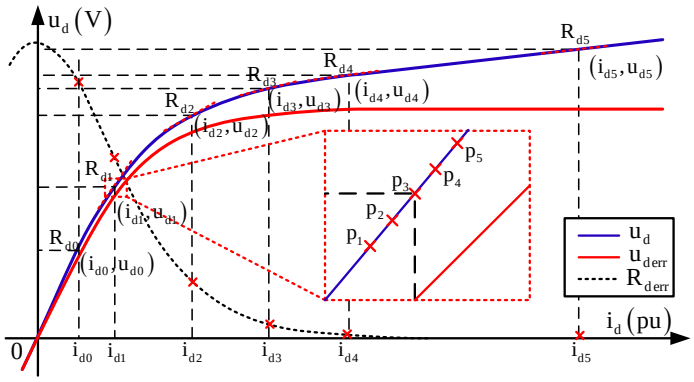

Fig. 1.10 – d-axis voltage error characteristic of the inverter nonlinearities [21]

Researches propose procedure of self-commissioning with included program for variation of $U_{dq\,out}$ and $I_{dq\,set}$ values to achieve better accuracy and estimation time of flux linkages for every current value. Moreover, rotor motion is considered during the test and rotation angle is included into voltage calculation to increase accuracy of determination. Also, time-delay effect is considered and correction method is proposed. Inductances are determined from fluxes basing on (1.3).

Low frequency injection method is proposed in [22]. Method is not influenced by stator resistance variation; cross-saturation and saturation are considered. Unlike, standard HF voltage injection method, it is proposed to decrease frequency of the injected voltage to the nominal operating frequency in order to reduce hysteresis effects. As the goal is to determine inductance values for different (d-q) currents, DC bias is included into injected voltage to provide different average current values.

Incremental inductance is proposed to compute from AC values of injected voltage v_{ac} and output current i_{ac} as follows:

$$\Delta L = \frac{Z \sin \varphi}{\omega_{ac}}, \tag{1.27}$$

where $Z = v_{ac}/i_{ac}$ - machine impedance; ω_{ac} - frequency of the applied voltage; φ - phase angle between the resultant stator terminal voltage and current.

Quadrature axis component of the current creates torque. In order to maintain motor speed close to zero, test has to be modified. It is proposed to vary DC bias of the applied voltage so that average current value has near zero value. Frequency of the DC bias curve is selected in a such way that torque oscillations are filtered by the machine mechanical properties.

Flux linkages along d-q axes can be determined from incremental inductance in the following way:

$$\Psi_{dq}(k) = \Psi_{dq}(k-1) + \Delta L_{dq}(k) \Delta i_{dq}(k), \tag{1.28}$$

where k – sampling index; Δi_{dq} - current change between two consecutive DC bias.

In the paper comparison of computed flux linkages with locked rotor and without locked is made. According to the received results rotor condition does not influence on the results. Moreover, results are not affected by stator resistance value as well as inverter nonlinearities as inductance value is determined basing on phase shift.

In the papers [23] and [25], procedure for determination of electrical parameters is presented. Stability is proved using the second Lyapunov method. Drawbacks are following: inductances are considered as constants and inverter nonlinearities are considered as constants.

Resistance and inductances are determined at the first stage of the self-commissioning procedure. Observer is based on non-saturated model of the IPMSM. D-axis current dynamics equation can be written as

$$\dot{i}_d = -\varphi_1 i_d + \varphi_2 \omega p_n i_q + u_d/\varphi_3, \tag{1.29}$$

where $\varphi_1 = R/L_d, \varphi_2 = L_q/L_d, \varphi_3 = L_d$ - constant parameters.

Adaptive d-axis current controller is constructed as

$$u_d = \hat{\varphi}_3\left(\hat{\varphi}_1 i_d^* - p_n \omega \hat{\varphi}_2 i_q + \dot{i}_d^* - k_{id}\tilde{i}_d\right), \tag{1.30}$$

where $\hat{\varphi}_1$, $\hat{\varphi}_2$, $\hat{\varphi}_3$ - parameter estimates, i_d^* - d-axis current reference value, $\tilde{i}_d = i_d - i_d^*$ - d-axis current error, $k_{id} > 0$ - proportional gain of the d-axis current controller.

After that, current error dynamics is derived by substitution (1.30) into (1.29). Following Lyapunov function is chosen:

$$V = \frac{1}{2}\left(\tilde{i}_d^2 + \frac{1}{\lambda_1}\tilde{\varphi}_1^2 + \frac{1}{\lambda_2}\tilde{\varphi}_2^2 + \frac{1}{\lambda_3\varphi_3}\tilde{\varphi}_3^2\right). \tag{1.31}$$

where $\tilde{\varphi}_k = \varphi_k - \hat{\varphi}_k$, $k=\{1,2,3\}$ - parameters estimation error.

Derivative of the Lyapunov function is

$$\dot{V} = -k_{iid}\tilde{i}_d^2, \tag{1.32}$$

if parameters estimation derivatives are chosen as

$$\begin{aligned} \dot{\hat{\varphi}}_1 &= -\dot{\tilde{\varphi}}_1 = -\lambda_1 i_d^* \tilde{i}_d, \\ \dot{\hat{\varphi}}_2 &= -\dot{\tilde{\varphi}}_2 = \lambda_2 p_n \omega i_q \tilde{i}_d, \\ \dot{\hat{\varphi}}_3 &= -\dot{\tilde{\varphi}}_3 = -\lambda_3 \xi_d \tilde{i}_d, \end{aligned} \tag{1.33}$$

where λ_1, λ_2, λ_3 - estimation gains.

Reference values of current and voltage are $i_d^* = 2\sin(50t)$, $u_q = 10\sin(50t)$.

1.2.2 Online identification methods

Online identification methods allow to estimate inductances during operation and simultaneously modify algorithm with its new values to avoid performance deterioration due to parameter mismatch. Back - EMF based method is presented in [26]. Disadvantage is that it can be used only in steady state at nonzero speed. Inductances are determined from the model in steady state.

Estimation scheme for d-axis inductance determination $\hat{L}_q$ is presented in Fig. 1.11. Idea of determination d-axis inductance $\hat{L}_d$ is the same.

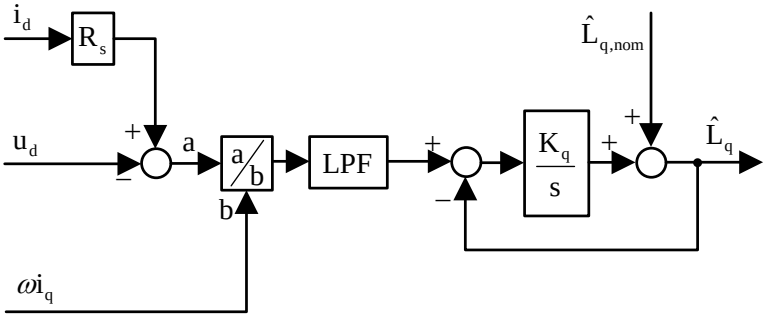

Fig. 1.11 – On-line IPM machine parameter estimation [26]

Low-pass filter (LPF) is used to filter unwanted high frequency components. Nominal values of inductances $\hat{L}_{q,nom}$ and $\hat{L}_{d,nom}$ feedforward compensation improves parameter estimation during transients. K_q -integral coefficient. The same approach is used in [27], however LPF is excluded from the scheme.

Current observer-based method for d-axis inductance estimation is presented in [28]. Similarly to [26] and [27] proposed method can be used only in steady state at nonzero speed. Also, it requires knowledge of all other motor parameters and current i_d does not have to be zero.

Quadrature axis equation of the non-saturated motor model is utilized for d-axis inductance determination. Estimation scheme is presented in Fig. 1.12.

Adaptive mechanism from Fig. 1.12 is I-controller. Input of the controller is current error $e_i = i_d - \hat{i}_d$, where i_d - current measured in the real system, $\hat{i}_d$ - estimated current value, K_i - adaptive gain.

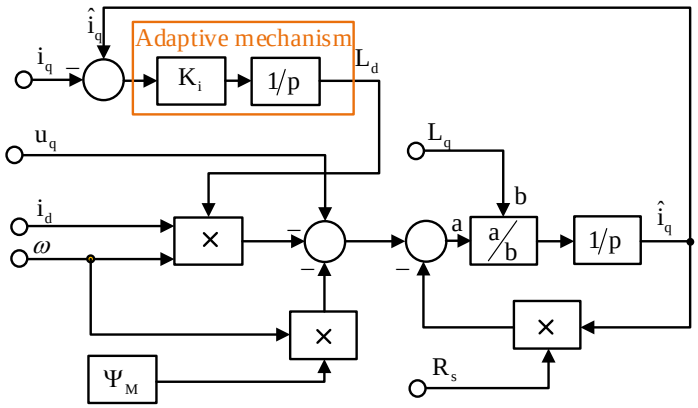

Fig. 1.12 – Structural scheme for L_d identification for online identification test [28]

The papers [29] and [30] present two methods for inductance estimation. Stability analysis and convergence behavior analysis are presented. In the first Section, analysis of identifiability of the motor parameters basing on Jacobian submatrix presented. Adaptive regulators are the same for both methods and have the following form:

$$\begin{aligned}
\hat{R}_s(t) &= \hat{R}_s(t_0) - \int_{t_0}^{t} K_R \tilde{i}_q(\tau)\,d\tau, \\
\hat{L}_q(t) &= \hat{L}_q(t_0) - \int_{t_0}^{t} K_{Lq} \tilde{i}_d(\tau)\,d\tau, \\
\hat{L}_d(t) &= \hat{L}_d(t_0) - \int_{t_0}^{t} K_{Ld} \tilde{i}_q(\tau)\,d\tau,
\end{aligned} \tag{1.34}$$

where $\hat{R}_s(t_0)$, $\hat{L}_q(t_0)$, $\hat{L}_d(t_0)$ - initial guesses of resistance and inductances; K_R, K_{Lq}, K_{Ld} - estimation gains.

The first method called “Model reference output cancellation method”. Functional diagram of the method is presented in Fig. 1.13. Current $i_s = \left[i_d, i_q \right]$, i_r and u_r are reference values of current and voltage, θ^* - reference value for the rotor position. System convergence is achieved for the next coefficients:

$$\begin{aligned}
K_R &= -K_{R0} \cdot \operatorname{sign}(i_q), \\
K_{Ld} &= K_{Ld0} \cdot \operatorname{sign}(\omega i_d), \\
K_{Lq} &= K_{Lq0} \cdot \operatorname{sign}(\omega i_q),
\end{aligned} \tag{1.35}$$

where K_{R0}, K_{Lq0}, K_{Ld0} - positive estimation gains.

Drawbacks of the method is that the convergence of the estimation is coupled. It means that even if initial guess of one of the parameters is correct, it becomes erroneous if initial guess of the other parameters is wrong.

The second method is called “Model-reference online identification using decoupling control”. It allows to exclude above mentioned drawback so that

convergence of each of the parameter estimation is decoupled. Functional diagram is shown in Fig. 1.14.

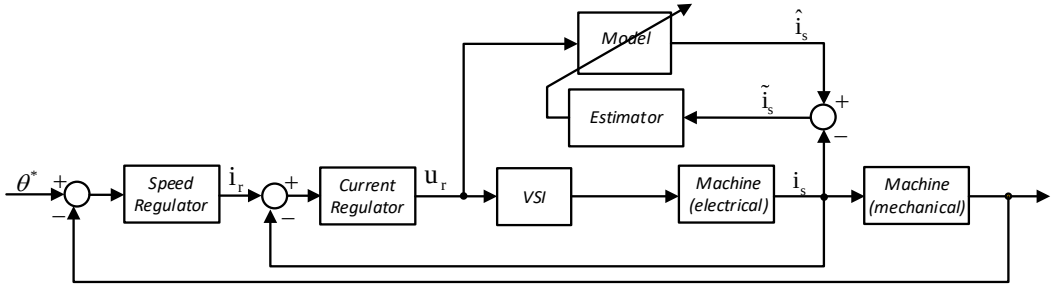

Fig. 1.13 – Functional diagram of the first MRAC method [29]

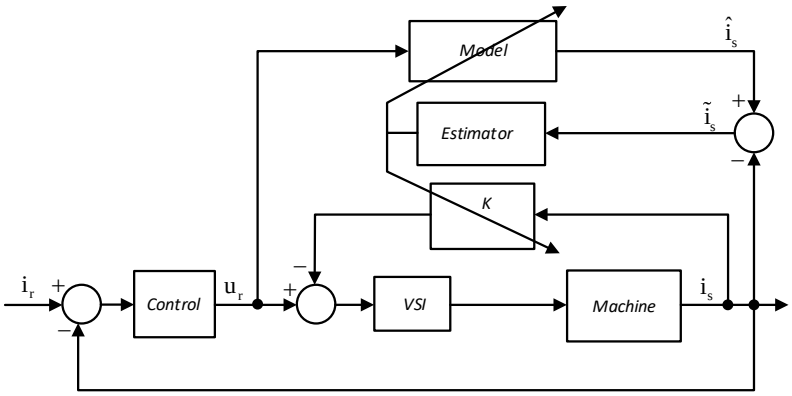

Fig. 1.14 – Functional diagram of the second MRAC method [29]

Decoupling control is provided with addition of decoupling block K to the control system. In this case motor model is simplified. Decoupling block and model are presented below:

$$\mathrm{K} = \frac{1}{\omega}\begin{bmatrix} 0 & \hat{\mathrm{L}}_\mathrm{q} \\ -\hat{\mathrm{L}}_\mathrm{d} & 0 \end{bmatrix},$$

$$\hat{\mathrm{L}}_\mathrm{d}\frac{\mathrm{di_d}}{\mathrm{dt}} = -\hat{\mathrm{R}}_\mathrm{s}\mathrm{i_d} + \mathrm{u_{dr}}, \qquad (1.36)$$

$$\hat{\mathrm{L}}_\mathrm{q}\frac{\mathrm{di_q}}{\mathrm{dt}} = -\hat{\mathrm{R}}_\mathrm{s}\mathrm{i_q} - \omega\Psi_\mathrm{M} + \mathrm{u_{qr}}.$$

Both methods are experimentally verified considering flux variation. The second one shows better performance.

Adaptive control algorithm [31] is designed using Lyapunov method. Inductances are estimated from both mechanical and electrical equations. Design

procedure is similar to proposed in [23] and [25], however voltage references are composed after Lyapunov function derivative is obtained. Such approach allows to deal with inductance components that are not from current equations only. At the first step, positive Lyapunov function is selected. Adaptive laws and voltage references are derived in a such way that Lyapunov function derivative becomes less that zero.

High frequency signal wave voltage injection method is proposed in [32]. Researches propose to inject HF square wave voltage $\left[\mathrm{u}_{\alpha\mathrm{h}},\mathrm{u}_{\beta\mathrm{h}}\right]$ in the stator coordinate system $(\alpha-\beta)$. Injected voltages forms are shown in Fig. 1.15.

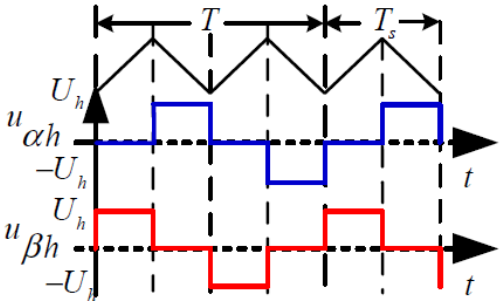

Fig. 1.15 – Injected voltages form for online identification test [32]

Where $\mathrm{T_s}$ is carried period, T - HF voltage signal period. From Fig. 1.15, it is clear that voltage has four different values per one period. For the future analysis each of this value has certain index $\mathrm{x}=\left[1\quad 2\quad 3\quad 4\right]$. The paper proposes to calculate the following variables:

$$\begin{bmatrix}\mathrm{I}_{\Delta\mathrm{Ls}}\\ \mathrm{I}_{\Delta\mathrm{Lc}}\\ \mathrm{I}_{\Sigma\mathrm{L}}\end{bmatrix}=\begin{cases}\left[-\mathrm{i}_{\alpha\mathrm{h1}}+\mathrm{i}_{\beta\mathrm{h4}},\mathrm{i}_{\beta\mathrm{h1}}+\mathrm{i}_{\alpha\mathrm{h4}},-\mathrm{i}_{\alpha\mathrm{h4}}+\mathrm{i}_{\beta\mathrm{h1}}\right]^{\mathrm{T}},\mathrm{x}=1\\ \left[-\mathrm{i}_{\alpha\mathrm{h2}}-\mathrm{i}_{\beta\mathrm{h1}},-\mathrm{i}_{\alpha\mathrm{h2}}+\mathrm{i}_{\beta\mathrm{h1}},\mathrm{i}_{\alpha\mathrm{h2}}+\mathrm{i}_{\beta\mathrm{h1}}\right]^{\mathrm{T}},\mathrm{x}=2\\ \left[\mathrm{i}_{\alpha\mathrm{h3}}-\mathrm{i}_{\beta\mathrm{h2}},-\mathrm{i}_{\beta\mathrm{h3}}-\mathrm{i}_{\alpha\mathrm{h2}},-\mathrm{i}_{\beta\mathrm{h3}}+\mathrm{i}_{\alpha\mathrm{h2}}\right]^{\mathrm{T}},\mathrm{x}=3\\ \left[\mathrm{i}_{\alpha\mathrm{h3}}+\mathrm{i}_{\beta\mathrm{h4}},\mathrm{i}_{\beta\mathrm{h4}}+\mathrm{i}_{\alpha\mathrm{h1}},-\mathrm{i}_{\beta\mathrm{h4}}-\mathrm{i}_{\alpha\mathrm{h3}}\right]^{\mathrm{T}},\mathrm{x}=4\end{cases},\tag{1.37}$$

where $\mathrm{i}_{\alpha\mathrm{hx}}$ and $\mathrm{i}_{\beta\mathrm{hx}}$ - are current caused by HF voltages at the different sampling points.

Direct and quadrature inductances are calculated from the variables in (1.37) as

$$L_d = \frac{TU_h}{I_{\Sigma L} - \sqrt{I_{\Delta Ls}^2 + I_{\Delta Lc}^2}},$$
$$L_q = \frac{TU_h}{I_{\Sigma L} + \sqrt{I_{\Delta Ls}^2 + I_{\Delta Lc}^2}}. \quad (1.38)$$

Proposed method is tested by means of simulation and experimentally. Identification is completed within 70ms, error is approximately 3%.

Recursive least squares (RLS) method with simultaneous identification of all electrical parameters is presented in [33]. Researches propose to determine inductances, resistance and PM flux simultaneously from two equations. RLS algorithm is following:

$$\begin{aligned} &Y(k) = \Theta(k) Z(k), \\ &\hat{\Theta}(k) = \hat{\Theta}(k-1) + K(k)\left\{Y(k) - Z^T(k)\hat{\Theta}(k-1)\right\}, \\ &K(k) = P(k-1)Z(k)\left\{\lambda I + Z^T(k)P(k-1)Z(k)\right\}^{-1}, \\ &P(k) = \frac{1}{\lambda}\left\{I - K(k)Z^T(k)\right\}P(k-1), \end{aligned} \quad (1.39)$$

where Y is output vector, Θ is parameter vector, Z is input vector, $\hat{\Theta}$ is estimated parameter vector, P is covariance matrix, λ is a positive forgetting factor which is chosen in range of 0.97 to 0.995.

Inductances are determined from d-axis equation. In this case parameters for (1.39) are

$$\begin{aligned} &Y_d(k) = u_d(k-1) - R_S(k-1)i_d(k-1), \\ &\Theta_d(k) = \begin{bmatrix} L_d(k) & L_q(k) \end{bmatrix}, \\ &Z_d(k) = \begin{bmatrix} \frac{i_d(k) - i_d(k-1)}{T_s} \\ -\omega(k) i_q(k-1) \end{bmatrix}. \end{aligned} \quad (1.40)$$

Resistance and PM flux determination is made in a similar way from the q-axis equation

$$\begin{aligned} &Y_d(k) = u_d(k-1) - \omega(k) L_d(k-1) i_d(k-1) - L_q(k-1) \frac{i_q(k) - i_q(k-1)}{T_s}, \\ &\Theta_d(k) = \begin{bmatrix} R_S(k) & \Psi_M(k) \end{bmatrix}, \; Z_d(k) = \begin{bmatrix} i_q(k-1) \\ \omega(k) \end{bmatrix}. \end{aligned} \tag{1.41}$$

It worth mentioning that both algorithms (1.39), (1.40) and (1.39), (1.41) are operating at the same time. In (1.40), resistance value from the previous iteration of (1.41) is used. In a similar way inductances from the previous step are utilized in (1.41)

The drawback of the method is that in the algorithms current derivative are calculated directly. It will cause a lot of errors if inverter is used and value of the error will depend on sample time.

In [34] RLS method with determination of the voltage drop on switches is presented. Relation between output voltages of the inverter (u_a, u_b, u_c) and reference $(u_{a\_ref}, u_{b\_ref}, u_{c\_ref})$ considering voltage drop on switches is following

$$\begin{aligned} u_a &= u_{a\_ref} - \Delta V \cdot \mathrm{sgn}(i_a), \\ u_a &= u_{a\_ref} - \Delta V \cdot \mathrm{sgn}(i_b), \\ u_a &= u_{a\_ref} - \Delta V \cdot \mathrm{sgn}(i_c), \end{aligned} \tag{1.42}$$

where ΔV - voltage error due to deadtime of the inverter and switches voltage drop.

In rotor reference frame model, (d-q) axis voltages are modified with components $\Delta V \cdot D_d$ and $\Delta V \cdot D_q$ respectively. Variables D_d, D_q are calculated using park transformation from sign functions of the stator currents. RLS algorithm the same as in (1.39) is proposed.

The first step of the identification is standstill test. Resistance R_S and voltage error ΔV are calculated from the d-axis equation at standstill:

$$\begin{aligned} &Y(k) = u_{d\_ref}(k), \\ &Z(k) = \begin{bmatrix} i_d(k) & D_d(k) \end{bmatrix}^T, \\ &\hat{\Theta}(k) = \begin{bmatrix} \hat{R}(k) & \Delta\hat{V}(k) \end{bmatrix}^T. \end{aligned} \tag{1.43}$$

After that inductances are determined from (1.39) and (1.40).

In the paper [35], RLS method with two algorithms with different time rate is proposed. It allows reducing controller computation efforts during operation. Resistance R_S and PM flux are mainly constants and are changing depending on temperature. Therefore, their dynamics is quite slow. In case of inductances, iron core saturation directly influences on inductance values. Fast RLS is utilized to estimate inductances and it runs at sampling rate. Resistance and PM flux are estimated in a separate program - slow RLC - and runs at lower frequency. RLS algorithm the same as in (1.39) is proposed.

Faster algorithm has the simpler structure and assumes that stator resistance and PM flux are constant during at the sampling period. RLS algorithm parameters are following:

$$\begin{aligned} Y(k) &= \begin{bmatrix} v_q(k) - R_S i_q(k) - \Psi_M \omega(k) \\ v_d(k) - R_S i_d(k) \end{bmatrix}, \\ Z^T(k) &= \begin{bmatrix} 0 & \omega(k) i_d(k) \\ -\omega(k) i_q(k) & 0 \end{bmatrix}, \\ \hat{\Theta}(k) &= \begin{bmatrix} L_q(k) & L_d(k) \end{bmatrix}^T. \end{aligned} \tag{1.44}$$

Slow RLS algorithm parameters are presented below.

$$\begin{aligned} Y(k) &= \begin{bmatrix} v_q(k) \\ v_d(k) \end{bmatrix}, \\ Z^T(k) &= \begin{bmatrix} 0 & i_d(k)\omega(k) & i_q(k) & \omega(k) \\ -\omega(k) i_q & 0 & i_d(k) & 0 \end{bmatrix}, \\ \hat{\Theta}(k) &= \begin{bmatrix} L_q(k) & L_d(k) & R_S(k) & \Psi_M(k) \end{bmatrix}^T. \end{aligned} \tag{1.45}$$

Problem of persistency of excitation with slower algorithm can be solved by means of providing small perturbations to the d-axis of the machine. Size of the perturbations has to be small enough in order not to cause torque ripple and large enough to provide proper operation of the algorithm (1.45).

Researches in [36] propose affine projection method with two algorithms with fast and slow convergence. Algorithm structure is similar to proposed in [35]: Algorithm with slow convergence is utilized for load torque, resistance and flux PM estimation. Algorithm with fast convergence allows to estimate inductances. Affine projection method has the following structure:

$$\begin{aligned} &\mathrm{Y}(\mathrm{k}) = \mathrm{Z}^{\mathrm{T}}(\mathrm{k})\Theta(\mathrm{k}), \\ &\hat{\Theta}(\mathrm{k}) = \hat{\Theta}(\mathrm{k}-1) + \gamma \mathrm{Z}(\mathrm{k}) \frac{\mathrm{Y}(\mathrm{k}) - \mathrm{Z}^{\mathrm{T}}(\mathrm{k})\hat{\Theta}(\mathrm{k}-1)}{\lambda \mathrm{I} + \mathrm{Z}^{\mathrm{T}}(\mathrm{k})\mathrm{Z}(\mathrm{k})}. \end{aligned} \tag{1.46}$$

From (1.46) it is clear that affine projection algorithm has simpler structure comparing to RLS algorithm. Fast convergence algorithm parameters for inductance estimation are determined from current dynamics equation. Current derivatives are calculated as difference between adjacent currents measurements. Low convergence RLS algorithm parameters for resistance, load torque and PM flux estimation are determined from speed and currents dynamics equations.

In the paper experimental comparison of conventional RLS method and proposed method is presented. Results show better performance of the affine projection method (faster response, more accurate estimation, better robustness to load torque variation, etc.).

Extended Kalman filter proposed in [37] can be implemented if common IPMSM model is transformed to the following structure

$$\begin{aligned} &\dot{\mathbf{x}}(\mathrm{t}) = \mathbf{f}\left(\mathbf{x}(\mathrm{t})\right) + \mathbf{G}\mathbf{u}(\mathrm{t}) + \sigma(\mathrm{t}), \\ &\mathbf{y}(\mathrm{t}) = \mathbf{H}\mathbf{x}(\mathrm{t}) + \mu(\mathrm{t}), \end{aligned} \tag{1.47}$$

where $\mathbf{u} = \left[\mathrm{u_d}, \mathrm{u_q}\right]^{\mathrm{T}}, \mathbf{y} = \left[\mathrm{i_d}, \mathrm{i_q}\right]^{\mathrm{T}}$ are input and output vectors, $\mathbf{x} = \left[\mathrm{i_d}\, \mathrm{i_q}\, \mathrm{a}\, \mathrm{b}\right]^{\mathrm{T}}$ - system state vector $\left(\mathrm{a} = 1/\mathrm{L_d}, \mathrm{a} = 1/\mathrm{L_q}\right)$, $\sigma(\mathrm{t})$ - system noise that includes model inaccuracies and $\mu(\mathrm{t})$ - measurement noises.

$$\mathbf{f}\left(\mathbf{x}(t)\right)=\begin{bmatrix} a\left(-R_s i_d\right)+a\omega_r i_q/b \\ b\left(-R_s i_q-\omega_r \Psi_M\right)-b\omega_r i_d/a \\ 0 \\ 0 \end{bmatrix},\mathbf{G}=\begin{bmatrix} a & 0 \\ 0 & b \\ 0 & 0 \\ 0 & 0 \end{bmatrix},\mathbf{H}=\begin{bmatrix} 1 & 0 & 0 & 0 \\ 0 & 1 & 0 & 0 \end{bmatrix}. \quad (1.48)$$

Filter consists of two steps called the prediction step and innovation step. The first step performs prediction of state vector value and covariance matrix basing on previous estimates and mean voltage in the period between t_{k-1} and t_k. The next step corrects value of covariance matrix.

1) Prediction step

$$\begin{aligned} \hat{\mathbf{x}}_{k|k-1} &= \hat{\mathbf{x}}_{k-1|k-1}+\left[\mathbf{f}\left(\hat{\mathbf{x}}_{k-1|k-1}\right)+\mathbf{G}v_{k-1}\right]T_s, \\ \mathbf{P}_{k|k-1} &= \mathbf{P}_{k-1|k-1}+\left(\mathbf{F}_{k-1}\mathbf{P}_{k-1|k-1}+\mathbf{P}_{k-1|k-1}\mathbf{F}_{k-1}^{T}\right)T_s+\mathbf{Q}. \end{aligned} \quad (1.49)$$

2) Innovation step

$$\begin{aligned} \hat{\mathbf{x}}_{k|k} &= \hat{\mathbf{x}}_{k|k-1}+\mathbf{K}_k\left(\mathbf{y}_k-\mathbf{H}\hat{\mathbf{x}}_{k|k-1}\right), \\ \mathbf{P}_{k|k} &= \mathbf{P}_{k|k-1}-\mathbf{K}_k\mathbf{H}\mathbf{P}_{k|k-1}. \end{aligned} \quad (1.50)$$

3) Kalman gain

$$\mathbf{K}_k=\mathbf{P}_{k|k-1}H^{T}\left(H\mathbf{P}_{k|k-1}+\mathbf{R}\right)^{-1}. \quad (1.51)$$

Parameters **Q** and **R** are chosen with trial-and-error procedure to get the best tradeoff between filter stability and convergence time. In the paper, filter is tested by means of simulation and experiment.

1.3 Finite element method for inductance determination

All modern machines are designed with FEA method [38]. Currently two types of the FEA models existed: radial flux geometries can be describes using 2D FEA models with a decent level of accuracy; 3D FEA models require much more computational efforts, but allow to achieve more precise description of magnetic processes in the motor. Current supply is simulated and flux is evaluated by means of

integration of the vector magnetic potential [39]. Inductances are evaluated from fluxes to obtain motor models with the different level of simplification (see Section 2) [40], [41].

1.4 Mechanical parameters identification methods

Importance of accurate mechanical parameters estimation cannot be emphasized for precise speed and position control especially in robotics, high efficiency/speed applications. Existing papers are focused on moment of inertia, different types of friction and load torque identification.

Most of the researches are focused on the moment of inertia identification. Moment of inertia is estimated using Unscented Kalman Filer in [42]. Paper also compares proposed method with estimation using conventional Extended Kalman filter. In [43] position is changing sinusoidally. The idea of the test is to multiply torque reference by position and take its average value during one position reference sine period. Moment of inertia is calculated basing on this average value and amplitude of the position reference sine. In [44] moment of inertia estimation method is based on full-order state observer. Method also allows to estimate disturbance torque. Sinusoidal quadrature current component reference is applied in [45]. Speed form is also sinusoidal if load torque equals to zero. Speed derivative can be found analytically. Moment of inertia is determined from the mechanical equation in the moment of time when speed equals to zero.

Some articles consider simultaneous estimation of the mechanical parameters as all of them are presented in one equation and erroneous value of one of them can have negative impact on the accuracy of designation of the others.

In [46], it is proposed to determine viscous friction, moment of inertia and load toque. The main idea is to differentiate both sides of the mechanical equation of the model and after that multiply it by speed derivative. Speed derivative is calculated directly from the speed value with implementation of lowpass filter to avoid amplifying system noises. Each of parameters determination is based on neglection of obtained equation components if special test is conducted.

In [47] another approach is proposed. Disturbance torque, caused by torque coefficient and moment of inertia inaccuracy, friction and load toque, is determined as difference between calculated from currents value of torque reference and calculated from measured speed value of dynamic torque. After that this value can be used to modify torque reference and as a result achieve better performance.

Moment of inertia and friction torque coefficients simultaneous estimation method is proposed in [48]. Total friction is caused by Coulomb friction and viscous friction. The idea is to apply low frequency sinusoidal speed. In this case friction torque is in phase with speed and dynamic torque is out of phase. Friction coefficients and moment of inertia calculations are based on half period integration of reference torque.

Conventional load torque sliding mode observer is analyzed in [49]. According to the analysis, observer accuracy deteriorates if moment of inertia and viscous friction coefficient are determined not correctly. In the paper new sliding mode observer is proposed. Observation errors caused by the mismatch moment of inertia are removed as two additional methods for moment of inertia determination are proposed: direct method when the drive system has just entered into a steady state; and PI controller method, when the drive system entered into the dynamic state.

Conclusions to the Section 1

A lot of methods are existed to determine inductances. However, problem of accurate inductance determination is not fully solved, as accurate methods usually requires special test with additional equipment and methods that are convenient in usage do not consider saturation. Existed mechanical parameter identification methods usually require special test, as a result, control system does not adapt to mechanical parameters variation during operation.

From the survey follows that following tasks has to be solved:

1. Development of the test for inductance determination methods that combine simplicity and accuracy of estimation.

2. Development of the high-performance speed and position control algorithms.

3. Development of the position algorithm that provides online estimation of the mechanical parameters and adjust to its variation.

2 INDUCTANCE DETERMINATION CONSIDERING SATURATION

In this Section derivation of the IPMSM model considering saturation and cross-coupling is presented. After that, by means of consequent simplification, model converts to the common non-saturated model [50]. Also, two methods for inductance determination are proposed and experimentally verified. Both methods are based on the model with partially considered saturation.

2.1 Derivation of the IPMSM models considering saturation

Process of the model derivation starts with the model in flux linkage terms in rotor reference frame. Conversion to the stator reference frame model can be done using Inverse Park Transformation [50]:

$$\begin{aligned} &\mathbf{x}^{(\alpha-\beta)} = \left[\mathbf{e}^{-\mathbf{J}\theta}\right]^{-1}\mathbf{x}^{(\mathrm{d-q})}, \\ &\mathbf{e}^{-\mathbf{J}\theta} = \begin{bmatrix} \cos\theta & \sin\theta \\ -\sin\theta & \cos\theta \end{bmatrix}, \\ &\left[\mathbf{e}^{-\mathbf{J}\theta}\right]^{-1} = \left[\mathbf{e}^{-\mathbf{J}\theta}\right]^{\mathrm{T}}, \end{aligned} \tag{2.1}$$

where $\mathbf{x}^{(\mathrm{d-q})}$ - state vector in the rotor reference frame; $\mathbf{x}^{(\alpha-\beta)}$ - stator reference frame state vector, θ - rotor angle.

Equation (2.1) allows to convert model to the two phase $(\alpha-\beta)$ stator reference frame. Transformation to the three-phase coordinate system can be accomplished with Inverse Clark transformation [52]:

$$\begin{bmatrix} \mathrm{x_a} \\ \mathrm{x_b} \\ \mathrm{x_c} \end{bmatrix} = \begin{bmatrix} 1 & 0 & 1 \\ -\frac{1}{2} & \frac{\sqrt{3}}{2} & 1 \\ -\frac{1}{2} & -\frac{\sqrt{3}}{2} & 1 \end{bmatrix} \begin{bmatrix} \mathrm{x}_\alpha \\ \mathrm{x}_\beta \\ 0 \end{bmatrix}, \tag{2.2}$$

where $\begin{bmatrix} \mathrm{x_a} & \mathrm{x_b} & \mathrm{x_c} \end{bmatrix}^{\mathrm{T}}$ - three phase state vector, $\begin{bmatrix} \mathrm{x}_\alpha & \mathrm{x}_\beta & 0 \end{bmatrix}^{\mathrm{T}}$ - two phase state vector.

General model that consider saturation and cross-coupling effects in the IPMSM can be expressed in flux linkage terms [1]. Equations of the model in d-q axis rotor reference frame are presented below

$$\begin{aligned} u_d &= R_s i_d + \frac{d\Psi_d(i_d,i_q)}{dt} - \omega p_n \Psi_q(i_d,i_q), \\ u_q &= R_s i_q + \frac{d\Psi_q(i_d,i_q)}{dt} + \omega p_n \Psi_d(i_d,i_q), \\ \frac{d\omega}{dt} &= \frac{3p_n}{2J}\left(\Psi_d(i_d,i_q) i_q - \Psi_q(i_d,i_q) i_d\right) - \frac{\nu}{J}\omega - \frac{T_L}{J}, \end{aligned} \tag{2.3}$$

where J – moment of inertia; ν – viscous friction, T_L is load torque.

Assuming that self and cross inductances are considered as a functions of both currents (i_d and i_q), flux equations are

$$\begin{bmatrix} \Psi_d(i_d,i_q) \\ \Psi_q(i_d,i_q) \end{bmatrix} = \begin{bmatrix} L_d(i_d,i_q) & L_{dq}(i_d,i_q) \\ L_{qd}(i_d,i_q) & L_q(i_d,i_q) \end{bmatrix} \begin{bmatrix} i_d \\ i_q \end{bmatrix} + \begin{bmatrix} \Psi_M \\ 0 \end{bmatrix}. \tag{2.4}$$

Model (2.3) allows to describe saturation and cross-coupling effects in the IPMSM, but it cannot be used for closed loop control design due to complexity of flux measurement. In most of the cases model (2.3) has to be transformed to a model with explicit current derivatives.

2.1.1 Model of the IPMSM if self-inductances and mutual inductances are functions of both currents

Transformation to the model in current terms can be done by means of expression of flux derivative as derivative of complex function:

$$\frac{d\Psi_d(i_d,i_q)}{dt} = \frac{di_d}{dt}\frac{\partial\Psi_d(i_d,i_q)}{\partial i_d} + \frac{di_q}{dt}\frac{\partial\Psi_d(i_d,i_q)}{\partial i_q}. \tag{2.5}$$

Analogically to (2.5), quadrature axis flux linkage derivative is

$$\frac{d\Psi_q(i_d,i_q)}{dt} = \frac{di_q}{dt}\frac{\partial\Psi_q(i_d,i_q)}{\partial i_q} + \frac{di_d}{dt}\frac{\partial\Psi_q(i_d,i_q)}{\partial i_d}. \tag{2.6}$$

Substitution of (2.5) and (2.6) into (2.3) gives

$$\begin{aligned}
&\frac{d\omega}{dt}=\frac{3p_n}{2J}\left(\Psi_d\left(i_d,i_q\right)i_q-\Psi_q\left(i_d,i_q\right)i_d\right)-\frac{\nu}{J}\omega-\frac{T_L}{J},\\
&\frac{di_d}{dt}\frac{\partial\Psi_d\left(i_d,i_q\right)}{\partial i_d}+\frac{di_q}{dt}\frac{\partial\Psi_d\left(i_d,i_q\right)}{\partial i_q}=-R_s i_d+\Psi_q\left(i_d,i_q\right)p_n\omega+u_d,\\
&\frac{di_q}{dt}\frac{\partial\Psi_d\left(i_d,i_q\right)}{\partial i_d}+\frac{di_d}{dt}\frac{\partial\Psi_d\left(i_d,i_q\right)}{\partial i_q}=-R_s i_q-\Psi_d\left(i_d,i_q\right)p_n\omega+u_q.
\end{aligned}\tag{2.7}$$

Flux derivatives by currents in model (2.7) can presented from inductances. In this case, model will have more conventional form. If $\Psi_M=\text{const}$, partial derivatives of flux linkages by currents from (2.4) are

$$\begin{aligned}
&\frac{\partial\Psi_d\left(i_d,i_q\right)}{\partial i_d}=L_d\left(i_d,i_q\right)+i_d\frac{\partial L_d\left(i_d,i_q\right)}{\partial i_d}+i_q\frac{\partial L_{dq}\left(i_d,i_q\right)}{\partial i_d},\\
&\frac{\partial\Psi_d\left(i_d,i_q\right)}{\partial i_q}=L_{dq}\left(i_d,i_q\right)+i_d\frac{\partial L_d\left(i_d,i_q\right)}{\partial i_q}+i_q\frac{\partial L_{dq}\left(i_d,i_q\right)}{\partial i_q},\\
&\frac{\partial\Psi_q\left(i_d,i_q\right)}{\partial i_q}=L_q\left(i_d,i_q\right)+i_q\frac{\partial L_q\left(i_d,i_q\right)}{\partial i_q}+i_d\frac{\partial L_{qd}\left(i_d,i_q\right)}{\partial i_q},\\
&\frac{\partial\Psi_q\left(i_d,i_q\right)}{\partial i_d}=L_{qd}\left(i_d,i_q\right)+i_q\frac{\partial L_q\left(i_d,i_q\right)}{\partial i_d}+i_d\frac{\partial L_{qd}\left(i_d,i_q\right)}{\partial i_d}.
\end{aligned}\tag{2.8}$$

Substitution (2.8) and (2.4) into (2.7) allows to obtain model that is free from flux linkages. Obtained model requires knowledge of self and cross-inductances together with its derivatives, however information about each component does not lead to advantages from control design point of view. Therefore, it is more rational to use model (2.7) as it requires 7 parameters to describe electrical part of the motor instead of 13 parameters in case of the model that is free from flux linkages. The flux derivatives by currents can be considered as dynamic inductances (1.3), which fully describe magnetizing processes.

2.1.2 Model of the IPMSM if self-inductances and mutual inductances are functions of both currents and cross-coupling is neglected

Equation (2.4) is simplified in this case, as cross-inductances $L_{dq}\left(i_d,i_q\right)$ and $L_{qd}\left(i_d,i_q\right)$ are neglected. However, this aspect has no influence on the model (2.7). And as a result, neglection of the cross coupling does not simplify electrical part of the motor model.

2.1.3 Model of the IPMSM if self-inductances are functions of one correspond current and cross-coupling is neglected

Derivation of the model starts with model in flux linkage terms (2.3), however fluxes are functions of self-currents:

$$\begin{aligned} u_d &= R_s i_d + \frac{d\Psi_d\left(i_d\right)}{dt} - \omega p_n \Psi_q\left(i_q\right), \\ u_q &= R_s i_q + \frac{d\Psi_q\left(i_q\right)}{dt} + \omega p_n \Psi_d\left(i_d\right), \\ \frac{d\omega}{dt} &= \frac{3p_n}{2J}\left(\Psi_d\left(i_d\right)i_q - \Psi_q\left(i_q\right)i_d\right) - \frac{\nu}{J}\omega - \frac{T_L}{J}. \end{aligned} \tag{2.9}$$

Fluxes derivatives are expressed as

$$\frac{d\Psi_d\left(i_d\right)}{dt} = \frac{di_d}{dt}\frac{\partial\Psi_d\left(i_d\right)}{\partial i_d}; \frac{d\Psi_q\left(i_q\right)}{dt} = \frac{di_q}{dt}\frac{\partial\Psi_q\left(i_q\right)}{\partial i_q}. \tag{2.10}$$

Substitution (2.10) into (2.9) gives

$$\begin{aligned} \frac{d\omega}{dt} &= \frac{3p_n}{2J}\left(\Psi_d\left(i_d\right)i_q - \Psi_q\left(i_q\right)i_d\right) - \frac{\nu}{J}\omega - \frac{T_L}{J}, \\ \frac{di_d}{dt}\frac{\partial\Psi_d\left(i_d\right)}{\partial i_d} &= -R_s i_d + \Psi_q\left(i_q\right)p_n\omega + u_d, \\ \frac{di_q}{dt}\frac{\partial\Psi_d\left(i_d\right)}{\partial i_d} &= -R_s i_q - \Psi_d\left(i_d\right)p_n\omega + u_q. \end{aligned} \tag{2.11}$$

Model (2.11) can be used for algorithm design if fluxes $\Psi_d\left(i_d\right)$ and $\Psi_q\left(i_q\right)$ are known values. However, some identification methods determine inductances not from the

fluxes, but directly from the model. According to made simplifications and assumptions flux linkages are defined as

$$\begin{aligned}\Psi'_d(i_d) &= L_d(i_d)i_d,\\ \Psi_d(i_d) &= \Psi'_d(i_d) + \Psi_M,\\ \Psi_q(i_q) &= L_q(i_q)i_q.\end{aligned} \tag{2.12}$$

In this case model (2.11) can be presented as

$$\begin{aligned}\frac{d\omega}{dt} &= \frac{3p_n}{2J}\left(\left(L_d(i_d) - L_q(i_q)\right)i_q i_d + \Psi_M i_q\right) - \frac{\nu}{J}\omega - \frac{T_L}{J},\\ L_{dd}(i_d)\frac{di_d}{dt} &= -R_s i_d + \omega p_n \Psi_q(i_q) + u_d,\\ L_{qq}(i_q)\frac{di_q}{dt} &= -R_s i_q - \omega p_n \Psi_d(i_d) + u_q,\end{aligned} \tag{2.13}$$

where $L_{dd}(i_d)$ and $L_{qq}(i_q)$ are dynamic inductances along d- and q-axis as functions of the correspond current. If $\Psi_M = \text{const}$, dynamic inductances are

$$\begin{aligned}L_{dd}(i_d) &= \frac{\partial\Psi_d(i_d)}{\partial i_d} = \frac{\partial\left(L_d(i_d)i_d\right)}{\partial i_d} = L_d(i_d) + i_d\frac{\partial L_d(i_d)}{\partial i_d},\\ L_{qq}(i_q) &= \frac{\partial\Psi_q(i_q)}{\partial i_q} = \frac{\partial\left(L_q(i_q)i_q\right)}{\partial i_q} = L_q(i_q) + i_q\frac{\partial L_q(i_q)}{\partial i_q}.\end{aligned} \tag{2.14}$$

Model (2.13) is comparably simple, and saturation is partially considered.

Further simplification leads to obtaining conventional IPMSM model [53] when inductances are constants and cross-coupling is neglected:

$$\begin{aligned}\frac{d\omega}{dt} &= \frac{3p_n}{2J}\left(\left(L_d - L_q\right)i_d i_q + \Psi_M i_q\right) - \frac{\nu}{J}\omega - \frac{T_L}{J},\\ L_d\frac{di_d}{dt} &= -R_s i_d + p_n\omega L_q i_q + u_d,\\ L_q\frac{di_q}{dt} &= -R_s i_q - p_n\omega\left(L_d i_d + \Psi_M\right) + u_q.\end{aligned} \tag{2.15}$$

2.2 Description of the test 1

The first test is made in standstill [54]. Basic idea is similar to methods proposed in [6]. Test is made for the motor #1 and experimental setup described in Appendix A.

The static and dynamic inductances are determined from the single test for two relative rotor positions with respect to the applied locked stator voltage vector. The functional diagram of the experimental setup is presented in Fig. 2.1.

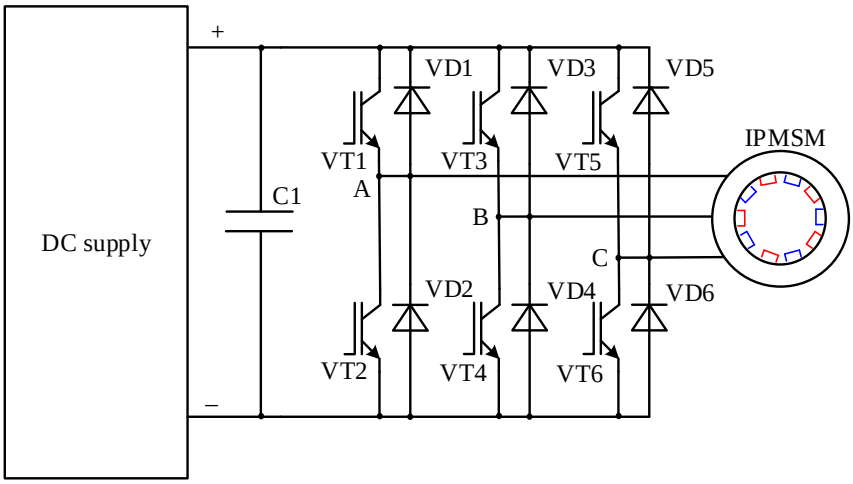

Fig. 2.1. – Functional diagram of the experimental setup for the stand-still test

Voltage u_{ab} between phases A and B and the current in phase A are measured using differential probes and an oscilloscope. The measured values are either d-axis or q-axis voltage and current depending on the rotor position. Idea of the test is to observe the current and voltage during *transients* from active states to zero state, where the states are as follows:

1. Active positive state. +DC voltage is applied to phase A and -DC to B and C phase. In this case transistors VT1, VT4 and VT6 are opened.

2. Active negative state. -DC voltage is applied to phase A and +DC to B and C phase. In this case transistors VT2, VT3 and VT5 are opened.

3. Zero state: all transistors are closed.

In the rotor reference frame, d-axis is aligned with the direction of the permanent magnet flux. In order to determine d-axis inductance, the rotor d-axis has to be aligned with the locked stator voltage vector corresponding to either active positive or active negative state (Fig. 2.2a). Voltage u_{ab} in this case is d-axis voltage and current measured in phase A is d-axis current. In order to set the rotor position, +DC voltage is applied to phase A and –DC to B and C phases. After that, the rotor is locked. To determine q-axis inductance, the rotor q-axis is aligned with the locked stator voltage vector described above (Fig. 2.2b). Rotor alignment is done with applying +DC voltage

to phase B and –DC voltage to phase C (transistors VT3 and VT6 are opened only). After rotor is locked transients from active states to zero state are considered as q-axis transients.

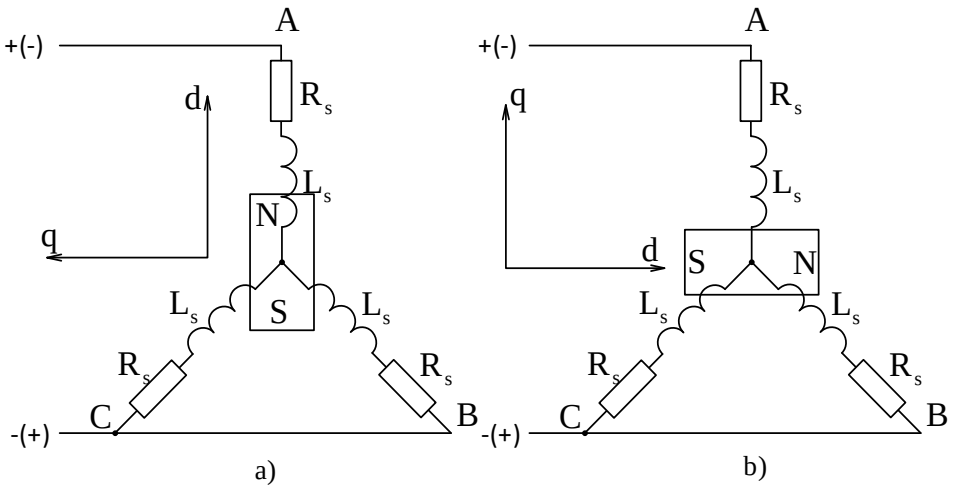

Fig. 2.2. – Stand-still test configurations for a) d-axis, and b) q-axis inductance determination

When switched to active states, the inductances accumulate magnetic energy. Fig. 2.3 shows current path in positive active state. Once the inverter is turn off to zero state, the stored magnetic energy continues the current flow and induces a voltage higher than the DC supply and with opposite polarity. The current starts to flow through diodes as it is shown in Fig. 2.4. At the moment of time, when current falls to zero, all energy stored in inductances has been dissipated.

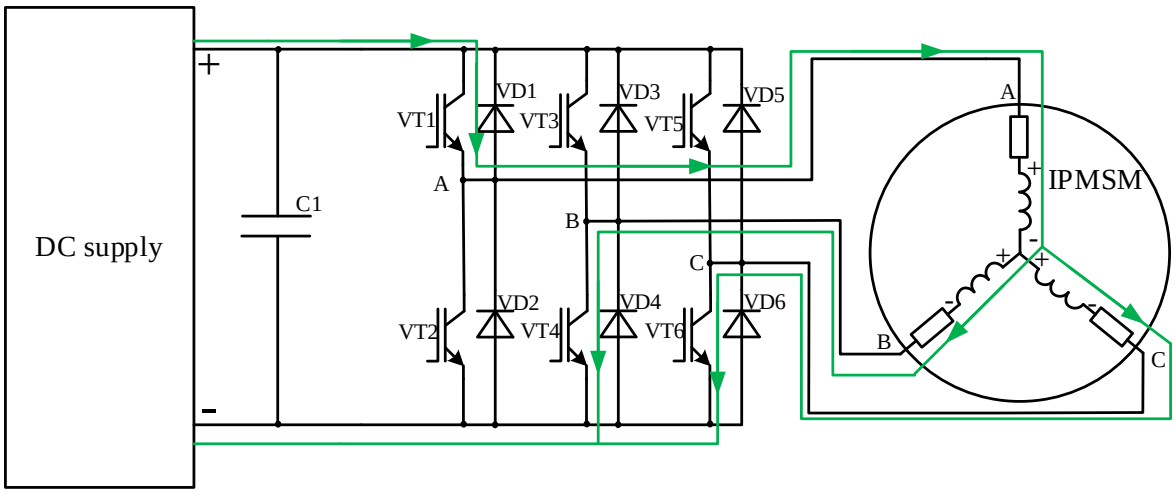

Fig. 2.3. – Current flow in the active positive state

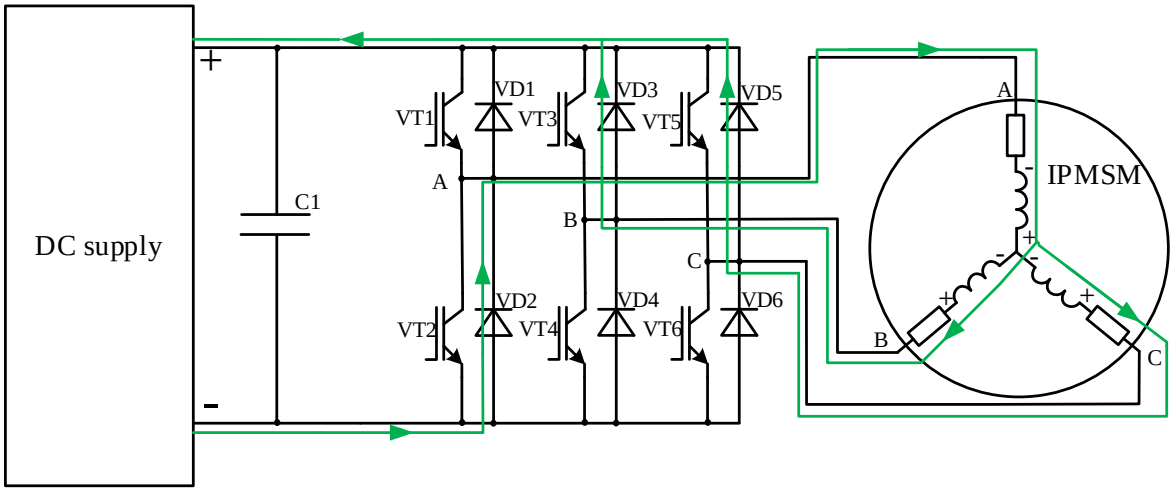

Fig. 2.4. – Current flow when switched from the active positive state to zero state

It should be mentioned that currents in phases B and C are assumed to be the same and therefore voltage drop on transistors VT4, VT6 and diodes VD3, VD5 is the same. As a result, points B and C are directly connected, what is important for further data analysis.

According to Fig. 2.2, equivalent resistance and inductance of this circuit are $R_{eqv}=1.5R_s$, $L_{eqv}(i_a)=1.5L_s(i_a)$, considering that impedance in each phase is the same, where $L_s(i_a)$ is phase inductance.

2.3 Description of the test 2

The second test is a test with constant speed. Idea is similar to proposed in [12]-[16]. Test is made for the motor #2 and experimental setup described in the Appendix B. The functional diagram of the experimental setup is shown in Fig. 2.5.

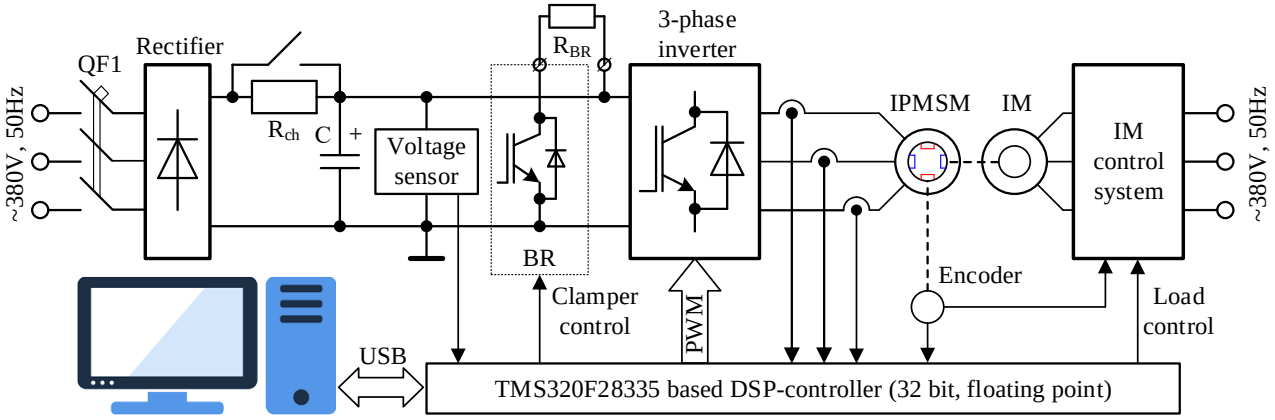

Fig. 2.5. – Functional diagram of the experimental setup

The test allows to estimate the flux linkages $\Psi_d(i_d)$, $\Psi_q(i_q)$ and permanent magnets flux Ψ_m. The constant non-zero speed is achieved by the additional induction motor (IM) velocity stabilization. IPMSM stator current tracking is organized using PI current controllers, implemented in rotor coordinate reference frame:

$$\begin{aligned} u_d &= -k_i\tilde{i}_d - x_d, \quad & u_q &= -k_i\tilde{i}_q - x_q, \\ \dot{x}_d &= k_{ii}\tilde{i}_d, & \dot{x}_q &= k_{ii}\tilde{i}_q, \end{aligned} \tag{2.16}$$

where $\tilde{i}_q = i_q - i_q^*$, $\tilde{i}_d = i_d - i_d^*$ are current tracking errors, i_d^*, i_q^* are references, x_d, x_q denote integral components, $k_i > 0$, $k_{ii} > 0$ are the proportional and integral gains of the controllers.

These two high gain PI-current controllers (2.16) are configured to achieve asymptotic current tracking with $\tilde{i}_q = 0$ and $\tilde{i}_d = 0$ provided that current references are slow enough.

For the flux linkage $\Psi_d(i_d)$ estimation, the reference value $i_q^* = 0$; d-axis current reference value is changing linearly in the range $[i_{max}, i_{min}]$, where i_{min}, i_{max} are minimum and maximum operation currents respectively. The rate of the change has to be slow enough so that current dynamics can be neglected. As a result, d-axis flux as a function of d-axis current is found from model (2.13) as

$$\Psi_d(i_d) = \frac{u_q}{\omega p_n}. \tag{2.17}$$

For the determination of flux $\Psi_q(i_q)$, the testing procedure is the same, but in this case $i_d^* = 0$ and q-axis reference current value is changing linearly. As a result, q-axis flux as a function of q-axis current can be found from model (2.13) as

$$\Psi_q(i_q) = -\frac{u_d}{\omega p_n}. \tag{2.18}$$

Permanent magnets flux Ψ_m can be calculated from d-axis flux when $i_d = 0$:

$$\Psi_m = \Psi_d(i_d = 0). \tag{2.19}$$

The inductances can be determined using four methods described below.

2.4 Methods for inductance calculation

Four methods are proposed for static and dynamic inductance calculation of the IPMSM.

1. Method based on flux model. Dynamic inductances can be determined from the fluxes as

$$L_{dd}\left(i_d\right)=\frac{\partial\Psi_d\left(i_d\right)}{\partial i_d},\ L_{qq}\left(i_q\right)=\frac{\partial\Psi_q\left(i_q\right)}{\partial i_q}. \tag{2.20}$$

In case of motionless test, the flux linkages $\Psi_d\left(i_d\right), \Psi_q\left(i_q\right)$ are found from measured current and voltage curves:

$$\begin{aligned}\Psi_d\left(i_d\right)&=\int\left(u_d-R_s i_d\right)dt+C_d,\\ \Psi_q\left(i_q\right)&=\int\left(u_q-R_s i_q\right)dt+C_q,\end{aligned} \tag{2.21}$$

where C_d, C_q are initial conditions.

Drawbacks of using (2.21) are the following: direct integration tends to accumulate errors and necessity of precise determination of initial conditions for accurate flux computation. However, if dynamic inductances are determined from (2.20), these drawbacks have no influence on accuracy of determination, as flux gradient is used but not its absolute value. Therefore, initial conditions C_d, C_q can be taken as zero.

2. Method based on current model. Another approach is to determine dynamic inductances directly from the motor model (2.13). As test is made in stand-still, model is simplified and inductances are

$$L_{dd}\left(i_d\right)=\frac{u_d-R_s i_d}{di_d/dt},\ L_{qq}\left(i_q\right)=\frac{u_q-R_s i_q}{di_q/dt}. \tag{2.22}$$

Equations (2.22) require accurate knowledge of current derivative. In order to exclude influence of noises it is proposed to approximate current curve and calculate the derivative directly. Flux can be also approximated to receive dynamic inductance from (2.20) analytically.

3. Method based on steady-state model. Static inductance can be determined from flux as

$$L_d(i_d) = \frac{\Psi_d(i_d) - \Psi_m}{i_d},\ L_q(i_q) = \frac{\Psi_q(i_q)}{i_q}. \tag{2.23}$$

The mentioned drawback of flux calculation using (2.21) has higher impact on accuracy of static inductance determination in this case since absolute values of flux are used. Inaccurate computation of the flux linkages for (2.23) leads to singularities for currents close to zero. Initial conditions can be found from the point when current and voltage decay to zero. In this case $\Psi_q = 0$, $\Psi_d = \Psi_m$ and initial conditions are

$$C_d = \Psi_m - \int_0^{t_{cond}} (u_d - R_s i_d)dt,\ C_q = -\int_0^{t_{cond}} (u_q - R_s i_q)dt. \tag{2.24}$$

4. Method based on discrete time model. It is also possible to compute the static inductance using dynamic inductances from their relationship in (2.14). However, it requires solving difference equations in the following form:

$$\begin{aligned} L_d[k+1] &= L_d[k] + (L_{dd}[k+1] - L_d[k])\Delta i_d / i_d[k+1], \\ L_q[k+1] &= L_q[k] + (L_{qq}[k+1] - L_q[k])\Delta i_q / i_q[k+1], \end{aligned} \tag{2.25}$$

where k is a sampling index, Δi_d, Δi_q are changes of (d-q) currents between adjacent iterations. Initial values for static inductances are $L_d[0] = L_{dd}[0]$, $L_q[0] = L_{qq}[0]$ if $k = 0$ corresponds to zero current.

Computation of the static inductances using (2.25) doesn't have problems of method based on (2.23), due to the fact that calculations in (2.25) are based on dynamic inductances and currents. Dynamic inductances can be determined from the methods proposed above.

2.5 Experimental results

2.5.1 Stand-still test 1

An example of transients for tested motor #1 is presented in Fig. 2.6. The stator resistance is determined from the measured current and voltage values in active state.

The active state corresponds to the period of time $t \in [0, 0.5]$ ms in Fig. 2.6, in which equivalent resistances are $R_{eqv} = u_{ab}(0)/i_a(0) = 0.2$ Ohm, $R_s = R_{eqv}/1.5 = 0.13$ Ohm.

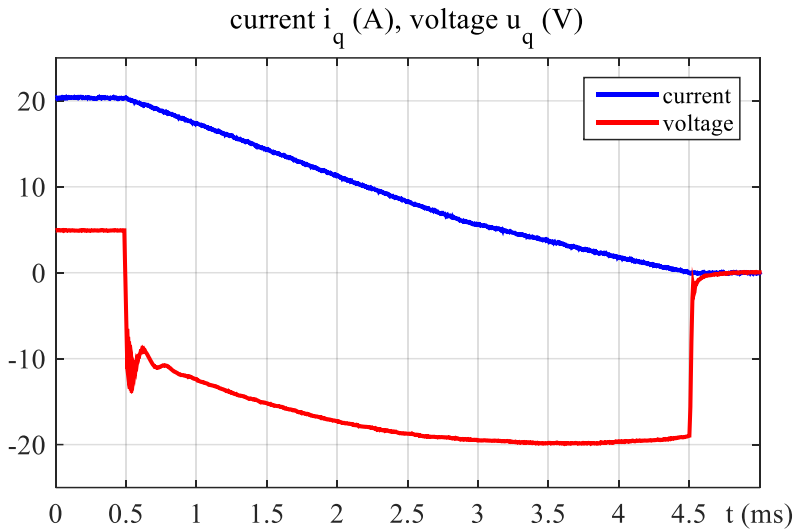

Fig. 2.6. – Transients of voltage and current if q-axis inductance is calculated

The problem of method #2 comparing to method #1 for dynamic inductance calculation is that precise approximation of current curve is not always possible; equation (2.22) can be used only during transient, preferably with current derivative that does not change its sign.

Drawbacks of static inductance determination using method #3 are dependence on initial conditions in flux calculation (2.21) and as a result, singularities at zero currents are present. In case of using method #4, there is no problem with singularity if condition of equality of static and dynamic inductances is accepted for non-zero currents.

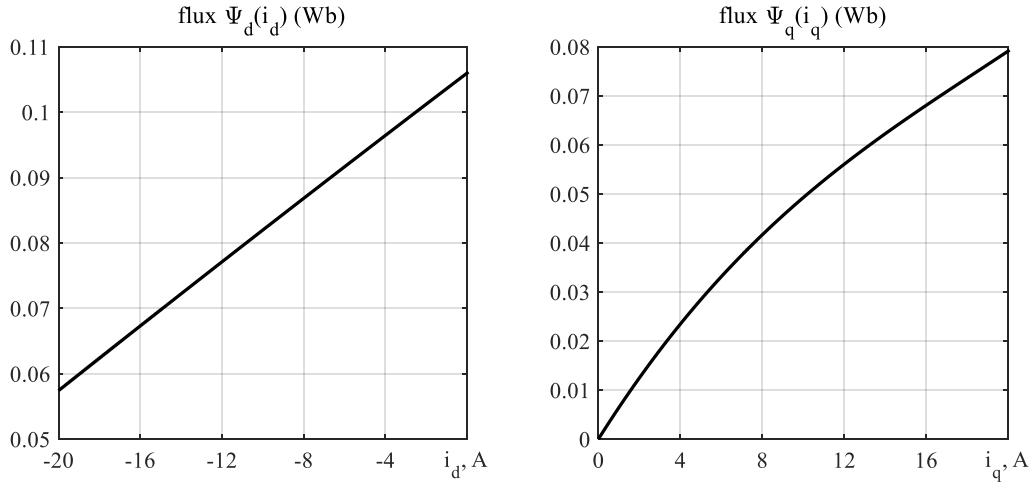

Fig. 2.7. – Flux linkages along d- and q-axis

The (d-q) flux linkages, computed from (2.21) and (2.24) are presented in Fig. 2.7. The q-axis static and dynamic inductances using presented methods are shown in. Static inductance (method #4) is calculated based on dynamic inductance determined using method #1. The d-axis inductances are not shown since they remain constant for this motor if $i_d < 0$ and equal $L_d = L_{dd} = 1.62$ mH.

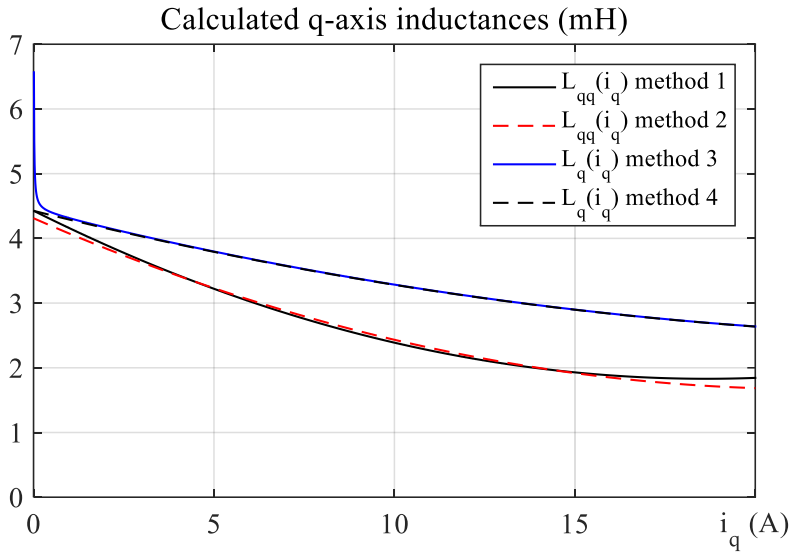

Fig. 2.8. – Calculated values of the q-axis inductance of the motor #1

2.5.2 Constant speed test 2

In this test, motor rotates with the speed $\omega = 157$ rad/s, which corresponds to 50 Hz motor supply frequency. Currents i_d and i_q are changing linearly from $i_{max} = 7.5$ A to $i_{min} = -7.5$ A (values close to rated ones). The transients last for 60 s. Current controller gains $k_i = 30$ and $k_{ii} = 1250$ ensure sufficiently fast dynamics of the current control loops to consider the regulation processes as quasi-static.

The transients for estimation of $\Psi_d(i_d)$ and $\Psi_q(i_q)$ are presented in Fig. 2.9. Measured flux characteristics (2.17), (2.18) for motor #2 are shown in Fig. 2.10. From the analysis of Fig. 2.9 and Fig. 2.10 it is seen that under condition $i_q = 0$ the flux $\Psi_q(i_q = 0) \neq 0$, that needs further investigations. From condition $i_d = 0$ it follows that $\Psi_m = 0.615$ Wb. Both flux linkages were approximated as 3rd-order polynomials. The d-axis flux shown for negative values, which corresponds to field-weakening operation mode.

From Fig. 2.10, it follows that the saturation of magnetic circuit is negligibly small.

Advantages of the constant speed test are possibility to determine fluxes as functions of both currents and as a result to take into account cross-coupling effects of the motor. Moreover, implementation of the closed-loop system provides mitigation of inverter nonlinearities. However, it requires using the additional drive for testing machine rotation.

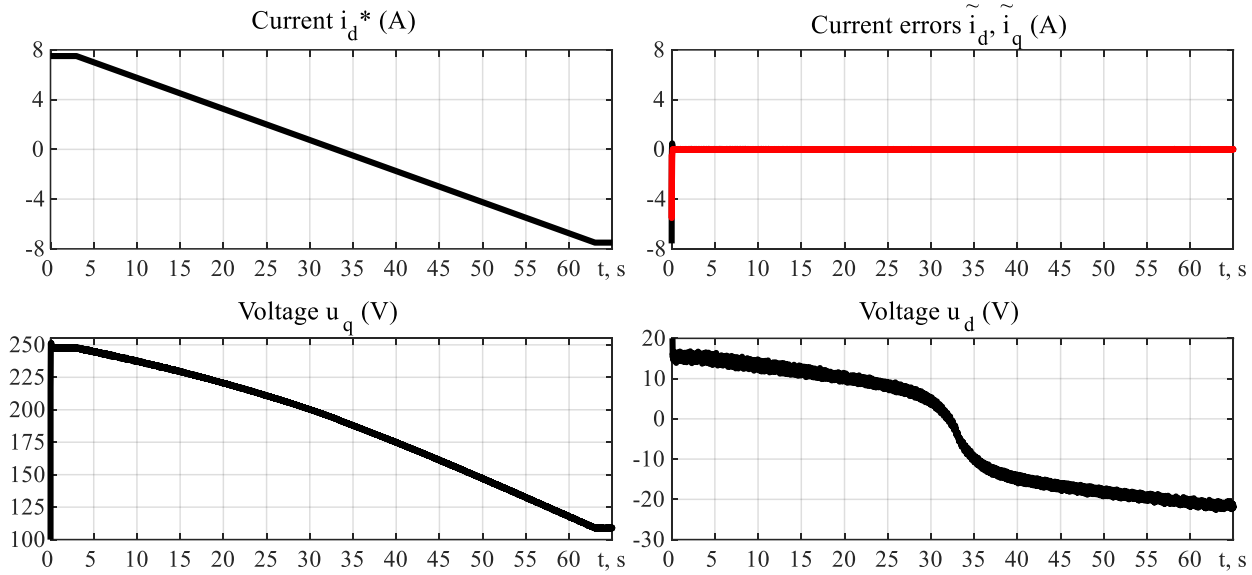

a) transients of the flux $\Psi_d(i_d)$ estimation

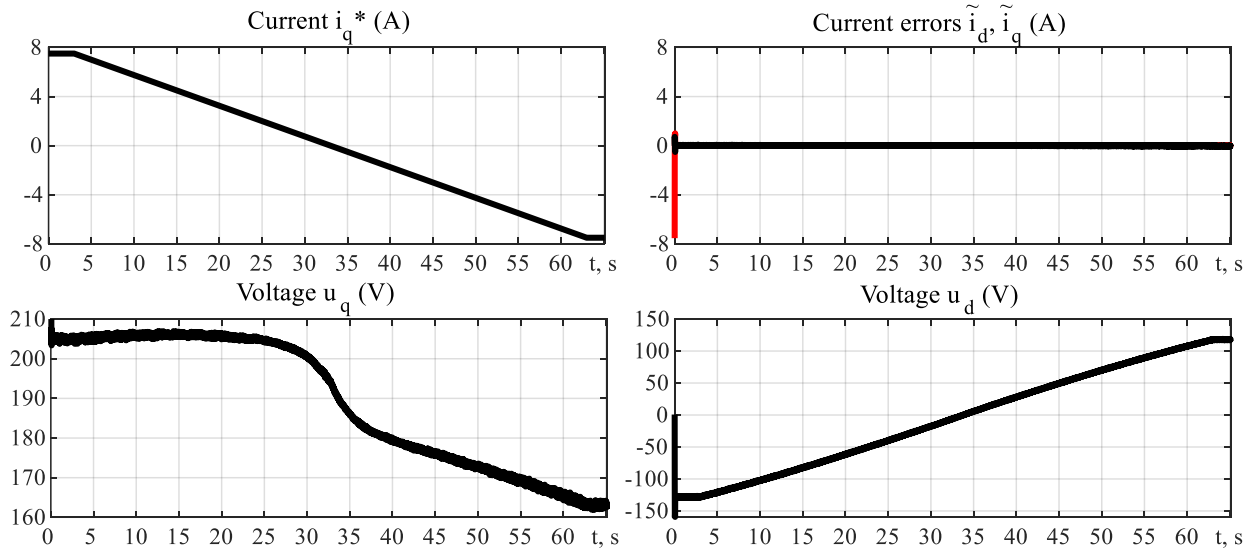

b) transients of the flux $\Psi_q(i_q)$ estimation

Fig. 2.9. – Transients for estimation of the fluxes for the motor #2

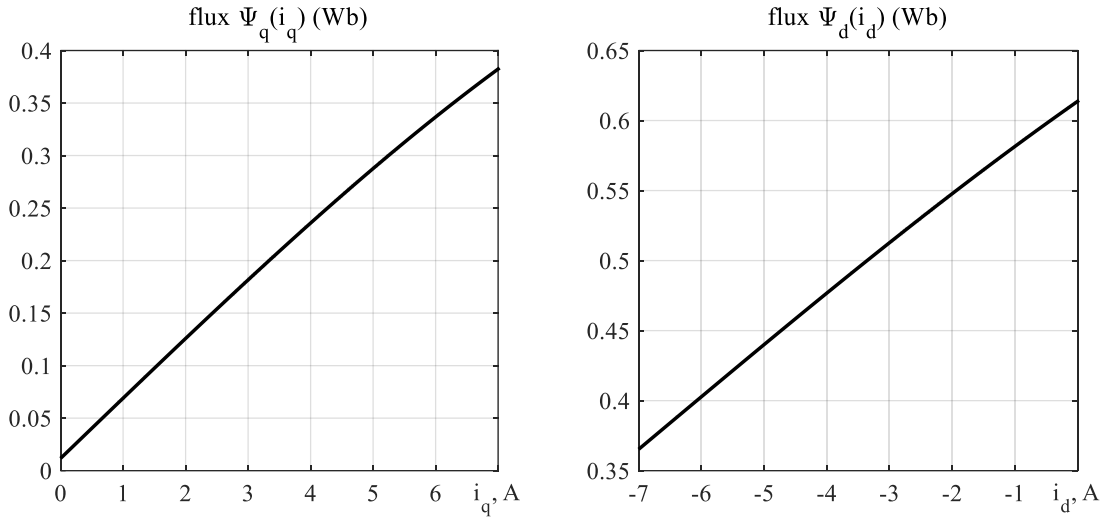

Fig. 2.10. – Flux curves for the second method

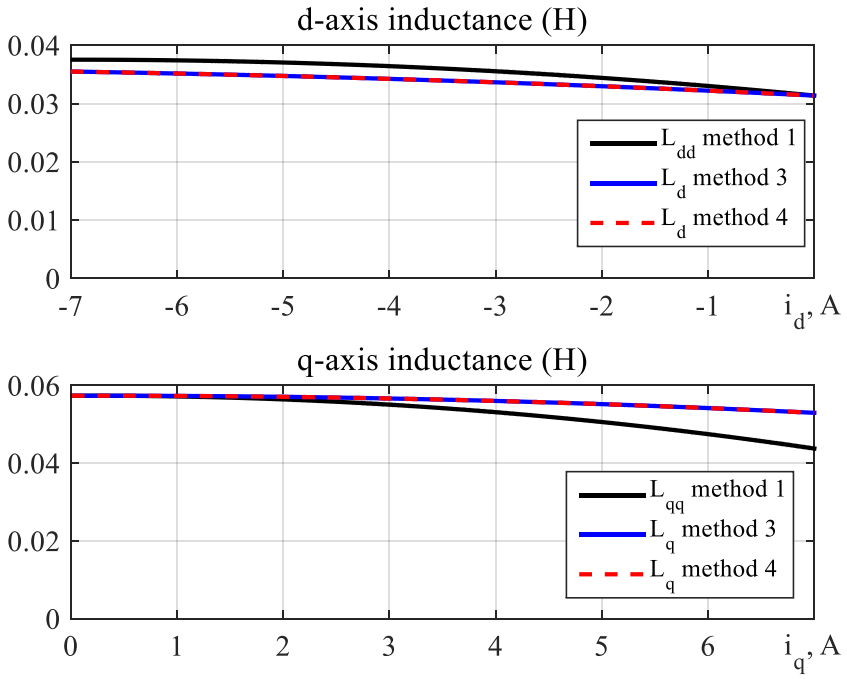

Fig. 2.11. – Calculated values of (d-q) inductances of the motor #2

Three methods under consideration were used for inductances estimation using experimental data shown in Fig. 2.10. The dynamic inductances are determined using (2.20) (method #1). The static inductances can be either determined from (2.23) (method #3), or (2.25) (method #4). As the fluxes are determined directly, initial conditions are inherently known. The results of computations are presented in Fig. 2.11. The inductance $L_d(i_d)$ slightly rises in the field-weakening region; while the inductance $L_q(i_q)$ slightly decreases near the rated values of i_q, but they can be considered constant with sufficient accuracy.

From comparison of Fig. 2.8 with Fig. 2.11 follows that investigated motors have different level of the saturation of magnetic circuits, however proposed tests and methods provide accurate estimations of both static and dynamic inductances.

Conclusions to the Section 2

1. Presentation of the model with fluxes and flux derivatives requires a smaller number of parameters comparing to the model presented using self and cross inductances

2. If inductances are presented as functions of one current, system becomes coupled only with back-EMF components, and control algorithm based on the system does not have significant differences comparing to the one based on the non-saturated model

3. Two different tests are proposed and experimentally verified. The first one, called “stand-still method”, allows removing inverter nonlinearities from the calculation scheme and has high level of accuracy as voltages and currents are measured directly. At the same, this test requires to connect additional DC supply. The second method uses common inverter-based vector-controlled drive, however it has to be driven with prime mover. Inverter nonlinearities have less influence in this test.

4. Four methods are proposed to calculate inductances from data obtained in the tests. Dynamic inductances are determined either from fluxes or directly from the model. Static inductances can be found also from the fluxes or from the dynamic inductance.

3 SPEED CONTROL OF THE INTERIOR PERMANENT MAGNET SYNCHROLOUS MOTORS

In this Section design of the IPMSM speed vector control algorithm is presented [23].

3.1 Formulation of the control problem

Following assumptions are taken:

A.3.1. Stator currents, angular speed and angular position are measured values.

A.3.2. Parameters of the motor are known and constant values.

A.3.3. Torque T_L is unknown, limited, constant or those that is changing slowly.

A.3.4. The rotor speed reference ω^* is smooth and bounded function together with its first $\dot{\omega}^*$ and second $\ddot{\omega}^*$ time derivatives; d-axis current reference i_d^* is bounded together with its bounded derivative $\dot{i}_d^*$.

The control problem is to design a speed controller, which guarantees following control objectives:

CO.3.1. Asymptotic speed ω and direct current component i_d tracking:

$$\lim_{t\to\infty}\left(\tilde{\omega}, \tilde{i}_d\right) = 0, \tag{3.1}$$

where $\tilde{\omega} = \omega - \omega^*$ - rotor speed error, $\tilde{i}_d = i_d - i_d^*$ - direct current component error.

CO.3.2. Asymptotic decoupling of speed control and direct current control subsystems.

CO.3.3. Linearization of speed control subsystem.

3.2 Design of the speed control algorithm

As parameters are considered as constants, non-saturated model (2.15) is used for the control design. Algorithm is designed using back – stepping design procedure [54].

3.2.1 Speed controller design

From (2.15) speed error dynamics is following:

$$\dot{\tilde{\omega}} = \left(i_q^* + \tilde{i}_q\right)\cdot\mu\left(i_d^*\right) - \frac{\nu}{J}\omega^* - \frac{\nu}{J}\tilde{\omega} - \hat{T}_L - \tilde{T}_L - \dot{\omega}^* + \frac{3}{2}\frac{1}{J}p_n\left(L_d - L_q\right)\tilde{i}_d i_q, \qquad (3.2)$$

where $\tilde{i}_q = i_q - i_q^*$ - quadrature axis current error, i_q^* - reference value of the current; $\tilde{T}_L = \frac{T_L}{J} - \hat{T}_L$ - torque estimation error, $\hat{T}_L$ - torque estimation; $\mu\left(i_d^*\right) = \frac{3}{2}\frac{1}{J}p_n\left[\Psi_M + \left(L_d - L_q\right)i_d^*\right] > 0$.

Current controller can be formed from (3.2) as

$$\begin{aligned} i_q^* &= \frac{1}{\mu\left(i_d^*\right)}\left(\hat{T}_L + \frac{\nu}{J}\omega^* + \dot{\omega}^* - k_\omega\tilde{\omega}\right), \\ \dot{\hat{T}}_L &= -k_{\omega i}\tilde{\omega}, \end{aligned} \qquad (3.3)$$

where $\left(k_\omega, k_{\omega i}\right) > 0$ are speed controller proportional and integral gains respectively.

Substitution (3.3) into (3.2) gives

$$\begin{aligned} \dot{\tilde{\omega}} &= -\left(k_\omega + \frac{\nu}{J}\right)\tilde{\omega} - \tilde{T}_L + \mu\left(i_d^*\right)\tilde{i}_q + \frac{3}{2}\frac{1}{J}p_n\left(L_d - L_q\right)\tilde{i}_d\left(\tilde{i}_q + i_q^*\right), \\ \dot{\tilde{T}}_L &= k_{\omega i}\tilde{\omega}. \end{aligned} \qquad (3.4)$$

Torque is assumed to be constant in A.3. As a result, $\dot{\tilde{T}}_L = -\dot{\hat{T}}_L$. Worth mentioning that in case of current control, $\tilde{i}_d = \tilde{i}_q = 0$, so that system (3.4) becomes linear and asymptotically stable for every $\left(k_\omega, k_{\omega i}\right) > 0$.

For the further design, derivative of the quadrature current reference $\dot{i}_q^*$ has to be found

$$
\begin{aligned}
\dot{i}_q^* &= \frac{1}{\mu\left(i_d^*\right)}\left[\dot{\hat{T}}_L + \frac{\nu}{J}\dot{\omega}^* + \ddot{\omega}^*\right] + \\
&+ \frac{1}{\mu\left(i_d^*\right)}\left[-k_\omega\left(-\left(k_\omega + \frac{\nu}{J}\right)\tilde{\omega} + \mu\left(i_d^*\right)\tilde{i}_q + \frac{3}{2}\frac{1}{J}p_n\left(L_d - L_q\right)\tilde{i}_d i_q\right)\right] - \\
&- \frac{1}{\mu\left(i_d^*\right)^2}\left[\frac{3}{2}\frac{1}{J}p_n\left(L_d - L_q\right)i_d^*\right]\left[\frac{\nu}{J}\omega^* + \dot{\omega}^* - k_\omega\tilde{\omega}\right] + \\
&+ \frac{k_\omega}{\mu\left(i_d^*\right)}\tilde{T}_L \triangleq \dot{i}_{q1}^* + \dot{i}_{q2}^*,
\end{aligned}
\tag{3.5}
$$

where $\dot{i}_{q1}^*$ is known function; $\dot{i}_{q2}^* = \frac{k_\omega}{\mu\left(i_d^*\right)}\tilde{T}_L$ - unknown function.

3.2.2 Q-axis current controller design

From (2.15) q-axis current dynamics is following:

$$
\dot{\tilde{i}}_q = -\frac{R_s}{L_q}\left(\tilde{i}_q + i_q^*\right) - \frac{L_d}{L_q}i_d p_n\omega - \frac{1}{L_q}\Psi_M p_n\omega + \frac{1}{L_q}u_q - \dot{i}_q^*. \tag{3.6}
$$

Current controller can be composed from (3.6) as

$$
\begin{aligned}
u_q &= Ri_q^* + L_d p_n\omega i_d + \Psi_M p_n\omega + L_q\left(\dot{i}_{q1}^* - k_{i1}\tilde{i}_q - x_q\right), \\
\dot{x}_q &= k_{ii}\tilde{i}_q,
\end{aligned}
\tag{3.7}
$$

where $\left(k_{i1}, k_{ii}\right) > 0$ are current controller proportional and integral gains respectively.

Substitution (3.7) into (3.6) gives

$$
\begin{aligned}
\dot{\tilde{i}}_q &= -k_{iq}\tilde{i}_q - x_q - \frac{k_\omega}{\mu\left(i_d^*\right)}\tilde{T}_L, \\
\dot{x}_q &= k_{ii}\tilde{i}_q,
\end{aligned}
\tag{3.8}
$$

where $k_{iq} = k_{1i} + \frac{R_s}{L_q}$.

3.2.3 D-axis current controller design

Current controller for d-axis is designed similarly. From (2.15) d-axis current dynamics is

$$\dot{\tilde{i}}_d = -\frac{R_s}{L_d}\left(\tilde{i}_d + i_d^*\right) + \frac{L_q}{L_d} i_q p_n \omega + \frac{1}{L_d} u_d - \dot{i}_d^*. \tag{3.9}$$

Voltage reference along d-axis is formed from (3.9) as

$$\begin{aligned} u_d &= R_s i_d^* - L_q p_n \omega i_q + L_d\left(\dot{i}_d^* - k_{i1}\tilde{i}_d - x_d\right), \\ \dot{x}_d &= k_{ii}\tilde{i}_d, \end{aligned} \tag{3.10}$$

Substitution (3.7) into (3.6) gives

$$\begin{aligned} \dot{\tilde{i}}_d &= -k_{id}\tilde{i}_d - x_d, \\ \dot{x}_d &= k_{ii}\tilde{i}_d, \end{aligned} \tag{3.11}$$

where $k_{id} = k_{1i} + \frac{R_s}{L_d}$.

Total error dynamics of the system basing on (3.4), (3.8) and (3.11) are

$$\begin{aligned} \dot{\tilde{\omega}} &= -\left(k_\omega + \frac{\nu}{J}\right)\tilde{\omega} - \tilde{T}_L + \mu\left(i_d^*\right)\tilde{i}_q + \frac{3}{2}\frac{1}{J} p_n \left(L_d - L_q\right)\tilde{i}_d\left(\tilde{i}_q + i_q^*\right), \\ \dot{\tilde{T}}_L &= k_{\omega i}\tilde{\omega}, \\ \dot{\tilde{i}}_q &= -k_{iq}\tilde{i}_q - x_q - \frac{k_\omega}{\mu\left(i_d^*\right)}\tilde{T}_L, \\ \dot{x}_q &= k_{ii}\tilde{i}_q, \\ \dot{\tilde{i}}_d &= -k_{id}\tilde{i}_d - x_d, \\ \dot{x}_d &= k_{ii}\tilde{i}_d. \end{aligned} \tag{3.12}$$

In (3.12) first four equations describe behavior of the speed control subsystem and the last two – behavior of the direct current control subsystem. From (3.12) it is clear that these subsystems are decoupled. Direct current subsystem is asymptotically stable $\forall\left(k_{1i}, k_{ii}\right) > 0$. As a result, condition $\lim_{t\to\infty}\left(\tilde{i}_d, x_d\right) = 0$ is fulfilled. Speed control

subsystem is asymptotically stable with suitable tuning of the controller gains $(k_{\omega}, k_{\omega i}) > 0$ and $(k_{1i}, k_{ii}) > 0$. Results from theory of cascaded system proposes to adjust current control loop gains so that subsystem dynamics to be at least two times faster that speed dynamics.

If above mentioned requirements are fulfilled, system (3.12) is asymptotically stable:

$$\lim_{t\to\infty}\left(\tilde{\omega}, \tilde{T}_L, \tilde{i}_q, x_q, \tilde{i}_d, x_d\right) = 0, \tag{3.13}$$

Standard relation between proportional and integral gain is used:

$$\begin{aligned} k_i &= \frac{k_p^2}{2}, \text{ if } \xi = 0.707 \\ k_i &= \frac{k_p^2}{4}, \text{ if } \xi = 1 \end{aligned}, \tag{3.14}$$

where k_p is proportional gain, and k_i - integral gain, ξ - damping coefficient.

As a result, control objectives CO.3.1. – CO.3.3. are achieved. Block diagram of the electric drive with proposed controller (3.3), (3.5), (3.7) and (3.10) is presented in Fig. 3.1. Structural scheme of the controller is presented in Fig. 3.2.

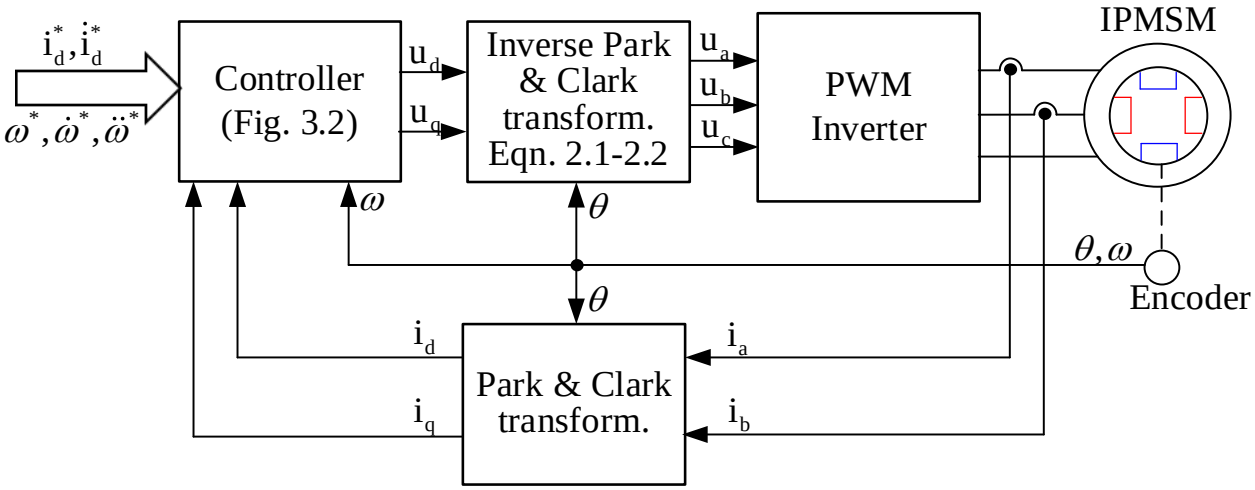

Fig. 3.1. – Block diagram of the electric drive with proposed speed controller

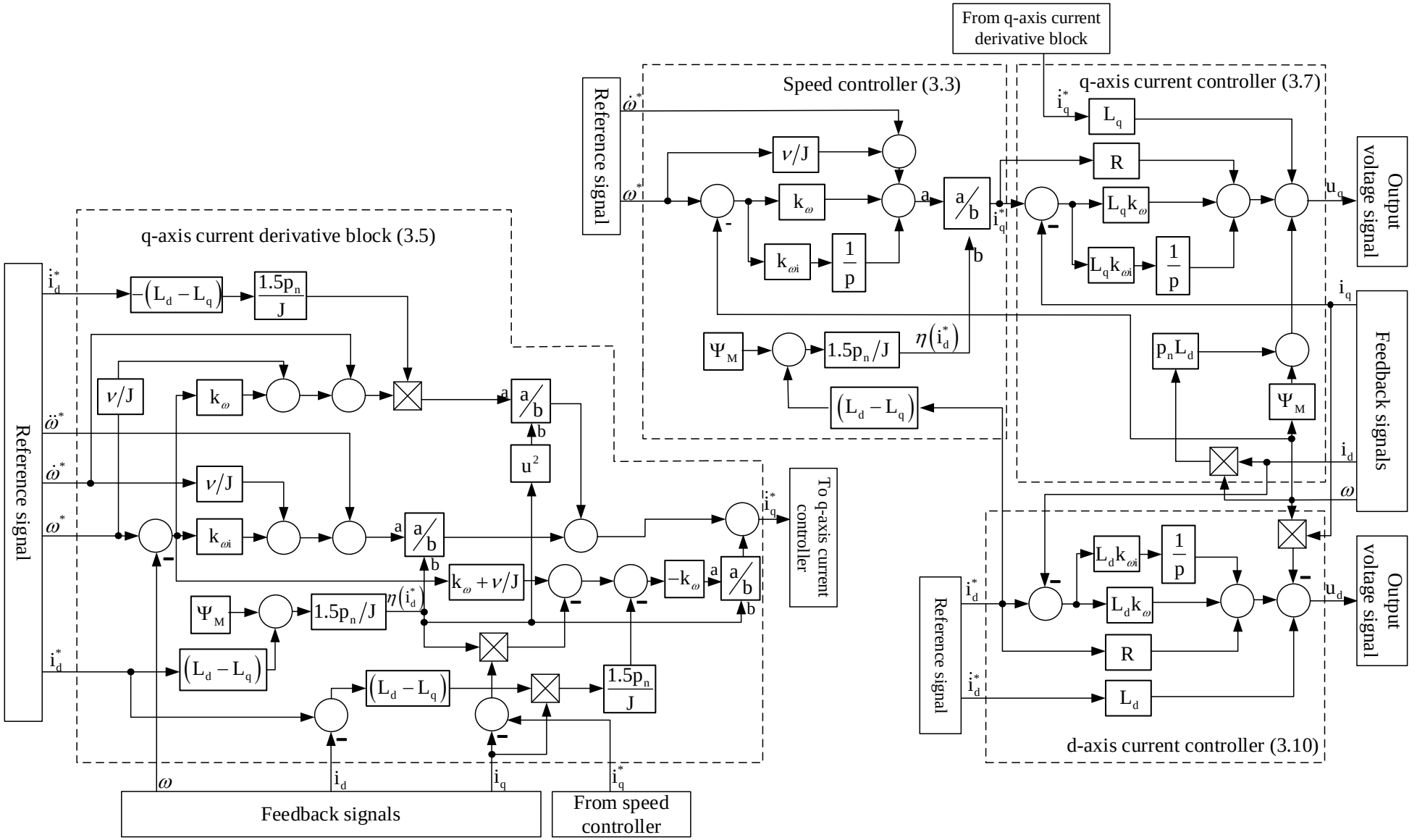

Fig. 3.2. – Structural scheme of the proposed speed controller

3.3. Research of the speed control algorithm

Following test is proposed to analyze behavior of the system if derived controller is used: Standard speed reference trajectory ω^* with bounded the first and the second derivative is proposed. Maximum value of the first derivative is $\dot{\omega}^* = 600\,\mathrm{rad/s^2}$ and the second time derivative $\ddot{\omega}^* = 3000\,\mathrm{rad/s^3}$. Acceleration occurred from $0.1\mathrm{s}$ to $0.28\mathrm{s}$. Steady state speed value is $\omega_{ss} = 100\,\mathrm{rad/s}$. Deceleration to zero speed starts at $1.4\mathrm{s}$ and longs for $0.18\mathrm{s}$. Direct current $\mathrm{i}_\mathrm{d}^* = -5\mathrm{A}$ is applied at $0.8\mathrm{s}$ for $0.4\mathrm{s}$. Acceleration and deceleration of the current last for $0.01\mathrm{s}$. Nominal load torque $(14\mathrm{Nm})$ is applied from $0.4\mathrm{s}$ to $1.8\mathrm{s}$. Controller gains are $\mathrm{k}_{1\mathrm{i}} = 1000$, $\mathrm{k}_{\mathrm{ii}} = \mathrm{k}_{1\mathrm{i}}^2/4$, $\mathrm{k}_\omega = 100$, $\mathrm{k}_{\omega\mathrm{i}} = \mathrm{k}_\omega^2/2$.

Test combines standard test when torque is applied only at nonzero speed and the most difficult for control system condition, when torque is applied when speed reference $\omega^* = 0\,\mathrm{rad/s}$.

Motor is modelled using derived model (2.12), (2.13). Static and dynamic inductance values determined in the previous Section are used (Fig. 2.11). Simulation is performed using software MATLAB 2014B for the motor, which parameters are presented in Appendix B. The main cycle of the modelling program is presented in Appendix C. Simulation results are presented for controller (3.3), (3.5), (3.7) and (3.10) in Fig. 3.3.

From Fig. 3.3, it is clear that processes in speed control and direct current subsystems are not fully decoupled. It can be explained by the fact that controller is designed for non-saturated model. At the same time simulation and experiments were made for the motor that is some level of saturation. However, control performance degradation due to this aspect is negligibly small. Controllers based on the non-saturated model can be used for high performance control if motor saturation is comparatively small (as in tested motor). Otherwise, controller have to be based on the model where saturation is considered.

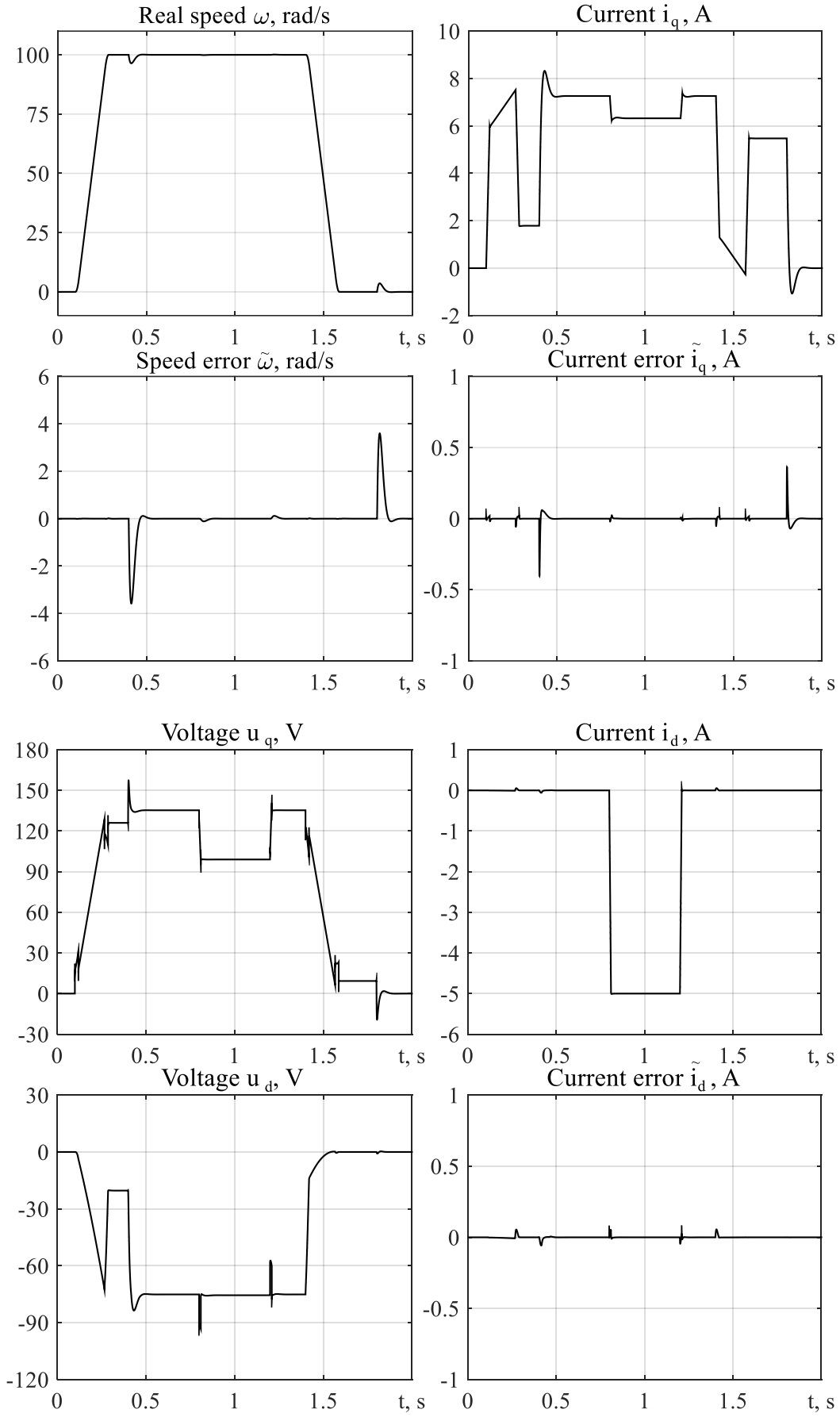

Fig. 3.3 –Transients during simulation if derived speed algorithm is used

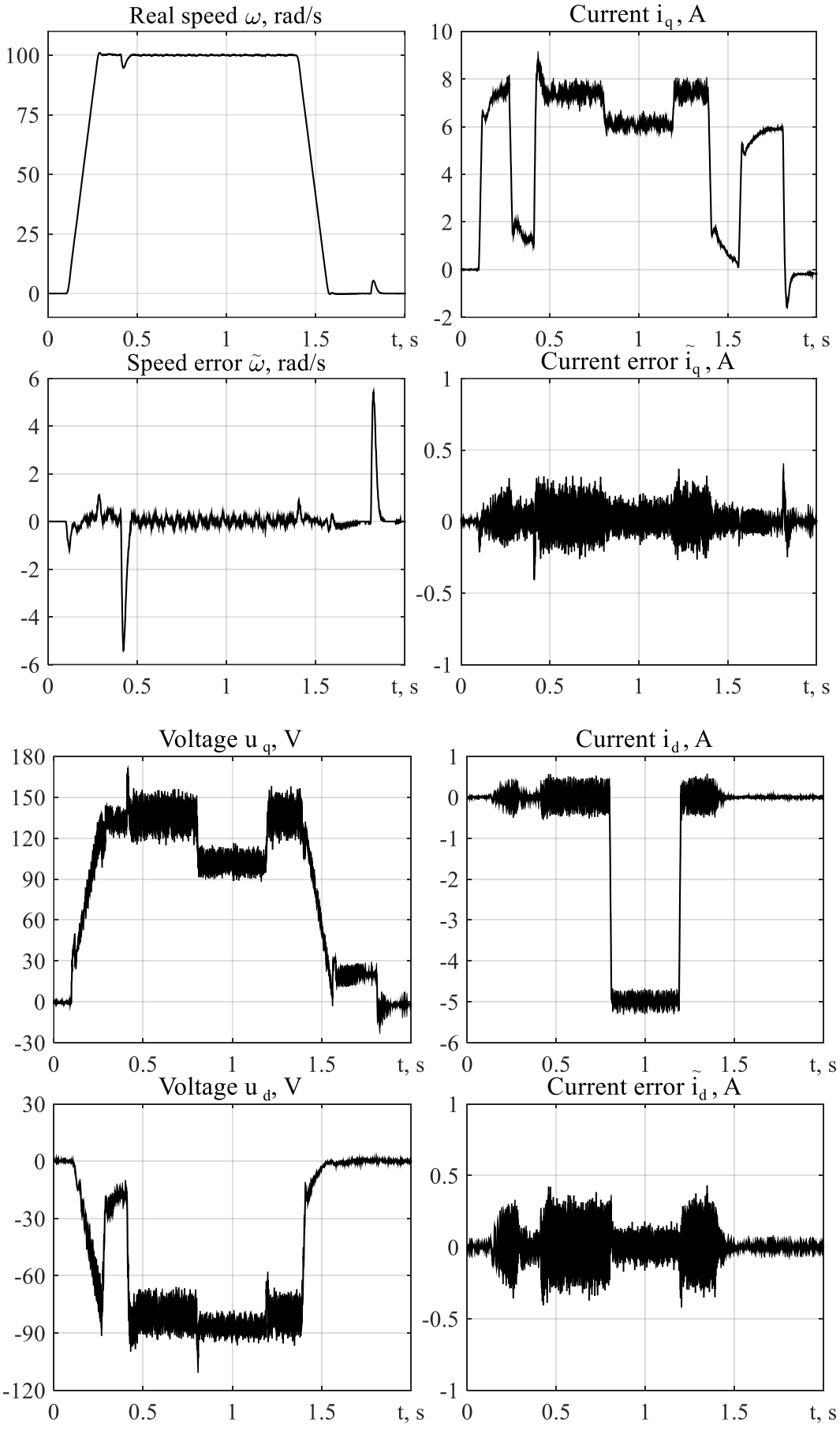

Fig. 3.4. – Transients during experiment if derived speed algorithm is used

The same test is made on the experimental setup presented in the Appendix B. Results are shown in Fig. 3.4. From the comparison of the simulation and experimental results follows that mechanical and electrical parameters are determined correctly as current and voltage curves are almost fully coincide. Differences can be explained by presence of inverter nonlinearities in the experiment, variation of motor parameters that were not evaluated in the motor model.

Conclusions to the Section 3

1. In the Section speed controller for IPMSM was derived. Algorithm provides asymptotic tracking of direct current component and angular speed reference trajectories. Processes in these two subsystems are almost fully decoupled. In low saturated motors (like tested one) performance degradation is negligibly small, so algorithm based on non-saturated model can be used.

2. Controller was tested by means of simulation and experimentally. Experiment almost fully coincides with simulation. Results proof the effectiveness of theoretical findings.

4 POSITION CONTROL OF THE INTERIOR PERMANENT MAGNET SYNCHROLOUS MOTORS

In this Section design of the IPMSM position vector control algorithm is presented [25].

4.1 Formulation of the control problem

Following assumptions are taken:

A.4.1. Stator currents, angular speed and angular position are measured values.

A.4.2. Parameters of the motor are known and constant values.

A.4.3. Torque T_L is unknown, limited, constant or those that is changing slowly.

A.4.4. The rotor position reference θ^* is smooth and bounded function together with its first $\dot{\theta}^*$, second $\ddot{\theta}^*$ and third $\dddot{\theta}^*$ time derivatives; d-axis current reference i_d^* is bounded together with its bounded derivative $\dot{i}_d^*$.

The control problem is to design a position controller, which guarantees following control objectives:

CO.4.1. Asymptotic position θ and direct current component i_d tracking:

$$\lim_{t\to\infty}\left(\tilde{\theta}, \tilde{i}_d\right) = 0, \tag{4.1}$$

where $\tilde{\theta} = \theta - \theta^*$ - rotor position error.

CO.4.2. Asymptotic decoupling of position control and direct current control subsystems.

CO.4.3. Linearization of position control subsystem.

4.2 Design of the position control algorithm

Algorithm is designed in a similar way as proposed in the previous Section for speed control. As parameters are considered as constants, non-saturated model (2.15) is used for the control design. Algorithm is designed using back – stepping design procedure [54].

4.2.1 Position controller design

Relation between speed and position is presented below

$$\dot{\theta} = \omega . \tag{4.2}$$

From (4.2) position error dynamics is

$$\dot{\tilde{\theta}} = \omega - \dot{\theta}^* . \tag{4.3}$$

Speed reference ω^* from (4.3) can be derived as

$$\omega^* = \dot{\theta}^* - \mathrm{k}_\theta \tilde{\theta}, \tag{4.4}$$

where k_θ - proportional position gain.

Substitution (4.4) into (4.3) gives

$$\dot{\tilde{\theta}} = \tilde{\omega} - \mathrm{k}_\theta \tilde{\theta} . \tag{4.5}$$

Solution of the equation (4.5) shows that condition $\lim_{t\to\infty}\left(\tilde{\theta}\right) = 0$ can be achieved if condition $\lim_{t\to\infty}\left(\tilde{\omega}\right) = 0$ is achieved.

For the further design, derivative of the speed reference has to be found. In case of position control, it is not known data, but has to be derived from speed reference (4.4) considering (4.5):

$$\dot{\omega}^* = \ddot{\theta}^* - \mathrm{k}_\theta \dot{\tilde{\theta}} = \ddot{\theta}^* - \mathrm{k}_\theta \tilde{\omega} + \mathrm{k}_\theta^2 \tilde{\theta} . \tag{4.6}$$

4.2.2 Speed controller design

From (2.15) speed error dynamics is following:

$$\dot{\tilde{\omega}} = \left(\mathrm{i}_\mathrm{q}^* + \tilde{\mathrm{i}}_\mathrm{q}\right) \cdot \mu\left(\mathrm{i}_\mathrm{d}^*\right) - \frac{\nu}{\mathrm{J}}\omega^* - \frac{\nu}{\mathrm{J}}\tilde{\omega} - \hat{\mathrm{T}}_\mathrm{L} - \tilde{\mathrm{T}}_\mathrm{L} - \dot{\omega}^* + \frac{3}{2}\frac{1}{\mathrm{J}}\mathrm{p}_\mathrm{n}\left(\mathrm{L}_\mathrm{d} - \mathrm{L}_\mathrm{q}\right)\tilde{\mathrm{i}}_\mathrm{d}\mathrm{i}_\mathrm{q}, \tag{4.7}$$

Quadrature current reference i_q^* from (4.7) taking into account (4.6) is

$$\begin{aligned} i_q^* &= \frac{1}{\mu\left(i_d^*\right)}\left(\hat{T}_L + \frac{\nu}{J}\omega^* + \ddot{\theta}^* + k_\theta^2\tilde{\theta} - \left(k_\omega + k_\theta\right)\tilde{\omega}\right), \\ \dot{\hat{T}}_L &= -k_{\omega i}\tilde{\omega}, \end{aligned} \tag{4.8}$$

Speed error dynamics after substitution (4.8) into (4.7) is

$$\begin{aligned} \dot{\tilde{\omega}} &= -\left(k_\omega + \frac{\nu}{J}\right)\tilde{\omega} - \tilde{T}_L + \mu\left(i_d^*\right)\tilde{i}_q + \frac{3}{2}\frac{1}{J}p_n\left(L_d - L_q\right)\tilde{i}_d\left(\tilde{i}_q + i_q^*\right), \\ \dot{\tilde{T}}_L &= k_{\omega i}\tilde{\omega}. \end{aligned} \tag{4.9}$$

Condition $\lim_{t\to\infty}\left(\tilde{\theta},\tilde{\omega}\right) = 0$ can be achieved only if current errors $\lim_{t\to\infty}\left(\tilde{i}_d,\tilde{i}_q\right) = 0.$

Quadrature current reference derivative is required for the current controller design. It can be taken from (4.8):

$$\begin{aligned} \dot{i}_q^* &= \frac{1}{\mu\left(i_d^*\right)}\left[\dot{\hat{T}}_L + \frac{\nu}{J}\dot{\omega}^* + \dddot{\theta}^* + k_\theta^2\dot{\tilde{\theta}}\right] + \\ &+ \frac{1}{\mu\left(i_d^*\right)}\left[-\left(k_\theta + k_\omega\right)\left(-\left(k_\omega + \frac{\nu}{J}\right)\tilde{\omega} + \mu\left(i_d^*\right)\tilde{i}_q + \frac{3}{2}\frac{1}{J}p_n\left(L_d - L_q\right)\tilde{i}_d i_q\right)\right] - \\ &- \frac{1}{\mu\left(i_d^*\right)^2}\left[\frac{3}{2}\frac{1}{J}p_n\left(L_d - L_q\right)i_d^*\right]\left[\frac{\nu}{J}\omega^* + \ddot{\theta}^* + k_\theta^2\tilde{\theta} - \left(k_\omega + k_\theta\right)\tilde{\omega}\right] + \\ &+ \frac{\left(k_\theta + k_\omega\right)}{\mu\left(i_d^*\right)}\tilde{T}_L \triangleq \dot{i}_{q1}^* + \dot{i}_{q2}^*, \end{aligned} \tag{4.10}$$

where $\dot{i}_{q1}^*$ is known function; $\dot{i}_{q2}^* = \frac{\left(k_\theta + k_\omega\right)}{\mu\left(i_d^*\right)}\tilde{T}_L$ - unknown function.

4.2.3 Q-axis current controller design

From (2.15) q-axis current dynamics is following:

$$\dot{\tilde{i}}_q = -\frac{R_s}{L_q}\left(\tilde{i}_q + i_q^*\right) - \frac{L_d}{L_q}i_d p_n\omega - \frac{1}{L_q}\Psi_M p_n\omega + \frac{1}{L_q}u_q - \dot{i}_q^*. \tag{4.11}$$

Current controller can be composed from (3.6) as

$$\begin{aligned} u_q &= R_s i_q^* + L_d p_n \omega i_d + \Psi_M p_n \omega + L_q \left(\dot{i}_{q1}^* - k_{i1} \tilde{i}_q - x_q \right), \\ \dot{x}_q &= k_{ii} \tilde{i}_q. \end{aligned} \tag{4.12}$$

In (4.12) only known part of the current reference derivative $\dot{i}_{q1}^*$ can be compensated.

Substitution (4.12) into (4.11) gives

$$\begin{aligned} \dot{\tilde{i}}_q &= -k_{iq} \tilde{i}_q - x_q - \frac{\left(k_\theta + k_\omega \right)}{\mu \left(i_d^* \right)} \tilde{T}_L, \\ \dot{x}_q &= k_{ii} \tilde{i}_q. \end{aligned} \tag{4.13}$$

System (4.13) is the same as current error dynamics in speed control controller (3.8) but $k_\theta + k_\omega$ is substituted instead of k_ω.

4.2.4 D-axis current controller design

Current controller for d-axis is designed similarly. From (2.15) d-axis current dynamics is

$$\dot{\tilde{i}}_d = -\frac{R_s}{L_d} \left(\tilde{i}_d + i_d^* \right) + \frac{L_q}{L_d} i_q p_n \omega + \frac{1}{L_d} u_d - \dot{i}_d^*. \tag{4.14}$$

Voltage reference along d-axis is formed from (3.9) as

$$\begin{aligned} u_d &= R_s i_d^* - L_q p_n \omega i_q + L_d \left(\dot{i}_d^* - k_{i1} \tilde{i}_d - x_d \right), \\ \dot{x}_d &= k_{ii} \tilde{i}_d. \end{aligned} \tag{4.15}$$

Substitution (4.15) into (4.14) gives

$$\begin{aligned} \dot{\tilde{i}}_d &= -k_{id} \tilde{i}_d - x_d, \\ \dot{x}_d &= k_{ii} \tilde{i}_d. \end{aligned} \tag{4.16}$$

Total error dynamics of the system is

$$
\begin{aligned}
&\dot{\tilde{\theta}} = \tilde{\omega} - k_{\theta}\tilde{\theta},\\
&\dot{\tilde{\omega}} = -\left(k_{\omega} + \frac{\nu}{J}\right)\tilde{\omega} - \tilde{T}_{L} + \mu\left(i_{d}^{*}\right)\tilde{i}_{q} + \frac{3}{2}\frac{1}{J}p_{n}\left(L_{d} - L_{q}\right)\tilde{i}_{d}\left(\tilde{i}_{q} + i_{q}^{*}\right),\\
&\dot{\tilde{T}}_{L} = k_{\omega i}\tilde{\omega},\\
&\dot{\tilde{i}}_{q} = -k_{iq}\tilde{i}_{q} - x_{q} - \frac{\left(k_{\theta} + k_{\omega}\right)}{\mu\left(i_{d}^{*}\right)}\tilde{T}_{L},\\
&\dot{x}_{q} = k_{ii}\tilde{i}_{q},
\end{aligned}
\tag{4.17}
$$

$$
\begin{aligned}
&\dot{\tilde{i}}_{d} = -k_{id}\tilde{i}_{d} - x_{d},\\
&\dot{x}_{d} = k_{ii}\tilde{i}_{d}.
\end{aligned}
\tag{4.18}
$$

In the system (4.17) three subsystems are presented: the first equation describes rotor position error dynamics, the second and third equations show speed error dynamics, in the last two equations q- axis current error dynamics is presented. Controller gains $\left(k_{\theta}, k_{\omega}, k_{\omega i}, k_{i}, k_{ii}\right) > 0$ can be selected in a such way that whole system will be stable. Results from theory of cascaded systems suggest to construct the current dynamics given by two latest equations in (4.17) to be at least two times faster than speed loop dynamics. The speed dynamics must be faster than position dynamics. In this case, system stability can be achieved.

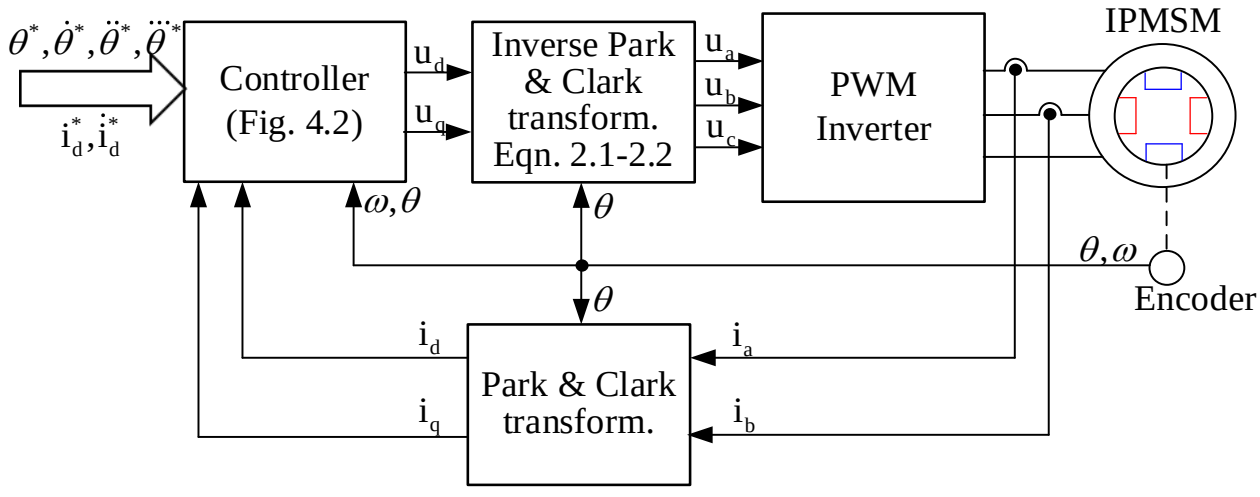

Fig. 4.1. – Block diagram of the electric drive with proposed position controller

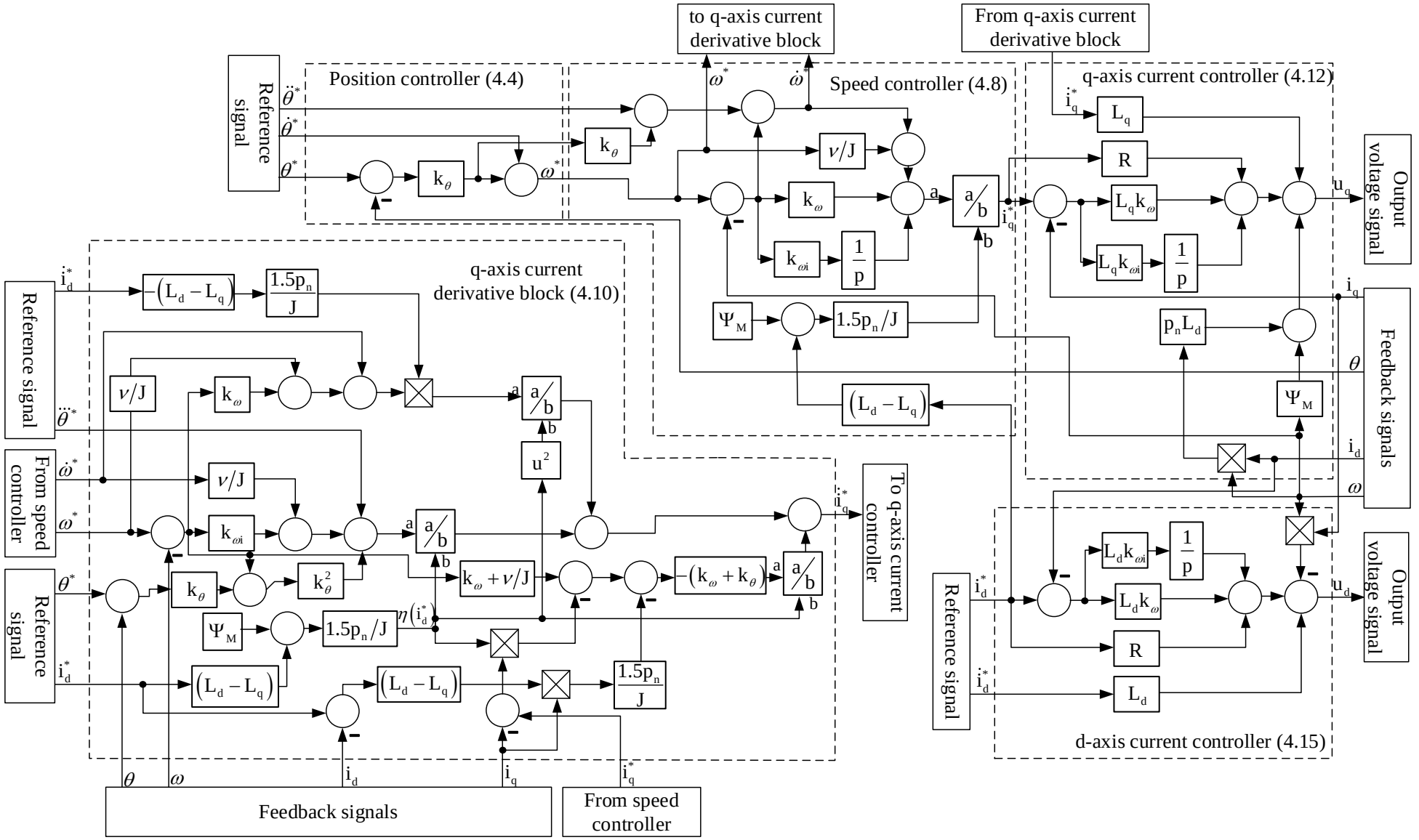

Fig. 4.2. – Structural scheme of the proposed position controller

System (4.18) determine direct current error dynamics are not connected with system (4.17) dynamics. Thus, control objective CO.4.2. is achieved. Moreover, system (4.18) has a typical structure, as a result condition $\lim_{t\to\infty}\left(\tilde{i}_d\right)=0$ is fulfilled for all $\left(k_i, k_{ii}\right)>0$.

Block diagram of the electric drive with proposed controller (4.4),(4.6), (4.8), (4.10), (4.12) and (4.15) is presented in Fig. 4.1. Structural scheme of the controller is presented in Fig. 4.2.

4.3. Research of the position control algorithm

Following test is proposed to analyze behavior of the derived controller.

Standard position reference trajectory θ^* with bounded the first, the second and the third derivative is proposed. Maximum value of the first derivative is $\dot{\theta}^*=100\,\text{rad/s}$, the second time derivative $\ddot{\theta}^*=600\,\text{rad/s}^2$ and the third time derivative $\dddot{\theta}^*=3000\,\text{rad/s}^3$. Motor accelerates from 0.1s to 0.28s. Position is changing linearly from 0.28s to 1.4s. After that motor start to decelerate for 0.18s until position remains constant. Direct current $i_d^*=-5\text{A}$ is applied at 0.8s for 0.4s. Current acceleration and deceleration last for 0.01s. Nominal load torque (14Nm) is applied from 0.4s to 1.8s. Controller gains are $k_{1i}=1000,\ k_{ii}=k_{1i}^2/4,\ k_\omega=100,\ k_{\omega i}=k_\omega^2/2,\ k_\theta=50.$

Motor is modelled using derived model (2.12), (2.13). Static and dynamic inductance values determined in the previous Section are used (Fig. 2.11). Simulation is performed using software MATLAB 2014B for the motor which parameters are presented in Appendix B. Main cycle of the modelling program is presented in Appendix D. From position error and speed error transients in Fig. 4.3, it is clear that processes in position control and direct current subsystems are not fully decoupled as variation of the current i_d causes dynamic errors to the position transient. The reason of this error appearance is following: Controller was designed for non-saturated model, moreover it requires accurate knowledge of the motor parameters. Real motor

parameters tend to variate due to temperature, saturation, time, etc. As a result, coupling between current equations is not fully compensated and such errors emerge.

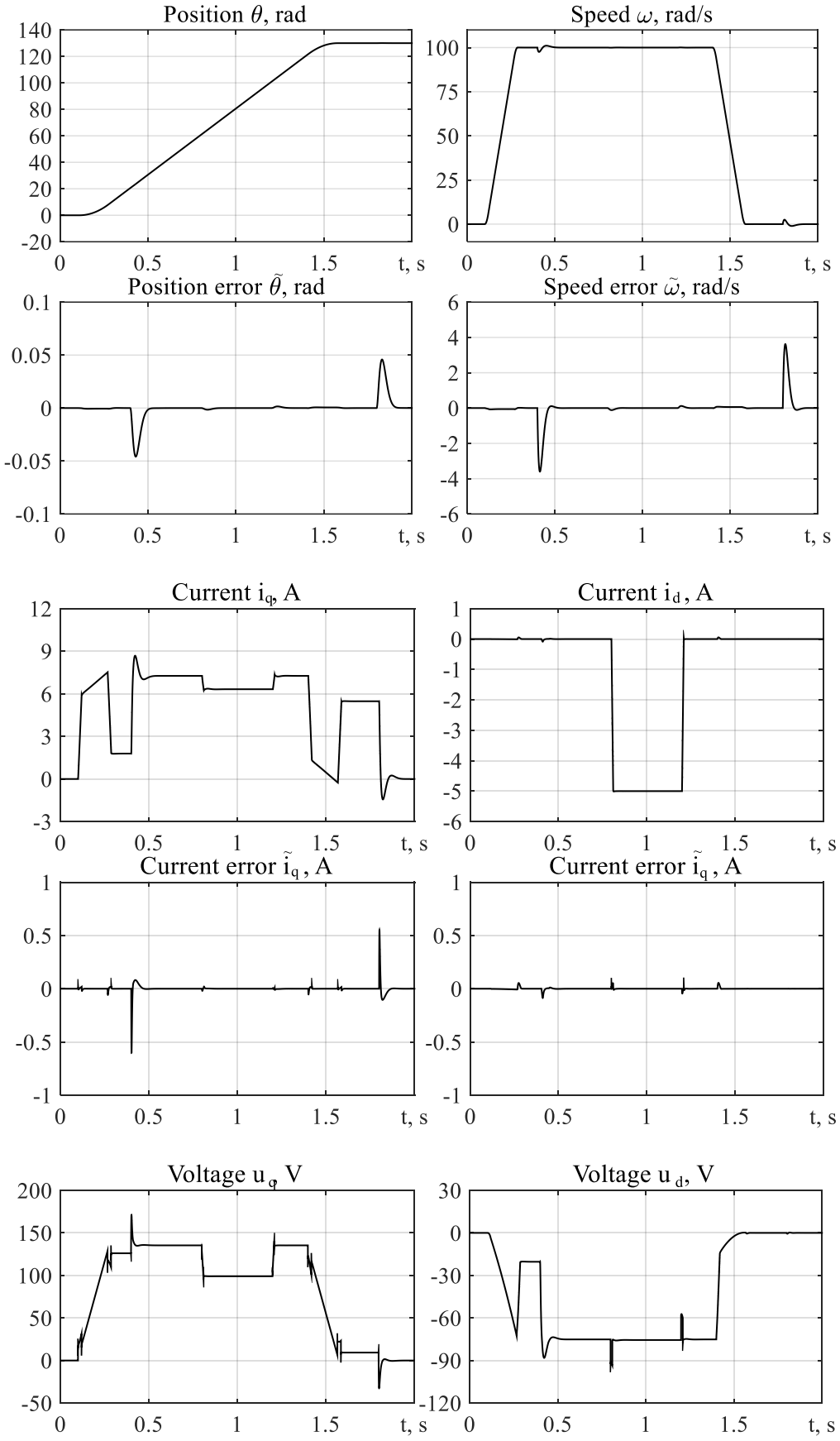

Fig. 4.3. – Transients during simulation if derived speed algorithm is used

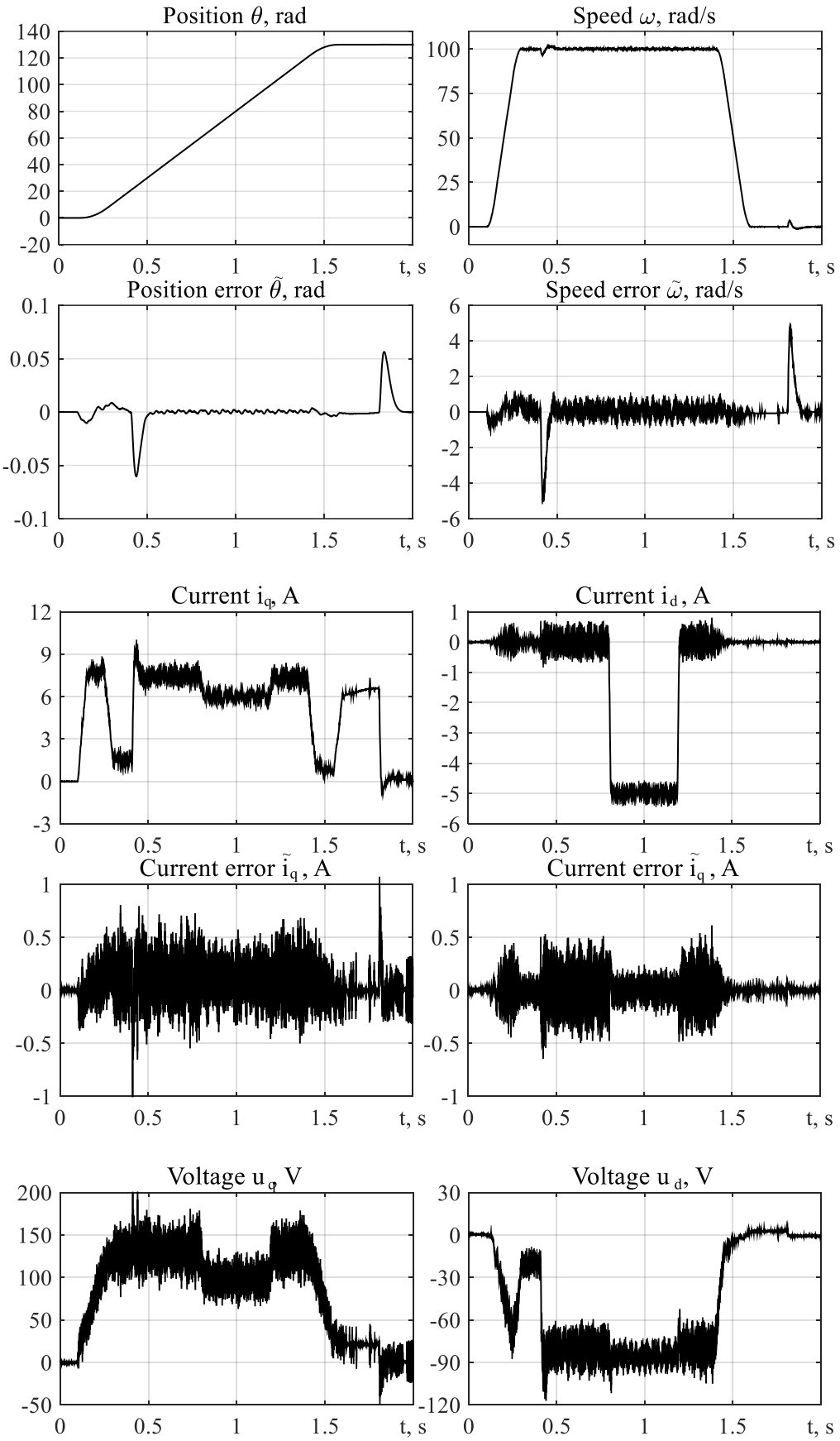

Fig. 4.4. – Transients during experiment if derived position algorithm is used

In case of experiment, inverter nonlinearities can be added to the above-mentioned reasons of control performance deterioration. The same test is made on the experimental setup presented in the Appendix B. Results are shown in Fig. 3.4. From the comparison of the simulation and experimental results, follows that mechanical and electrical parameters are determined correctly as current and voltage curves are almost fully coincide.

Conclusions to the Section 4

1. In the Section position controller for IPMSM was derived. Algorithm provides asymptotic tracking of direct current component and angular position reference trajectories. Processes in these two subsystems are decoupled according to the analysis of error dynamics. Proposed algorithm structure allows to provide high efficient control as position and current i_d are controlled separately.

2. Controller was tested by means of simulation and experimentally. In case of simulation, performance degradation is caused by motor model saturation that was not considered during controller design. The same situation is with experiment, but errors may be also caused by inverter nonlinearities. Saturation of the tested motor in negligibly small, as a result, designed algorithm can be used without significant performance degradation.

5 POSITION CONTROL OF THE INTERIOR PERMANENT MAGNET SYNCHROLOUS MOTORS WITH ADAPTATION TO MECHANICAL PARAMETERS

In this Section design of the IPMSM position vector control algorithm adaptation to mechanical parameters is presented [25].

5.1 Formulation of the control problem

Following assumptions are taken:

A.5.1. Stator currents, angular speed and angular position are measured values.

A.5.2. Resistance R_s, inductances L_d, L_q and PM flux Ψ_M are known and constant values.

A.5.3. Viscous friction coefficient ν, moment of inertia J and load torque T_L are unknown, limited, constant or those that is changing slowly.

A.5.4. The rotor position reference θ^* is smooth and bounded function together with its first $\dot{\theta}^*$, second $\ddot{\theta}^*$ and third $\dddot{\theta}^*$ time derivatives; d-axis current reference i_d^* is bounded together with its bounded derivative $\dot{i}_d^*$.

The control problem is to design adaptive position controller, which guarantees following control objectives:

CO.5.1. Asymptotic position θ and direct current component i_d tracking:

$$\lim_{t\to\infty}\left(\tilde{\theta}, \tilde{i}_d\right) = 0, \tag{5.1}$$

where $\tilde{\theta} = \theta - \theta^*$ - rotor position error.

CO.5.2. Asymptotic decoupling of position control and direct current control subsystems.

CO.5.3. Identification of the unknown parameters.

5.2 Design of the adaptive position control algorithm

Algorithm is designed in a similar way as proposed in the previous Section for position control. As parameters are considered as constants, non-saturated model (2.15)

is used for the control design. Algorithm is designed using back – stepping design procedure [54]. Stability of the adaptive controller is proved using the second Lyapunov method.

Following substitutions are introduced for the speed dynamics equation in the model (2.15):

$$\begin{aligned} \varphi_1 &= \mathrm{J}, \\ \varphi_2 &= \nu/\mathrm{J}, \\ \varphi_3 &= \mathrm{T_L}/\mathrm{J}. \end{aligned} \tag{5.2}$$

Position controller is the same as derived in Section 5.

5.2.1 Position controller design

Relation between speed and position is presented below

$$\dot{\theta} = \omega. \tag{5.3}$$

From (5.3) position error dynamics is

$$\dot{\tilde{\theta}} = \omega - \dot{\theta}^*. \tag{5.4}$$

Speed reference ω^* from (5.4) can be derived as

$$\omega^* = \dot{\theta}^* - \mathrm{k}_\theta \tilde{\theta}, \tag{5.5}$$

where k_θ - proportional position gain.

Substitution (5.5) into (5.4) gives

$$\dot{\tilde{\theta}} = \tilde{\omega} - \mathrm{k}_\theta \tilde{\theta}. \tag{5.6}$$

Solution of the equation (5.6) shows that condition $\lim_{\mathrm{t}\to\infty}\left(\tilde{\theta}\right) = 0$ can be achieved if condition $\lim_{\mathrm{t}\to\infty}\left(\tilde{\omega}\right) = 0$ is achieved.

Speed derivative reference from (5.5) is

$$\dot{\omega}^* = \ddot{\theta}^* - \mathrm{k}_\theta \tilde{\omega} + \mathrm{k}_\theta^2 \tilde{\theta}. \tag{5.7}$$

5.2.2 Speed controller design

Speed error dynamics from (2.15) considering substitutions (5.2) and (5.7) is

$$\dot{\tilde{\omega}} = \frac{3}{2}\frac{\mathrm{p_n}}{\varphi_1}\left(\left(\mathrm{L_d}-\mathrm{L_q}\right)\mathrm{i_d}+\Psi_\mathrm{M}\right)\mathrm{i_q}-\varphi_2\omega-\varphi_3-\left(\ddot{\theta}^*+\mathrm{k}_\theta^2\tilde{\theta}-\mathrm{k}_\theta\tilde{\omega}\right). \tag{5.8}$$

Adaptive speed controller is constructed as

$$\mathrm{i_q^*} = \frac{\hat{\varphi}_1}{\eta\left(\mathrm{i_d^*}\right)}\left(\hat{\varphi}_2\omega+\hat{\varphi}_3+\ddot{\theta}^*+\mathrm{k}_\theta^2\tilde{\theta}-\left(\mathrm{k}_\theta+\mathrm{k}_\omega\right)\tilde{\omega}\right), \tag{5.9}$$

where $\hat{\varphi}_\mathrm{k}$, $\mathrm{k}=(1,2,3)$ - estimated values of the motor parameters, $\tilde{\varphi}_\mathrm{k}=\varphi_\mathrm{k}-\hat{\varphi}_\mathrm{k}$ - estimation errors, $\eta\left(\mathrm{i_d^*}\right)=\frac{3}{2}\mathrm{p_n}\left[\Psi_\mathrm{M}+\left(\mathrm{L_d}-\mathrm{L_q}\right)\mathrm{i_d^*}\right]>0$.

Speed error dynamics after substitution (5.9) into (5.8) is

$$\dot{\tilde{\omega}} = -\mathrm{k}_\omega\tilde{\omega}-\tilde{\varphi}_2\omega-\tilde{\varphi}_3-\frac{\tilde{\varphi}_1}{\varphi_1}\xi+\frac{3}{2}\frac{\mathrm{p_n}}{\varphi_1}\left(\mathrm{L_d}-\mathrm{L_q}\right)\tilde{\mathrm{i}}_\mathrm{d}\mathrm{i_q}+\frac{\eta\left(\mathrm{i_d^*}\right)}{\varphi_1}\tilde{\mathrm{i}}_\mathrm{q}, \tag{5.10}$$

where $\xi=\hat{\varphi}_2\omega+\hat{\varphi}_3+\ddot{\theta}^*+\mathrm{k}_\theta^2\tilde{\theta}-\left(\mathrm{k}_\theta+\mathrm{k}_\omega\right)\tilde{\omega}$

Derivative of (5.9) is following

$$\dot{\mathrm{i}}_\mathrm{q}^* = \xi\frac{\dot{\hat{\varphi}}_1\eta\left(\mathrm{i_d^*}\right)-\hat{\varphi}_1\dot{\eta}\left(\mathrm{i_d^*}\right)}{\eta\left(\mathrm{i_d^*}\right)^2}+\frac{\hat{\varphi}_1}{\eta\left(\mathrm{i_d^*}\right)}\dot{\xi}=\dot{\mathrm{i}}_{\mathrm{q}1}^*+\dot{\mathrm{i}}_{\mathrm{q}2}^*, \tag{5.11}$$

where $\dot{\mathrm{i}}_{\mathrm{q}1}^*$ is known part, $\dot{\mathrm{i}}_{\mathrm{q}2}^*$ - unknown part:

$$\begin{aligned}\dot{\mathrm{i}}_{\mathrm{q}1}^* = {} & \xi\frac{\dot{\hat{\varphi}}_1\eta\left(\mathrm{i_d^*}\right)-\hat{\varphi}_1\frac{3\mathrm{p_n}}{2}\left(\mathrm{L_d}-\mathrm{L_q}\right)\dot{\mathrm{i}}_\mathrm{d}^*}{\eta\left(\mathrm{i_d^*}\right)^2}+\frac{\hat{\varphi}_1}{\eta\left(\mathrm{i_d^*}\right)}\left(\dot{\hat{\varphi}}_2\omega+\hat{\varphi}_2\dot{\omega}^*+\dot{\hat{\varphi}}_3+\dddot{\theta}^*+\mathrm{k}_\theta^2\dot{\tilde{\theta}}\right)- \\ & -\frac{1}{\eta\left(\mathrm{i_d^*}\right)}\left(\mathrm{k}_\theta+\mathrm{k}_\omega-\hat{\varphi}_2\right)\left(-\hat{\varphi}_1\mathrm{k}_\omega\tilde{\omega}+\frac{3}{2}\mathrm{p_n}\left(\mathrm{L_d}-\mathrm{L_q}\right)\tilde{\mathrm{i}}_\mathrm{d}\mathrm{i_q}+\eta\left(\mathrm{i_d^*}\right)\tilde{\mathrm{i}}_\mathrm{q}\right),\end{aligned} \tag{5.12}$$

$$\dot{i}_{q2}^{*}=\frac{\tilde{\varphi}_1}{\eta\left(i_d^{*}\right)\varphi_1}\left(k_\theta+k_\omega-\hat{\varphi}_2\right)\left(\frac{3}{2}p_n\left(L_d-L_q\right)\tilde{i}_d i_q+\eta\left(i_d^{*}\right)\tilde{i}_q\right)-$$
$$-\frac{\hat{\varphi}_1}{\eta\left(i_d^{*}\right)}\left(k_\theta+k_\omega-\hat{\varphi}_2\right)\left(-\tilde{\varphi}_2\omega-\tilde{\varphi}_3-\frac{\tilde{\varphi}_1}{\varphi_1}\xi\right). \quad (5.13)$$

5.2.3 Q-axis current controller design

From (2.15) q-axis current dynamics is following:

$$\dot{\tilde{i}}_q=-\frac{R_s}{L_q}\left(\tilde{i}_q+i_q^{*}\right)-\frac{L_d}{L_q}i_d p_n\omega-\frac{1}{L_q}\Psi_M p_n\omega+\frac{1}{L_q}u_q-\dot{i}_q^{*}. \quad (5.14)$$

Current controller in this case is almost the same as presented in (3.7) and (4.12) however integral component of the controller is absent.

Current controller can be composed from (5.14) as

$$u_q=R_s i_q^{*}+L_d p_n\omega i_d+\Psi_M p_n\omega+L_q\left(\dot{i}_{q1}^{*}-k_{i1}\tilde{i}_q\right). \quad (5.15)$$

In (4.12) only known part of the current reference derivative $\dot{i}_{q1}^{*}$ can be compensated.

Current error dynamics from (5.14) and (5.15) is

$$\dot{\tilde{i}}_q=-\left(k_{i1}+\frac{R}{L_q}\right)\tilde{i}_q-\dot{i}_{q2}^{*}. \quad (5.16)$$

5.2.4 D-axis current controller design

Current controller for d-axis is designed similarly. From (2.15) d-axis current dynamics is

$$\dot{\tilde{i}}_d=-\frac{R_s}{L_d}\left(\tilde{i}_d+i_d^{*}\right)+\frac{L_q}{L_d}i_q p_n\omega+\frac{1}{L_d}u_d-\dot{i}_d^{*}. \quad (5.17)$$

Voltage reference along d-axis is formed from (5.17) as

$$u_d=R_s i_d^{*}-L_q p_n\omega i_q+L_d\left(\dot{i}_d^{*}-k_{i1}\tilde{i}_d\right). \quad (5.18)$$

Substitution (5.18) into (5.17) gives

$$\dot{\tilde{i}}_d = -k_{id}\tilde{i}_d, \tag{5.19}$$

Error dynamics (5.19) guarantees that $\lim_{t\to\infty}\left(\tilde{i}_d\right)=0$ if controller (5.18) is used. Therefore, current component i_d can be excluded from further consideration and identification algorithm design.

5.2.5 Identification algorithm design

Speed error dynamics (5.10) and quadrature axis current error dynamics (5.16), (5.13) can be written in standard form

$$\dot{\tilde{\mathbf{x}}} = \mathbf{A}\tilde{\mathbf{x}} + \mathbf{W}\mathbf{D}^{-1}\tilde{\mathbf{\Phi}}, \tag{5.20}$$

where $\tilde{\mathbf{x}} = \left(\tilde{\omega}, \tilde{i}_q\right)^T$, $\mathbf{A} = \begin{bmatrix} -k_\omega & \eta\left(i_d^*\right)/\varphi_1 \\ 0 & -k_{iq} \end{bmatrix}$, $\mathbf{W} = \begin{bmatrix} w_{11} & w_{12} & w_{13} \\ w_{21} & w_{22} & w_{23} \end{bmatrix}$ is known regressor matrix, $w_{22} = \hat{\varphi}_1\omega\left(\hat{\varphi}_2 - k_\theta - k_\omega\right)/\left(\eta\left(i_d^*\right)\right)$, $w_{11} = -\xi$,

$w_{21} = \left(-\hat{\varphi}_1\xi - \frac{3}{2}p_n\left(L_d - L_q\right)\tilde{i}_d i_q + \eta\left(i_d^*\right)\tilde{i}_q\right)\left(\hat{\varphi}_2 - k_\theta - k_\omega\right)/\left(\eta\left(i_d^*\right)\right)$, $w_{12} = -\omega$,

$w_{13} = -1$, $w_{23} = \hat{\varphi}_1\left(\hat{\varphi}_2 - k_\theta - k_\omega\right)/\left(\eta\left(i_d^*\right)\right)$, $\mathbf{D} = \mathrm{diag}\left[\varphi_1 \quad 1 \quad 1\right]$ – positive-definite diagonal matrix, $\tilde{\mathbf{\Phi}} = \left[\tilde{\varphi}_1 \quad \tilde{\varphi}_2 \quad \tilde{\varphi}_3\right]^T$ – vector of estimation errors.

Let us consider following Lyapunov function

$$V = \frac{1}{2}\left(\tilde{\mathbf{x}}^T\mathbf{P}\tilde{\mathbf{x}} + \tilde{\mathbf{\Phi}}^T\mathbf{\Lambda}^{-1}\mathbf{D}^{-1}\tilde{\mathbf{\Phi}}\right), \tag{5.21}$$

where $\mathbf{P} = \mathrm{diag}\left[1 \quad \gamma\right]$ and $\Lambda = \mathrm{diag}\left[\lambda_1 \quad \lambda_2 \quad \lambda_3\right]$.

Function (5.21) can be transformed to an algebraic form

$$V = \frac{1}{2}\left(\gamma\tilde{i}_q^2 + \tilde{\omega}^2 + \frac{1}{\lambda_5}\frac{1}{\varphi_5}\tilde{\varphi}_5^2 + \frac{1}{\lambda_6}\tilde{\varphi}_6^2 + \frac{1}{\lambda_7}\tilde{\varphi}_7^2\right) \geq 0 \tag{5.22}$$

The time derivative of (5.21) is

$$\dot{V} = \frac{1}{2}\tilde{\mathbf{x}}^{T}\left(\mathbf{A}^{T}\mathbf{P} + \mathbf{P}\mathbf{A}\right)\tilde{\mathbf{x}} + \tilde{\mathbf{x}}^{T}\mathbf{W}\mathbf{D}^{-1}\tilde{\mathbf{\Phi}} + \dot{\tilde{\mathbf{\Phi}}}^{T}\mathbf{\Lambda}^{-1}\mathbf{D}^{-1}\tilde{\mathbf{\Phi}}. \tag{5.23}$$

Function (5.23) can be transformed to an algebraic form

$$\begin{aligned}
\dot{V} = &-\gamma\left(k_{i1} + \frac{R_s}{L_q}\right)\tilde{i}_q^2 - \gamma\tilde{i}_q\left(\hat{\varphi}_2 - k_\theta - k_\omega\right)\cdot \\
&\cdot\left(\hat{\varphi}_1\left(-\tilde{\varphi}_2\omega - \tilde{\varphi}_3 - \frac{\tilde{\varphi}_1}{\varphi_1}\xi\right) - \frac{\tilde{\varphi}_1}{\varphi_1}\left(\frac{3}{2}p_n\left(L_d - L_q\right)\tilde{i}_d i_q + \eta\left(i_d^*\right)\tilde{i}_q\right)\right) - \\
&-k_\omega\tilde{\omega}^2 - \tilde{\varphi}_2\omega\tilde{\omega} - \tilde{\varphi}_3\tilde{\omega} - \frac{\tilde{\varphi}_1}{\varphi_1}\xi\tilde{\omega} + \frac{\tilde{\omega}}{\varphi_1}\left(\frac{3}{2}p_n\left(L_d - L_q\right)\tilde{i}_d i_q + \eta\left(i_d^*\right)\tilde{i}_q\right) + \\
&+\frac{1}{\lambda_1}\frac{1}{\varphi_1}\tilde{\varphi}_1\dot{\tilde{\varphi}}_1 + \frac{1}{\lambda_2}\tilde{\varphi}_2\dot{\tilde{\varphi}}_2 + \frac{1}{\lambda_3}\tilde{\varphi}_3\dot{\tilde{\varphi}}_3.
\end{aligned} \tag{5.24}$$

As parameters φ_k are constants $\dot{\tilde{\mathbf{\Phi}}} = -\dot{\hat{\mathbf{\Phi}}}$ and adaptation algorithm is

$$\dot{\tilde{\mathbf{\Phi}}} = -\dot{\hat{\mathbf{\Phi}}} = -\mathbf{\Lambda}\mathbf{W}^{T}\tilde{\mathbf{x}}. \tag{5.25}$$

In the algebraic form (5.25) is

$$\begin{aligned}
\dot{\hat{\varphi}}_1 &= -\lambda_1\left[\xi\tilde{\omega} + \frac{\gamma\tilde{i}_q}{\eta\left(i_d^*\right)}\left(\hat{\varphi}_2 - k_\theta - k_\omega\right)\cdot\right. \\
&\left.\cdot\left(-\hat{\varphi}_1\xi - \frac{3}{2}p_n\left(L_d - L_q\right)\tilde{i}_d i_q - \eta\left(i_d^*\right)\tilde{i}_q\right)\right], \\
\dot{\hat{\varphi}}_2 &= -\lambda_2\left[\frac{\gamma\tilde{i}_q}{\eta\left(i_d^*\right)}\left(\hat{\varphi}_2 - k_\theta - k_\omega\right)\left(-\hat{\varphi}_1\omega\right) + \omega\tilde{\omega}\right], \\
\dot{\hat{\varphi}}_3 &= -\lambda_3\left[\frac{\gamma\tilde{i}_q}{\eta\left(i_d^*\right)}\left(\hat{\varphi}_2 - k_\theta - k_\omega\right)\left(-\hat{\varphi}_1\right) + \tilde{\omega}\right].
\end{aligned} \tag{5.26}$$

In this case

$$\dot{V} = -\left(k_{i1} + \frac{R}{L_q} \right) \tilde{i}_q^2 - k_\omega \tilde{\omega}^2 + \\ + \frac{3}{2} \frac{p_n}{\varphi_5} \tilde{\omega} \left(\left(L_d - L_q \right) \tilde{i}_d i_q + \left(\left(L_d - L_q \right) i_d^* + L_{md} i_f \right) \tilde{i}_q \right). \tag{5.27}$$

Condition $\dot{V} \le 0$ for stability of closed-loop system (5.20) can always be achieved by proper selection of k_θ, k_ω, k_{i1}.

From $V > 0$, $\dot{V} \le 0$, we conclude that vectors $\tilde{\mathbf{x}}$, $\tilde{\mathbf{\Phi}}$ are bounded $\forall\ t \ge 0$. Direct application of Barbalat's lemma [56] establishes that $\lim \left\| \tilde{\mathbf{x}}(t) \right\| = 0$.

If positive constant T exists, such that the 3×3 matrix

$$\int_t^{t+T} \mathbf{W}^T(\tau) \mathbf{W}(\tau) d\tau > 0 \tag{5.28}$$

is positive-definite $\forall\ t \ge 0$ (condition of persistency of excitation), then $\left(\tilde{\mathbf{x}}, \tilde{\mathbf{\Phi}} \right) = 0$ is globally exponentially stable equilibrium point for the linear time-varying system (5.20)

$$\dot{\tilde{\mathbf{x}}} = \mathbf{A}\tilde{\mathbf{x}} + \mathbf{W}\mathbf{D}^{-1}\tilde{\mathbf{\Phi}}, \\ \dot{\tilde{\mathbf{\Phi}}} = -\mathbf{\Lambda}\mathbf{W}^T\tilde{\mathbf{x}}. \tag{5.29}$$

Fulfilment of condition $\lim_{t \to \infty} \left(\tilde{\mathbf{x}} \right) = 0$, leads to $\lim_{t \to \infty} \left(\tilde{\theta} \right) = 0$. As a results control objectives CO.5.1 – CO.5.3 are achieved.

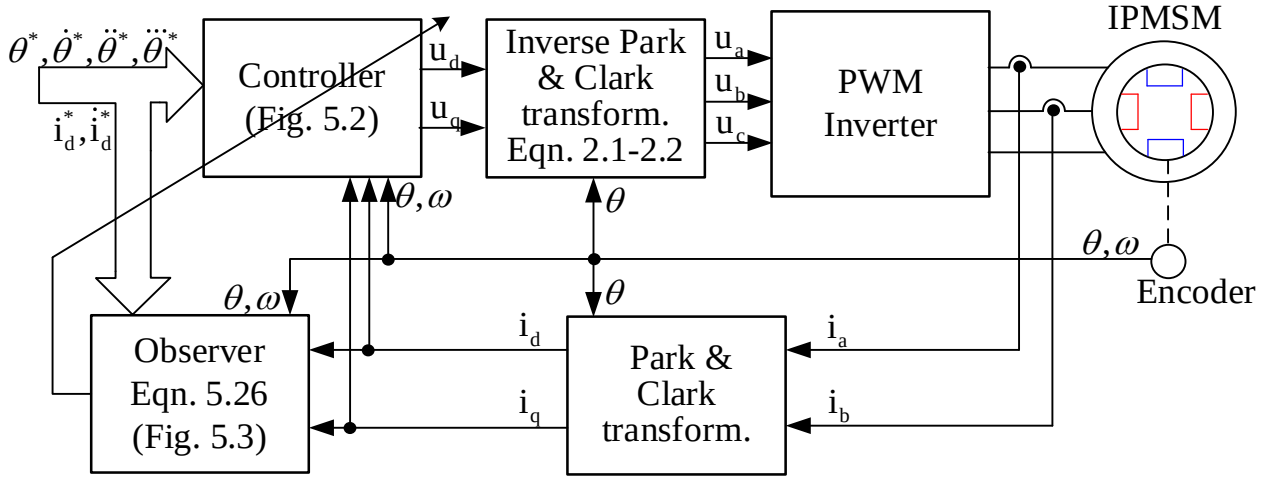

Fig. 5.1. – Block diagram of the electric drive with proposed position adaptive controller

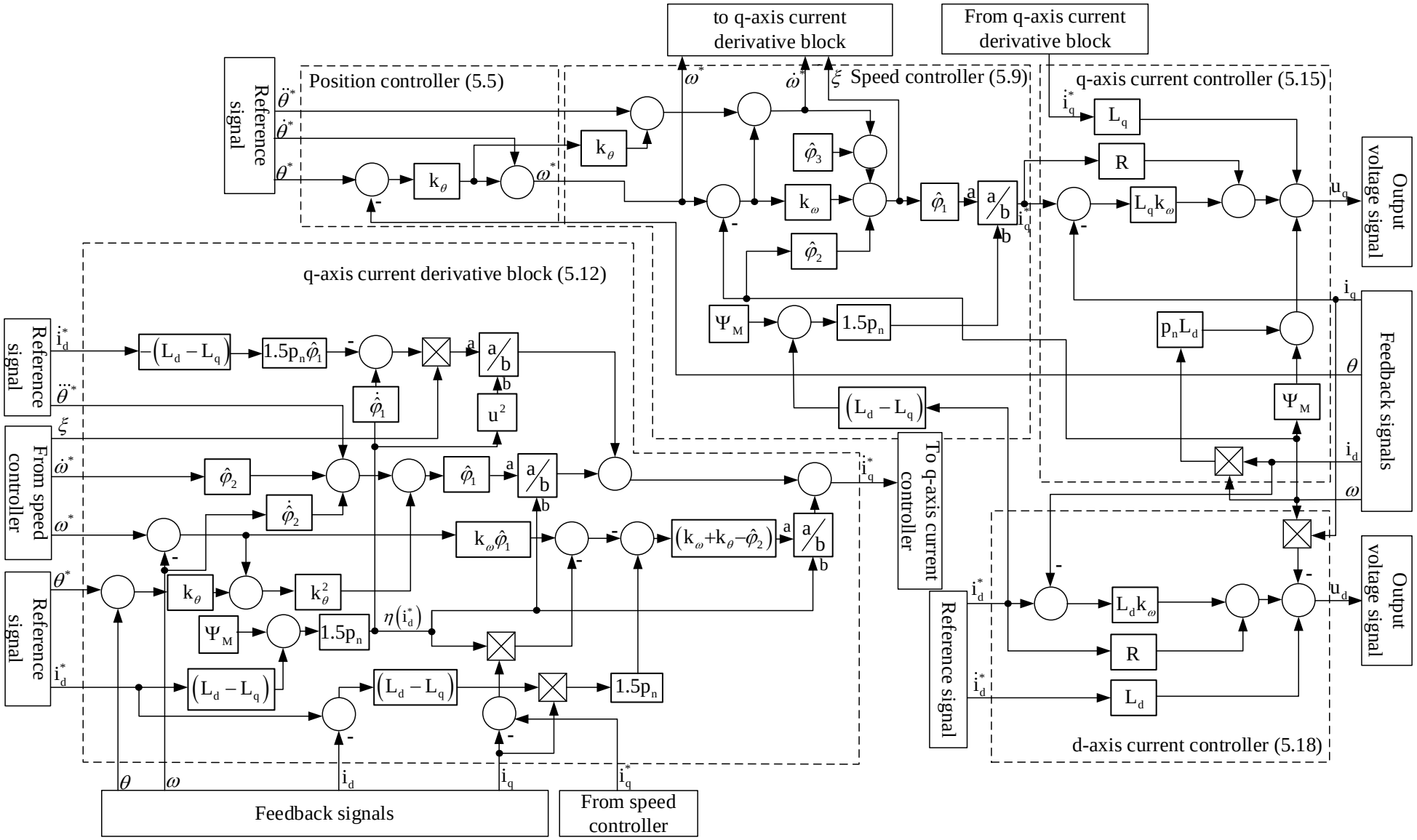

Fig. 5.2. – Structural scheme of the proposed position adaptive controller

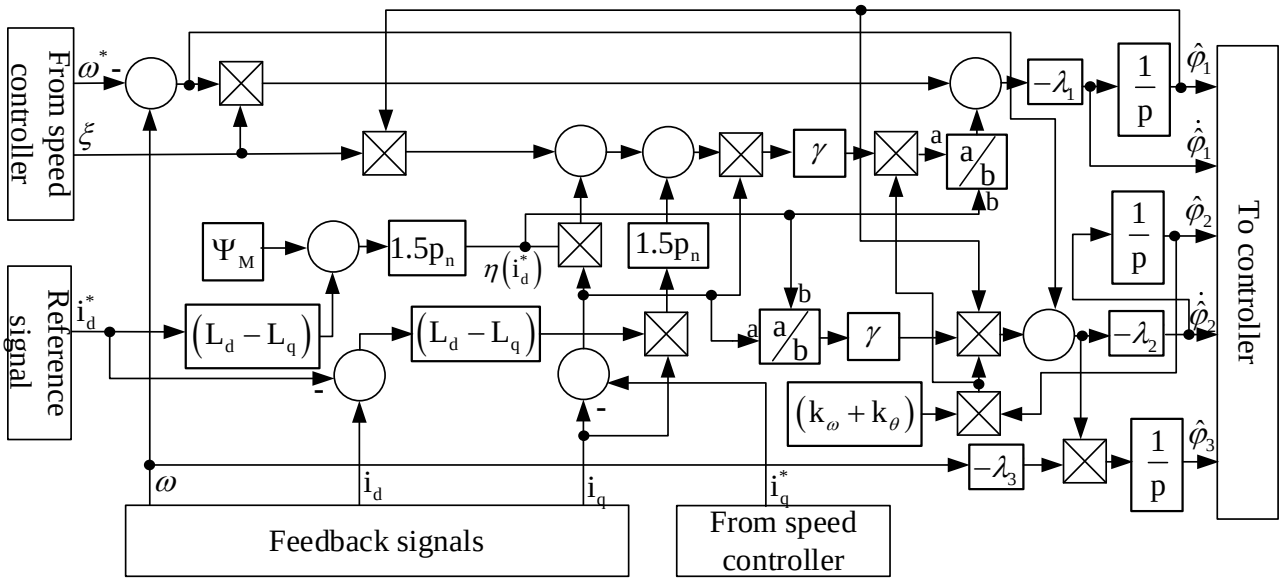

Fig. 5.3. – Structural scheme of the adaptive observer

Mechanical parameters can be correctly identified only if conditions of persistency of excitation are fulfilled, so speed and acceleration have to variate during the test. Block diagram of the electric drive with proposed controller (5.5), (5.7), (5.9) , (5.12), (5.15), (5.18) and (5.26) is presented in Fig. 5.1. Structural scheme of the controller is presented in Fig. 5.2. Structural scheme of the observer is presented in Fig. 5.3.

5.3 Research of the adaptive position control algorithm

Following test is proposed to test adaptive algorithm: Sinusoidal position reference θ^* is applied. Direct axis component falls to the value -2A at 0.9s and returns back to 0A at 2.2s. Nominal load torque (14Nm) is initially applied and its value does not change during the test. Following estimation gains are proposed for the faster mechanical parameter identification: $\lambda_1 = 10^{-4}$, $\lambda_2 = 120$, $\lambda_3 = 10^4$ and $\gamma = 0.3$. Coefficient gains are $\text{k}_{1\text{i}} = 1000$, $\text{k}_\omega = 200$ and $\text{k}_\theta = 100$. Simulation results are presented in Fig. 5.4 and Fig. 5.5. Algorithm is simulated for the motor which parameters are presented in Appendix B. Main cycle of the modelling program is presented in Appendix E.

From Fig. 5.4 and Fig. 5.5 follows that control objectives are achieved. Mechanical parameters are estimated correctly. After estimation is finished, position

error approaches to zero. Direct current component is changing during the test; however, it has no influence on speed and position transients.

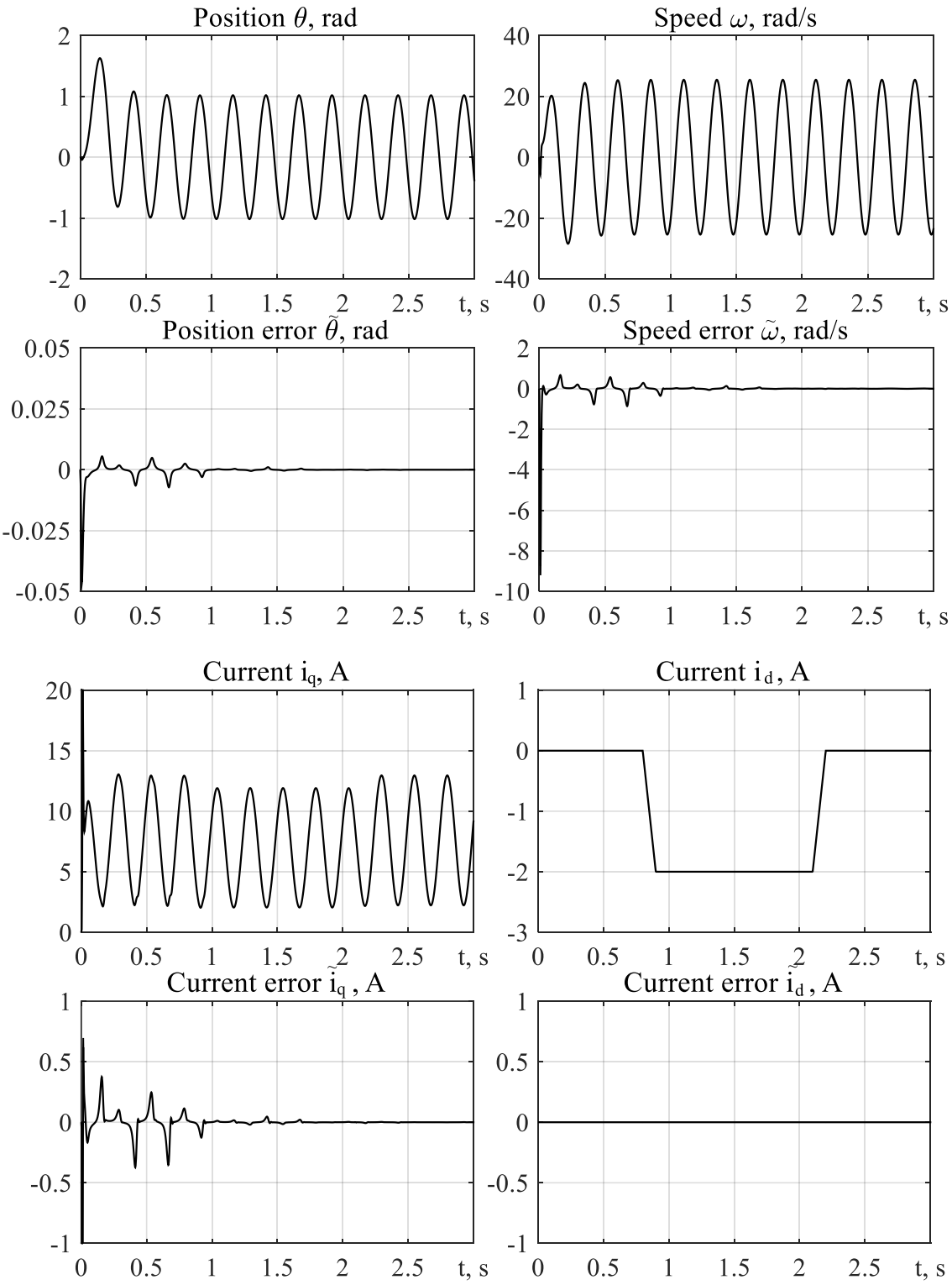

Fig. 5.4. – Transients during simulation if derived adaptive position algorithm is used

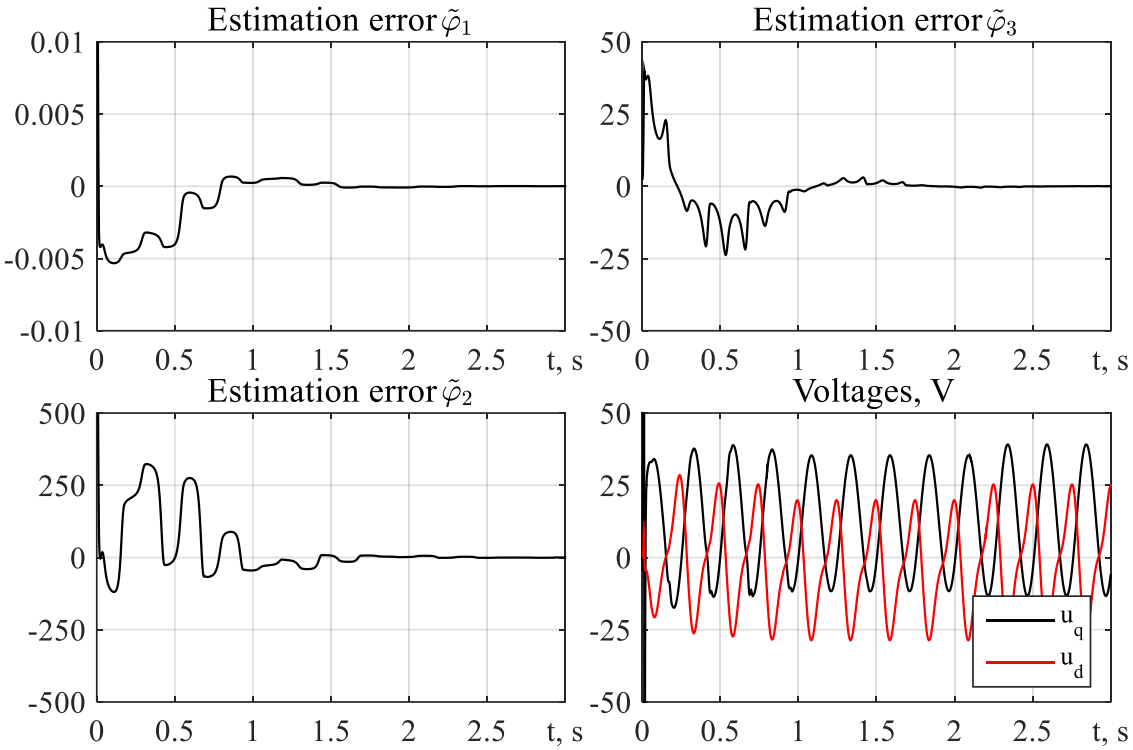

Fig. 5.5. – Transients of φ_1, φ_2, φ_3 estimations during simulation test

Conclusions to the Section 5

1. Adaptive position controller is designed and simulated. Algorithm allows online determination of mechanical parameters: moment of inertia, viscous friction coefficient and load torque.

2. Control objectives are fulfilled if conditions of persistency of excitation are met. Parameters are estimated correctly. Position control subsystem and direct current control subsystem are decoupled. Position and current error decays to zero when identification process is finished.

6 STARTUP PROJECT

Designed position algorithm with the adaptation to the mechanical parameters can be implemented to the standard frequency converters as a separate control program. The control algorithm utilization can be beneficial for the system where accurate positioning is required. Moreover, if system operates with variable moment of inertia, load torque and/or viscous friction coefficient, proposed control system will provide high performance unlike common vector systems where mechanical parameters mismatch lead to performance deterioration. Description of the startup idea, its pros and cons are presented in the table 6.1 – 6.2.

Table 6.1 – Description of the project idea

Content of the idea	Application directions	Benefits for users
Practical realization of the frequency converters with implemented position control algorithms with the adaptation to mechanical parameters. Converters with proposed algorithms allow increasing efficiency and performance of the systems that require accurate position tracking.	1. Asymptotic position tracking	Possibility to provide accurate position tracking for the systems where it is required
	2. Observation of the mechanical parameters	Possibility to obtain accurate values of the mechanical parameters of the system for the further analysis

Table 6.2 - Determination of strong, weak and neutral characteristics of the project idea

№	Technical-economic characteristics of the idea	(Potential) Competitor product/concepts				W (weak side)	N (neutral side))	S (strong side)
		My project	Competitor1	Competitor2	Competitor3			
1.	Possibility to provide position tracking	Yes	Yes	No	No		+	
2.	Possibility to observe load torque	Yes	Yes	Yes	No		+	
3.	Possibility to observe moment of inertia and adapt to its change online	Yes	No	No	No			+
4.	Necessity to measure speed/position	Yes	Yes	No	No	+		
5.	Cost	Low	Low	High	High			+

Competitiveness of the proposed product can be observed from the conducted analysis of strong, weak and neutral characteristics of the product. Technology of the

proposed project creation was discussed and results of the discussion are presented in table 6.3.

Table 6.3 – Technological feasibility of the project idea

№	The idea of the project	Technologies for its implementation	Availability of technologies	Accessibility of technologies
1	Production of the frequency converter	Assembly from existed components	Available	Accessible
		Assembly from self-created components	Must be developed	Inaccessible
2	Setting up the control system	Self-tuning instructions	Must be developed	Accessible
		Performed by specialists	Allowed	Accessible
Selected technology for the realization of the project idea: assembly of the frequency converter from the existed components. System tuning is performed by specialists.				

Analysis of the market opportunities to start project is presented in table 6.4 – 6.13.

Table 6.4 – Initial characteristic of the potential market for the start-up project

№	Indicators of the market condition (name)	Feature
1	Number of main players,	3
2	Total sales, UAH / s.u.	8000
3	Market Dynamics (Quality rating)	Growing
4	Existed restrictions (specify the character of restrictions)	None
5	Specific requirements for standardization and certification	None
6	Average rate of the profitability in the industry (or market), %	ARR=24,8%

Table 6.5 – Characteristics of potential clients of the startup project

№	Need that shapes the market	Target audience (target market segments)	Differences in behavior of different potential target customer groups	Consumer requirements
1.	Need to provide accurate position control of the electric drive (precision application, robotics)	Consumer whose goal is to provide accurate position control for the specific electromechanical system	The target group has no restrictions, except of the necessary means	Proposed frequency converter has to provide accurate position control for any applications. System tuning has to be performed by specialist.

Table 6.6 – Threat factors

№	Factor	Threat content	Possible company reaction
1.	Competition	Presence of the major international companies in the market	Advertising campaign.
2.	Cost	Initial cost for the product will be higher comparing to the other manufacturers	Find opportunities to use cheaper components without quality degradarion.

Table 6.7 – Opportunity factors

№	Factor	Content of opportunity	Possible reaction of the company
1.	Increasing the needs of potential users	Necessity of the customers to increase efficiency and performance of the controlled system/ process	Expanding the advertising campaign and providing free product service for some time
2.	Entering the International market	Expansion of the market, increase of the producing rates and as a result decrease of the one unit of the product.	Cooperation with international manufacturers.

Table 6.8 – Step-by-step analysis of competition in the market

Features of the competitive environment	What is this characteristic	Impact on the activity of the enterprise (possible actions of the company to be competitive)
1.Type of competition: oligopoly	There are 3 major companies.	Possible problems entering the market. Necessity to improve your advertising campaign
2. The level of - competition: international	Two companies are international, one is Ukrainian	Possibility to cooperate with international companies
3. Sectoral distribution: intersectoral	The product can be used different sectors	-

Table 6.8 continuation

4. Competition by type of goods	Competitor products are different because of different control algorithm is used	Created controller can be implemented in the frequency converters with different design.
5. By the nature of competitive advantages: non-price	Improvement of existing technologies in the field	Usage of the improved position control algorithm to provide better performance
6. By intensity	Competitors are well-known brands in this market segment	Creation your own brand and providing active advertising campaign or collaboration with famous trademarks

Table 6.9 - Analysis of competition in the industry by M. Porter

Analysis components	Direct competitors in the field	Potential competitors	Suppliers	Clients	Substitute products
	Provide a list of direct competitors	Identify entry barriers	Determine suppliers' force factors	Determine consumer force factors	Substitute threat factors
Conclusions	There are 3 competitors in the market. Each competitor offers products that	Opportunities to enter the market are existed. Depending on the consumers’	There are no suppliers. The company directly agrees with	Customers select products depending on required technical performance	Substitute goods may perform some of the functions that are proposed

	are similar to the offered but not identical	needs, all 3 companies can compete	the buyer the terms of the purchase.	and its price, usually choice falls under better-known companies	

Table 6.10 - Justification of competitiveness factors

№	Competitiveness Factor	Justification
1.	The ability to provide accurate position control	The product is more appealing for the customers as it provides precise position control
2.	The ability to observe mechanical parameters	Determination of the mechanical parameters allows providing more efficient system control

Table 6.11 – Comparative analysis of the strengths and weaknesses of the product

№	Competitiveness factor	Points 1-20	Rating of competing products compared to the proposed project						
			–3	–2	–1	0	+1	+2	+3
1	The ability to provide accurate position control	5			+				
2	The ability to observe mechanical parameters	10		+					

Table 6.12 – SWOT- analysis of the startup project

Strengths: ability to provide accurate position control without knowing mechanical parameters of the motor and system	Weaknesses: availability of the similar technologies in the market
Opportunities: entering the international market	Threats: High level of competition

Table 6.13 – Alternatives to market implementation of a startup project

№	Alternative (indicative set of actions) market behavior	Probability of receiving resources	Terms of implementation
1.	Assembly of the product from the existed components and tuning by the project developer.	90%	2 months
2.	Assembly of the product from the existed components and tuning using manual	45%	4 months

From the analysis of the market implementation opportunities follows that behavior 1 is more attractive as implementation terms are smaller and possibility to get resources is higher.

Results of development of the market strategy are presented in table 6.14 – 6.17.

Table 6.14 – Selection of target groups of potential consumers

№	Description of the target audience profile	Consumer willingness to accept the product	Target demand within the target group (segment)	Intensity of competition in the segment	Ease of entry into the segment
1.	For facilities	There may be a problem with implementation of the product into intellectual systems	Users will be interested in a such system, as it allows to achieve control objectives	There are 3 competitors in this market segment, however similar products do not allow to observe mechanical parameters.	In order to fully compete with the other companies, proposed product has to have high level of synergy with existed intellectual systems
2.	For individual use	At the start point of the sales, cost per one unit may be too high.			There may be some problems entering the segment due to product high cost
Which target groups are selected: Facilities are selected as a target group, as for the facilities achieving control objectives is more valuable than cost.					

Table 6.15 – Defining a Basic Development Strategy

№	Selected alternative to the project development	Market outreach strategy	Key competitive positions in line according to the chosen alternative	Basic development strategy
1	Build product from existed design details and tune by project developer	Mass marketing	Accurate position control, observation of the mechanical parameters	Differentiation strategy

Table 6.16 – Defining a basic competitive behavior strategy

№	Is the project a pioneer in the market?	Will the company look for new customers or take on existing competitors?	Will the company copy the key features of a competitor's product, and which ones?	Competitive behavior strategy
1	No	Finding new customers	Yes, developing the ability to perform additional types of transactions	Leader strategy

Table 6.17 – Definition of positioning strategy

№	Target product requirements	Basic development strategy	Key competitive positions of your own startup project	Selection of associations to form an integrated position for their own project (three key ones)

Table 6.17 Continuation

1	Provide high-precision position control	Differentiation strategy	Accurate position control, observation of the mechanical parameters	Position control, adaptation to mechanical parameters

Development of the mechanical strategy of the startup project is presented in table 6.18 – 6.22.

Table 6.18 – Identifying key benefits of the concept of a potential good

№	Need	The benefit that the product offers	Key Competitive Advantages (existing or which should be created)
1	Accurate position control	Ability to control rotor position without knowledge of the mechanical parameters	Common control techniques either require predefined values of the mechanical parameters or provide less accurate control.
2	Observation of the mechanical parameters	Ability to observe mechanical parameters during operation	Possibility to observe system state without additional equipment.

Table 6.19 – Description of the three levels of the product model

Product levels	Essence and components
I. Idea of the product	Creation of the frequency converter with implemented position algorithm with adaptation to the mechanical parameters

Table 6.19 Continuation

II. The product in the specific performance	Properties/characteristics	M/Nm	Wr/Tx /Tl/E/Op
	1. The ability to provide accurate position control 2. Ability to estimate mechanical parameters	-	-
	Product tuning will be done by the developer		
	Marking is present		
	The proposed project. Frequency converter with implemented position algorithm with adaptation to the mechanical parameters		
III. Product with reinforcement	Initial free tuning.		

Table 6.20 – Determination of price setting limit

№	Price level for substitute products	Price level for analog products	The level of income of the target consumer group	The upper and lower limits of setting the price for a product / service
1	10000	12000	50000	8000-15000

Table 6.21 – Formation of marketing system

№	Purchasing behavior of target customers	Marketing functions to be performed by the supplier	Depth of sales channel	Optimal sales system

Table 6.21 Continuation

1	Purchase of the frequency converter and its tuning and repair if needed	Selling	0 - directly, 1 - through one mediator	Own and involved

Table 6.22 – The concept of marketing communications

№	Specific behavior of target customers	Communication channels used by target customers	Key positions selected for positioning	Objectives of the advertising	The concept of advertising appeal
1	Purchase of the frequency converters to fulfill control objectives.	Internet, live communication.	position control, observation of the mechanical parameters.	Show the advantages of the developed algorithm and frequency converter comparing to competitors.	Online advertising, live communication with potential customers.

Conclusions to the Section 6

1. In the Section, startup project is presented. It is proposed to create frequency converter with implemented position control with adaptation to the mechanical parameters for IPMSM.

2. From the investigation follows that proposed product can compete with existed analogs as it allows controlling position without knowing mechanical parameters. As market dynamics is growing it can be predicted that product demand will increase. Also, analysis shows that assembly of the frequency converters from the existed components is more advantageous as it requires less amount of resources. Barriers are high initial cost and necessity to integrate the product into intellectual systems.

CONCLUSION

In the thesis, several control algorithms of the IPMSMs designed to improve efficiency and performance of the electromechanical systems are presented. Task of the inductance determination of the IPMSMs considering saturation and mechanical parameters estimation are solved. In the thesis following results were achieved:

1. Existed methods for inductances determination were observed, sorted and analyzed. As a result of the analysis, necessity to create tests that combine simplicity, high accuracy and convenience of usage is formulated. Similar analysis is made for mechanical parameters estimation methods and actuality of creation of the control algorithm with adaptation to mechanical parameters is justified.

2. IPMSM models with different level of simplification, starting from the model in flux linkage terms ending with conventional non-saturated IPMSM model, are derived and analyzed. Usage of the models with flux linkages instead of ones with inductances is proved.

3. Two tests are proposed and experimentally verified to determine inductances of the IPMSM considering saturation along one axis. Tests advantages and drawbacks are compared. Four methods for static and dynamic inductance calculation are presented and results are analyzed.

4. Speed control algorithm based on non-saturated model is designed. Algorithm provides asymptotic tracking of the speed and direct current component, asymptotic decoupling of the speed and direct current control subsystems. Derived algorithm is tested for the motor with small saturation level by means of simulation and experimentally. Derived position control algorithm is designed similarly and as a result has similar properties.

5. Position controller with the adaptation to mechanical parameters is designed. Algorithm provides speed, position and quadrature current tracking together with accurate estimation of the moment of inertia, viscous friction coefficient and load torque. Position control subsystem and direct current control subsystem are decoupled.

REFERENCES

[1]. Pellegrino, Gianmario, Jahns, Thomas, Bianchi, Nicola, Soong, Wen, Cupertino and Francesco. "The Rediscovery of Synchronous Reluctance and Ferrite Permanent Magnet Motors", SpringerBriefs in Electrical and Computer Engineering (2016)

[2]. W. L. Soong and T. J. E. Miller, "Field-weakening performance of brushless synchronous AC motor drives," in IEE Proceedings - Electric Power Applications, vol. 141, no. 6, pp. 331-340, Nov. 1994.

[3]. E. Levi and V. A. Levi, "Impact of dynamic cross-saturation on accuracy of saturated synchronous machine models," in *IEEE Transactions on Energy Conversion*, vol. 15, no. 2, pp. 224-230, June 2000.

[4]. B. Stumberger, G. Stumberger, D. Dolinar, A. Hamler and M. Trlep, "Evaluation of saturation and cross-magnetization effects in interior permanent-magnet synchronous motor," in IEEE Transactions on Industry Applications, vol. 39, no. 5, pp. 1264-1271, Sept.-Oct. 2003.

[5]. IEEE Standard Procedures for Obtaining Synchronous Machine Parameters by Standstill Frequency Response Testing (Supplement to ANSI/IEEE Std 115-1983, IEEE Guide: Test Procedures for Synchronous Machines), IEEE Std 115A-1987 (1987)

[6]. Viktor Bobek, PMSM Electrical Parameters Measurement Document Number:AN4680, Freescale Semiconductor, Inc. – 2013

[7]. Y. Jeong and S. Sul, "Adaptive Flux Observer with On-line Inductance Estimation of an IPMSM Considering Magnetic Saturation," *2005 IEEE 36th Power Electronics Specialists Conference*, Recife, 2005, pp. 2467-2473. doi: 10.1109/PESC.2005.1581979

[8]. Z. Li and H. Li, "MTPA control of PMSM system considering saturation and cross-coupling," *2012 15th International Conference on Electrical Machines and Systems (ICEMS)*, Sapporo, 2012, pp. 1-5.

[9]. S. Mukundan, H. Dhulipati, K. L. V. Iyer, N. C. Kar and K. Mukherjee, "Comparison of inductance determination methods of PMSMs for EV application,"

2017 IEEE 30th Canadian Conference on Electrical and Computer Engineering (CCECE), Windsor, ON, 2017, pp. 1-4.

[10]. T. Strinić and W. Gruber, "Self-Commissioning of Permanent Magnet Synchronous Machines by Considering Nonlinearities of the Voltage Source Inverter," IECON 2019 - 45th Annual Conference of the IEEE Industrial Electronics Society, Lisbon, Portugal, 2019, pp. 1320-1326.

[11]. T. L. Vandoorn, F. M. De Belie, T. J. Vyncke, J. A. Melkebeek and P. Lataire, "Generation of Multisinusoidal Test Signals for the Identification of Synchronous-Machine Parameters by Using a Voltage-Source Inverter," in IEEE Transactions on Industrial Electronics, vol. 57, no. 1, pp. 430-439, Jan. 2010.

[12]. D. Banerjee, Z. Li, S. Mukundan, A. Balamurali, C. Lai and N. C. Kar, "Online Parameter Estimation and Self Commissioning of Permanent Magnet Motor Drive," 2018 21st International Conference on Electrical Machines and Systems (ICEMS), Jeju, 2018, pp. 1401-1406.

[13]. C. Choi, W. Lee, S. Kwon and J. Hong, "Experimental Estimation of Inductance for Interior Permanent Magnet Synchronous Machine Considering Temperature Distribution," in IEEE Transactions on Magnetics, vol. 49, no. 6, pp. 2990-2996, June 2013.

[14]. F. Fernandez-Bernal, A. Garcia-Cerrada and R. Faure, "Determination of parameters in interior permanent magnet synchronous motors with iron losses without torque measurement," Conference Record of the 2000 IEEE Industry Applications Conference. Thirty-Fifth IAS Annual Meeting and World Conference on Industrial Applications of Electrical Energy (Cat. No.00CH37129), Rome, Italy, 2000, pp. 409-415 vol.1.

[15]. S. Jung, J. Hong and K. Nam, "Current Minimizing Torque Control of the IPMSM Using Ferrari's Method," in IEEE Transactions on Power Electronics, vol. 28, no. 12, pp. 5603-5617, Dec. 2013.

[16]. K. M. Rahman and S. Hiti, "Identification of machine parameters of a synchronous motor," in IEEE Transactions on Industry Applications, vol. 41, no. 2, pp. 557-565, March-April 2005.

[17]. Armando, E., Bojoi, R., Guglielmi, P., Pellegrino, G. and Pastorelli, M.: Experimental methods for synchronous machines evaluation by an accurate magnetic model identification. In: 2011 IEEE Energy Conversion Congress and Exposition (ECCE). pp. 1744–1749, 17-22 Sept 2011

[18]. C. Lascu and G. Andreescu, "Self-commissioning of electrical parameters for PMSM in sensorless drives," 2015 Intl Aegean Conference on Electrical Machines & Power Electronics (ACEMP), 2015 Intl Conference on Optimization of Electrical & Electronic Equipment (OPTIM) & 2015 Intl Symposium on Advanced Electromechanical Motion Systems (ELECTROMOTION), Side, 2015, pp. 605-610.

[19]. G. Wang, Lizhi Qu, Hanlin Zhan, Jin Xu, Li Ding, Guoqiang Zhang and Dianguo Xu, "Self-Commissioning of Permanent Magnet Synchronous Machine Drives at Standstill Considering Inverter Nonlinearities," in IEEE Transactions on Power Electronics, vol. 29, no. 12, pp. 6615-6627, Dec. 2014.

[20]. L. M. Gong and Z. Q. Zhu, "A Novel Method for Compensating Inverter Nonlinearity Effects in Carrier Signal Injection-Based Sensorless Control From Positive-Sequence Carrier Current Distortion," in IEEE Transactions on Industry Applications, vol. 47, no. 3, pp. 1283-1292, May-June 2011.

[21]. Q. Wang, G. Zhang, G. Wang, C. Li and D. Xu, "Offline Parameter Self-Learning Method for General-Purpose PMSM Drives With Estimation Error Compensation," in IEEE Transactions on Power Electronics, vol. 34, no. 11, pp. 11103-11115, Nov. 2019.

[22]. S. A. Odhano, R. Bojoi, Ş. G. Roşu and A. Tenconi, "Identification of the Magnetic Model of Permanent-Magnet Synchronous Machines Using DC-Biased Low-Frequency AC Signal Injection," in IEEE Transactions on Industry Applications, vol. 51, no. 4, pp. 3208-3215, July-Aug. 2015.

[23]. G. Pellegrino, B. Boazzo and T. M. Jahns, "Magnetic Model Self-Identification for PM Synchronous Machine Drives," in IEEE Transactions on Industry Applications, vol. 51, no. 3, pp. 2246-2254, May-June 2015.

[24]. S. Peresada, V. Reshetnyk, D. Rodkin and O. Zinchenko, "Linearizing speed control and self-commissioning of interior permanent magnet synchronous

motor", Bulletin of the National Technical University "KhPI". Problems of automated electric drive. Theory and practice, Kharkiv, 2019. no. 9, vol. 1334. pp. 36-42. (in Ukranian)

[25]. S. Peresada, Y. Nikonenko, V. Reshetnyk and D. Rodkin, "Adaptive position control and self-commissioning of the interior permanent magnet synchronous motors," 2019 IEEE International Conference on Modern Electrical and Energy Systems (MEES), Kremenchuk, Ukraine, 2019, pp. 498-501.

[26]. Hyunbae Kim, J. Hartwig and R. D. Lorenz, "Using on-line parameter estimation to improve efficiency of IPM machine drives," 2002 IEEE 33rd Annual IEEE Power Electronics Specialists Conference. Proceedings (Cat. No.02CH37289), Cairns, Qld., Australia, 2002, pp. 815-820 vol.2.

[27]. Aimeng Wang, Li Zhang and Shuhui Dong, "Dynamic performance improvement based on a new parameter estimation method for IPMSM used for HEVs," IECON 2011 - 37th Annual Conference of the IEEE Industrial Electronics Society, Melbourne, VIC, 2011, pp. 1825-1829.

[28]. I. Vesely, L. Vesely, and Z. Bradac, “MRAS identification of permanent magnet synchronous motor parameters,” IFAC-PapersOnLine, vol. 51, no. 6, pp. 250–255, 2018. 15th IFAC Conference on Programmable Devices and Embedded Systems PDeS 2018.

[29]. T. Boileau, N. Leboeuf, B. Nahid-Mobarakeh and F. Meibody-Tabar, "Online Identification of PMSM Parameters: Parameter Identifiability and Estimator Comparative Study," in IEEE Transactions on Industry Applications, vol. 47, no. 4, pp. 1944-1957, July-Aug. 2011.

[30]. T. Boileau, B. Nahid-Mobarakeh and F. Meibody-Tabar, "On-Line Identification of PMSM Parameters: Model-Reference vs EKF," 2008 IEEE Industry Applications Society Annual Meeting, Edmonton, AB, 2008, pp. 1-8.

[31]. M. N. Uddin and M. M. Islam Chy, "On-Line Parameter Estimation Based Speed Control of PM AC Motor Drive in Flux Weakening Region," Conference Record of the 2006 IEEE Industry Applications Conference Forty-First IAS Annual Meeting, Tampa, FL, 2006, pp. 1745-1751.

[32]. J. Zhou, K. Huang, S. Huang, S. Liu, H. Zhao and M. Shen, "Inductance Parameter Identification Method of Permanent Magnet Synchronous Motor Based on the HF Rotating Square Wave Voltage Injection," 2019 22nd International Conference on Electrical Machines and Systems (ICEMS), Harbin, China, 2019, pp. 1-4.

[33]. M. Cao and H. Migita, "A High Efficiency Control of IPMSM with Online Parameter Estimation," 2018 21st International Conference on Electrical Machines and Systems (ICEMS), Jeju, 2018, pp. 1421-1424.

[34]. S. Morimoto, M. Sanada and Y. Takeda, "Mechanical Sensorless Drives of IPMSM With Online Parameter Identification," in IEEE Transactions on Industry Applications, vol. 42, no. 5, pp. 1241-1248, Sept.-Oct. 2006.

[35]. S. J. Underwood and I. Husain, "Online Parameter Estimation and Adaptive Control of Permanent-Magnet Synchronous Machines," in IEEE Transactions on Industrial Electronics, vol. 57, no. 7, pp. 2435-2443, July 2010.

[36]. D. Q. Dang, M. S. Rafaq, H. H. Choi and J. Jung, "Online Parameter Estimation Technique for Adaptive Control Applications of Interior PM Synchronous Motor Drives," in IEEE Transactions on Industrial Electronics, vol. 63, no. 3, pp. 1438-1449, March 2016.

[37]. Y. Shi, K. Sun, H. Ma and L. Huang, "Permanent magnet flux identification of IPMSM based on EKF with speed sensorless control," IECON 2010 - 36th Annual Conference on IEEE Industrial Electronics Society, Glendale, AZ, 2010, pp. 2252-2257.

[38]. Bianchi, N.: Electrical machine analysis using finite elements. CRC press 10.1201/9781315219295, 2005

[39]. Bianchi, N., Bolognani, S.: Magnetic models of saturated interior permanent magnet motors based on finite element analysis. In: IEEE Industry Applications Conference IAS 1998, Oct 1998, pp. 27–34 (1998)

[40]. Ji-Young Lee, Sang-Ho Lee, Geun-Ho Lee, Jung-Pyo Hong and Jin Hur, "Determination of parameters considering magnetic nonlinearity in an interior permanent magnet synchronous motor," in IEEE Transactions on Magnetics, vol. 42, no. 4, pp. 1303-1306, April 2006.

[41]. B. Vaseghi, N. Takorabet and F. Meibody-Tabar, "Fault Analysis and Parameter Identification of Permanent-Magnet Motors by the Finite-Element Method," in IEEE Transactions on Magnetics, vol. 45, no. 9, pp. 3290-3295, Sept. 2009.

[42]. Z. Yin, R. Tang, C. Du and Y. Wang, "Moment of Inertia Identification Based on Unscented Kalman Filter for Permanent Magnet Synchronous Motors," 2019 14th IEEE Conference on Industrial Electronics and Applications (ICIEA), Xi'an, China, 2019, pp. 1141-1145.

[43]. F. Andoh, "Moment of Inertia Identification Using the Time Average of the Product of Torque Reference Input and Motor Position," in IEEE Transactions on Power Electronics, vol. 22, no. 6, pp. 2534-2542, Nov. 2007.

[44]. J. -. Choi, S. -. Lee and H. -. Kim, "Inertia identification algorithm for high-performance speed control of electric motors," in IEE Proceedings - Electric Power Applications, vol. 153, no. 3, pp. 379-386, 1 May 2006.

[45]. K. Liu and Z. Zhu, "Fast Determination of Moment of Inertia of Permanent Magnet Synchronous Machine Drives for Design of Speed Loop Regulator," in IEEE Transactions on Control Systems Technology, vol. 25, no. 5, pp. 1816-1824, Sept. 2017.

[46]. T. Kwon, S. Sul, H. Nakamura and K. Tsuruta, "Identification of the Mechanical Parameters for Servo Drive," Conference Record of the 2006 IEEE Industry Applications Conference Forty-First IAS Annual Meeting, Tampa, FL, 2006, pp. 905-910.

[47]. K. Ohnishi, N. Matsui and Y. Hori, "Estimation, identification, and sensorless control in motion control system," in Proceedings of the IEEE, vol. 82, no. 8, pp. 1253-1265, Aug. 1994.

[48]. S. Kim, "Moment of Inertia and Friction Torque Coefficient Identification in a Servo Drive System," in IEEE Transactions on Industrial Electronics, vol. 66, no. 1, pp. 60-70, Jan. 2019.

[49]. C. Lian, F. Xiao, S. Gao and J. Liu, "Load Torque and Moment of Inertia Identification for Permanent Magnet Synchronous Motor Drives Based on Sliding

Mode Observer," in IEEE Transactions on Power Electronics, vol. 34, no. 6, pp. 5675-5683, June 2019.

[50]. Rodkin D., Zinchenko O., Peresada S. "Survey of the interior permanent magnet synchronous motor models considering saturation and cross-magnetization", International scientific and technical journal of young scientists, graduate students and students "MODERN PROBLEMS OF ELECTRIC POWER ENGINEERING AND AUTOMATION", Kyiv, Ukraine, 2020.

[51]. Park, R. H. (1929). Two-reaction theory of synchronous machines generalized method of analysis-part I. Transactions of the American Institute of Electrical Engineers, 48(3), 716–727. doi:10.1109/t-aiee.1929.5055275

[52]. W. C. Duesterhoeft; Max W. Schulz; Edith Clarke (July 1951). "Determination of Instantaneous Currents and Voltages by Means of Alpha, Beta, and Zero Components". Transactions of the American Institute of Electrical Engineers. 70 (2): 1248–1255.

[53]. Krishnan R. “Permanent Magnet Synchronous and Brushless DC Motor Drives”, 2010.

[54]. Rodkin D., Zinchenko O., Peresada S., Kiselychnyk "Inductance determination of interior permanent magnet synchronous motor considering saturation" International scientific and technical journal of young scientists, graduate students and students "MODERN PROBLEMS OF ELECTRIC POWER ENGINEERING AND AUTOMATION", Kyiv, Ukraine, 2020.

[55]. Sepulchre R., Jankovic M., Kokotovic P. Constructive Nonlinear Control. Berlin: Springer-Verlag, 1997. 313 p.

[56]. K. S. Narendra and A. M. Annaswamy, Stable adaptive systems. Upper Saddle River, NJ: Prentice Hall, 1989.

APPENDIX A DESCRIPTION OF THE EXPERIMENTAL SETUP FOR THE STANDSTILL TEST

Function diagram of the setup is presented in Fig. 2.1. DC supply - Magna-power electronics TS series III. Current and voltage are measured using differential probes and oscilloscope ISO-TECH IDS-2074A. Inverter consists from 3 IGBT modules SKM75GB12V (2 switches in each module). Real time simulator OPAL-RT OP5600 is used to change transistor states.

Table A.1 – OPAL-RT real time simulator parameters.

Manufacturer	OPAL-RT Technologies Corp.
Model	OP5600 HIL Box
AC input	100-240 VAC, 50-60 Hz
Operating System	Redhat v2.6.29.6-opalrt-6
CPU	Intel Xeon QuadCore 2.40 GHz, 1333FSB,8M
Hard disk	250 Gb, 7200 rpm, SATA
Motherboard	X8DTL-I-O Supermicro Motherboard, Intel® Xeon® processor 5600/5500 series, with QPI up to 6.4 GT/s
I/O connectors	Spartan3: 4 panels of 4 DB37F connectors
PCI slots	2 PCI, 4 PCIe
Carrier board	Spartan3 configuration: 8 mezzanines
Input/output interface	- 16 Analog Inputs - 16 Analog Outputs - 32 Static Digital Inputs/ Time-Stamped Digital Inputs/ Pulse-Width Modulated Inputs - 32 Static Digital Outputs/ Time-Stamped Digital Outputs/ Pulse-Width Modulated Outputs

Rated data of the tested IPM synchronous motor #2 Tirius JEM02: rated power $P_r = 12\,\text{kW}$, rated current $I_r = 25\,\text{A}$ (RMS), rated DC voltage $U_{DC} = 560\,\text{V}$, rated torque $T_r = 28\,\text{Nm}$, rated speed $\omega_r = 387\,\text{rad/s}$ (308 Hz supply), pole pairs $p_n = 5$, stator resistance $R_s = 0.13\,\text{Ohm}$, d-axis inductance $L_d = 1.62\,\text{mH}$, q-axis inductance $L_q = 2.7\,\text{mH}$, PM flux $\Psi_M = 0.108\,\text{Wb}$.

APPENDIX B DESCRIPTION OF THE EXPERIMENTAL SETUP FOR THE TEST WITH CONSTANT SPEED AND ALGORITHM TESTING

Experimental setup is presented in Fig. 1.6. Setup is based on inverter module IXYS MUBW 30-12 and TMS320F28335 based DSP – controller (32-bit floating point).

Rated data of the tested IPM synchronous motor #1 NORD 100T2/4: rated power $P_r = 3\,\text{kW}$, rated current $I_r = 5.4\,\text{A}$ (RMS), rated torque $T_r = 13.6\,\text{Nm}$, rated speed $\omega_r = 220\,\text{rad/s}$ (70 Hz supply), pole pairs $p_n = 2$, stator resistance $R_s = 1.7\,\text{Ohm}$, d-axis inductance $L_d = 0.031\,\text{H}$, q-axis inductance $L_q = 0.058\,\text{H}$, PM flux $\Psi_M = 0.615\,\text{Wb}$, viscous friction coefficient $\nu = 0.033\,\text{Nm}(\text{rad/s})^{-1}$, total inertia (together with loading machine) $J_\Sigma = 0.0155\,\text{kg}\cdot\text{m}^2$.

Loading induction machine NORD 100LP/4 TF with rated power $2.2\,\text{kW}$ is controlled by frequency converter SINUS PENTA 0005 4T BA2K2.

APPENDIX C MAIN CYCLE OF THE MODELLING PROGRAM FOR SPEED CONTROL SIMULATION

```
while (ct<sim_t)
  k=k+1;
  %time
  ct=ct+t_step;
  % reference
  dthetr=wra(k);
  ddthetr=dwra(k);
  dddthetr=ddwra(k);
  thetr=thetra(k);
  didr=didra(k);
  idr=idra(k);

%load
 if ((ct>0.4)&&(ct<=1.8))
    Tl=14;
 else
     Tl=0;
 end

 %inductacnes
Ldd=interp1(id_table,Ldd_table,-
abs(id),'linear',Ldd_table(1));
Ld=interp1(id_table,Ld_table,-
abs(id),'linear',Ld_table(1));
Lqq=interp1(iq_table,Lqq_table,-
abs(iq),'linear',Lqq_table(1));
Lq=interp1(iq_table,Lq_table,-
abs(iq),'linear',Lq_table(1));

%motor equations
id=id+t_step*(-R*id+pn*w*Lq*iq+ud)/Ldd;
iq=iq+t_step*(-R*iq-pn*w*Ld*id-
pn*w*km+uq)/Lqq;
w=w+t_step*(1.5*pn*((Ld-
Lq)*id*iq+iq*km)-mu*w-Tl)/J;
thet=thet+t_step*w;

%errors
eid=id-idr;
eiq=iq-iqr;
ew=w-wr;
ethet=thet-thetr;

%control algorithm
Tlo=Tlo-t_step*(kwi*ew);
iqr=(Tlo+mu*wr/J+dwr-
kw*ew)/(nuc*(km+(Ldm-Lqm)*idr));

edw=-(kw+mu/J)*ew+(nuc*(km+(Ldm-
Lqm)*idr))*eiq+(nuc*(Ldm-Lqm)*eid*iq);
diqr=(-kwi*ew+mu*dwr/J+ddwr-
kw*edw)/(nuc*(km+(Ldm-Lqm)*idr))-
(nuc*((Ldm-Lqm)*didr))*(Tlo+mu/J*wr+dwr-
kw*ew)/((nuc*(km+(Ldm-Lqm)*idr))^2);

xd=xd-t_step*(kii*eid);
xq=xq-t_step*(kii*eiq);
ud=R*idr-Lqm*pn*w*iq+Ldm*(didr-ki*eid+xd);

uq=R*iqr+Ldm*pn*w*id+km*pn*w+Lqm*(diqr-
ki*eiq+xq);

%monitoring
tm(k)=ct;
wm(k)=w;
thetm(k)=thet;
ethetm(k)=ethet;
idm(k)=id;
iqm(k)=iq;
eidm(k)=eid;
eiqm(k)=eiq;
udm(k)=ud;
uqm(k)=uq;
wrm(k)=wr;
iqrm(k)=iqr;

end
```

APPENDIX D MAIN CYCLE OF THE MODELLING PROGRAM FOR POSITION CONTROL SIMULATION

```
while (ct<sim_t)
  k=k+1;
  %time
  ct=ct+t_step;
  % reference
  dthetr=wra(k);
  ddthetr=dwra(k);
  dddthetr=ddwra(k);
  thetr=thetra(k);
  didr=didra(k);
  idr=idra(k);

%load
 if ((ct>0.4)&&(ct<=1.8))
    Tl=14;
 else
     Tl=0;
 end

 %inductacnes
Ldd=interp1(id_table,Ldd_table,-
abs(id),'linear',Ldd_table(1));
Ld=interp1(id_table,Ld_table,-
abs(id),'linear',Ld_table(1));
Lqq=interp1(iq_table,Lqq_table,-
abs(iq),'linear',Lqq_table(1));
Lq=interp1(iq_table,Lq_table,-
abs(iq),'linear',Lq_table(1));

%motor equations
id=id+t_step*(-R*id+pn*w*Lq*iq+ud)/Ldd;
iq=iq+t_step*(-R*iq-pn*w*Ld*id-
pn*w*km+uq)/Lqq;
w=w+t_step*(1.5*pn*((Ld-
Lq)*id*iq+iq*km)-mu*w-Tl)/J;
thet=thet+t_step*w;

%errors
eid=id-idr;
eiq=iq-iqr;
ew=w-wr;
ethet=thet-thetr;

%control algorithm
wr=dthetr-kthet*ethet;
dwr=ddthetr-kthet*ew+kthet^2*ethet;

Tlo=Tlo-t_step*(kwi*ew);
iqr=(Tlo+mu*wr/J+dwr-
kw*ew)/(nuc*(km+(Ldm-Lqm)*idr));

edthet=ew-kthet*ethet;

edw=-(kw+mu/J)*ew+(nuc*(km+(Ldm-
Lqm)*idr))*eiq+(nuc*(Ldm-Lqm)*eid*iq);
diqr=(-kwi*ew+mu*dwr/J+dddthetr+
kthet^2*edthet-
(kw+kthet)*edw)/(nuc*(km+(Ldm-Lqm)*idr))-
(nuc*((Ldm-Lqm)*didr))*(Tlo+mu*wr/J+dwr-
kw*ew)/((nuc*(km+(Ldm-Lqm)*idr))^2);

xd=xd-t_step*(kii*eid);
xq=xq-t_step*(kii*eiq);
ud=R*idr-Lqm*pn*w*iq+Ldm*(didr-ki*eid+xd);
uq=R*iqr+Ldm*pn*w*id+km*pn*w+Lqm*(diqr-
ki*eiq+xq);

%monitoring
tm(k)=ct;
wm(k)=w;
thetm(k)=thet;
ethetm(k)=ethet;
idm(k)=id;
iqm(k)=iq;
eidm(k)=eid;
eiqm(k)=eiq;
udm(k)=ud;
uqm(k)=uq;
wrm(k)=wr;
iqrm(k)=iqr;

end
```

APPENDIX E MAIN CYCLE OF THE MODELLING PROGRAM FOR ADAPTIVE POSITION CONTROL SIMULATION

```
while (ct<sim_t)
  k=k+1;
  %time
  ct=ct+t_step;
  % reference
  dthetr=dthetra(k);
  ddthetr=ddthetra(k);
  dddthetr=dddthetra(k);
  thetr=thetra(k);
  didr=didra(k);
  idr=idra(k);

%motor equations
id=id+t_step*(-
R*id+pn*w*Lq*iq+ud)/Ldd;
iq=iq+t_step*(-R*iq-pn*w*Ld*id-
pn*w*km+uq)/Lqq;
w=w+t_step*(1.5*pn*((Ld-
Lq)*id*iq+iq*km)-mu*w-Tl)/J;
thet=thet+t_step*w;

%errors
eid=id-idr;
eiq=iq-iqr;
ew=w-wr;
ethet=thet-thetr;

%identification controller
ksi=fi2*w+fi3+ddthetr+kthet*kthet*e
thet-(kthet+kw)*ew;
muid=1.5*pn*(km+(Ld-Lq)*idr);

dfi1=-lm1*(ksi*ew+gm*eiq*(fi2-
kthet-kw)*(-fi1*ksi-1.5*pn*(Ld-
Lq)*eid*iq-muid*eiq)/(muid));
fi1=fi1+t_step*dfi1;

dfi2=-lm2*(gm*eiq*(fi2-kthet-
kw)*(-fi1)/muid+ew)*w;
fi2=fi2+t_step*dfi2;

dfi3=-lm3*(gm*eiq*(fi2-kthet-
kw)*(-fi1)/muid+ew);
fi3=fi3+t_step*dfi3;

%control algorithm
wr=dthetr-kthet*ethet;
dwr=ddthetr-kthet*ew+kthet^2*ethet;

iqr=fi1*ksi/muid;

edthet=ew-kthet*ethet;

diqr=ksi*(dfi1*muid-fi1*1.5*pn*(Ld-Lq)*didr)/muid^2+
fi1*(dfi2*w+fi2*dwr+dfi3+dddthetr+kthet*kthet*edthet)
/muid+ (fi2-kthet-kw)*(-fi1*kw*ew+1.5*pn*(Ld-
Lq)*eid*iq+muid*eiq)/muid;

ud=R*idr-Lqm*pn*w*iq+Ldm*(didr-ki*eid);
uq=R*iqr+Ldm*pn*w*id+km*pn*w+Lqm*(diqr-
ki*eiq);


fi1r=J;
fi2r=mu/J;
fi3r=Tl/J;

%monitoring
tm(k)=ct;
wm(k)=w;
thetm(k)=thet;
ethetm(k)=ethet;
idm(k)=id;
iqm(k)=iq;
eidm(k)=eid;
eiqm(k)=eiq;
udm(k)=ud;
uqm(k)=uq;
wrm(k)=wr;
iqrm(k)=iqr;
fi1m(k)=fi1;
fi2m(k)=fi2;
fi3m(k)=fi3;
fi1rm(k)=fi1r;
fi2rm(k)=fi2r;
fi3rm(k)=fi3r;
end
```